

# **CHEMICAL AND PHYSICAL STRUCTURAL STUDIES ON TWO INERTINITE-RICH LUMP COALS.**

**Nandi Malumbazo**

A thesis submitted in fulfilment of the requirements for the degree of Doctor of Philosophy in the School of Chemical and Metallurgical Engineering at the University of the Witwatersrand.

**Johannesburg, 2011**

---

## DECLARATION

I, Nandi Malumbazo, declare that the thesis entitled:

**“CHEMICAL AND PHYSICAL STRUCTURAL STUDIES ON TWO INERTINITE-RICH LUMP COALS”**

is my own work and that all sources I have used or quoted have been indicated and acknowledged by means of references.

Signature: .....

Date:.....

# ABSTRACT

---

## ABSTRACT

Two Highveld inertinite-rich lump coals were utilized as feed coal samples in order to study their physical, chemical structural and petrographic variations during heat treatment in a packed-bed reactor unit combustor.

The two feed lump coals were selected as it is claimed that Coal B converts at a slower rate in a commercial coal conversion process when compared to Coal A. The reason for this requires detailed investigation.

Chemical structural variations were determined by proximate and coal char CO<sub>2</sub> reactivity analysis. Physical structural variations were determined by FTIR, BET adsorption methods, XRD and <sup>13</sup>C Solid state NMR analysis. Carbon particle type analysis was conducted to determine the petrographic constituents of the reactor generated samples, their maceral associations (microlithotype), and char morphology. This analysis was undertaken with the intention of tracking the carbon conversion and char formation and consumption behaviour of the two coal samples within the reactor.

Proximate analysis revealed that Coal A released 10 % more of its volatile matter through the reactor compared to Coal B. Unburnt carbon in the ash bed zone was observed for both coal samples (Coal A and B), and it was attributed to incomplete carbon conversion. Coal char CO<sub>2</sub> reactivity analysis showed that indeed Coal A is more reactive than Coal B.

## ABSTRACT

---

Qualitative FTIR analysis showed that both coals follow similar trends when exposed to high temperatures. Coal structural characterization revealed that Coal A has higher surface area when compared to Coal B. XRD analysis revealed that Coal A has less aromatic crystallites and lower Lc values compared to Coal B. It was observed that the coal structural properties of Coal A became more ordered and aligned at lower temperatures (289 °C), whereas Coal B starts at higher temperatures (693 °C). <sup>13</sup>C Solid state NMR results showed that Coal B is more aromatic than Coal A implying that it is difficult to gasify/combust Coal B. Petrography analysis showed that Coal A has 34.6 vol % reactive macerals of which 78 % is from liptinite and vitrinite contents. Coal B has 53.6 vol % of reactive macerals of which 49 % was from liptinite and vitrinite, the other 51 % is from reactive semifusinite and inertodetrinite. The 49/51 split between reactive maceral value for Coal B may explain the lower reactivity compared to Coal A. Coal B appeared to produce more inert char particles, ran at higher temperatures in the ash bed because of its aromatic richness than Coal A. This was also attributed to the fact that Coal B has higher inertinite content than Coal A. The allocation of parent coal samples to “reactive” and “inert” macerals gave more in depth results that were able to show a possible reason behind reactivity difference occurring during the coal conversion process and support the structural analysis results obtained for these parent coal samples. The reactivity difference of these parent lump coal samples appears to be greatly influenced by the chemical reactions (structure) of these samples more than the kinetic reactions (pressure, temperature, reaction rates etc.) of these samples.

## DEDICATION

---

I dedicate this work to my son Hlumelo and my husband Mvuselelo Mathebula.

# ACKNOWLEDGEMENTS

---

## ACKNOWLEDGEMENTS

I would like to extend my gratitude to the following:

God almighty for guiding me throughout my studies and making my dreams come true.

To my ancestors for opening doors and guiding me throughout the difficulties of my varsity life.

My ancestors from maternal side: Oonkomo, Oogolela, Oomasikela, Ooyongwane, Oomntungwa, Oomalinga, Oomasikane, Oonkumbuzo. My ancestors from my paternal side: Oonyawuza, Oofaku, Oompondo, Oondayeli, Uziqelekazi uhlamba ngobubende, OoDakile.

To my parents (Mrs. Bukelwa Malumbazo-Ndayi and Mr. Makwedinana Ndayi) for giving me this life and raising me to be the person that I am today. To my siblings Thabiso Malumbazo, Zikhona "titi" Malumbazo and Yanga Ndayi, I was doing this to motivate you guys to continue with your studies no matter what.

To my husband Mvuselelo Mathebula for his encouragement and motivation for me to study this far.

To my supervisors, Prof. Wagner and Prof. Bunt for your constant guidance, support and patience to develop my skills in coal research and also for believing in me.

To Sasol for financial assistance and to the following people working at Coal processing Technologies Prof. J. van Heerden, Dr. D. van Niekerk, Ms. H. Assumption, Mr Ben Ashton, Dr. R. Coetzer, Mr. S. Duplessis and Dr. B. Hlatshwayo for your constructive support and always avail yourselves when I needed your help.

To my close friends and Carbon and Coal Group colleagues for always putting a smile on my face whenever I need it, you know who you are.

# CONTENTS

---

## Contents

<b>Chapter 1</b> .....	<b>1</b>
1. INTRODUCTION.....	1
1.1 Background and motivation of the study.....	1
1.1.1 Coal Structure .....	2
1.2 Research Questions .....	4
1.3 Aim and Objectives of the study .....	5
1.4 Scope of the thesis.....	6
<b>Chapter 2</b> .....	<b>7</b>
2. LITERATURE REVIEW.....	7
2.1 Origins and Formation of Coal .....	7
2.2 Geological Occurrence and uses of Coal in South Africa .....	9
2.2.1 South African Coalfields.....	11
2.3 Classification of Coal .....	13
2.4 Coal Structure .....	15
2.4.1 Analytical methods utilized for the Coal Structural Studies.....	17
2.4.1.1 Fourier Transform Infrared Spectroscopy (FTIR) studies for Coals.....	18
2.4.1.2 X-ray powder diffraction studies for Coals .....	21
2.4.1.3 <sup>13</sup> C Solid State Nuclear Magnetic Resonance Spectroscopy studies for Coals.....	26
2.4.1.4 BET Adsorption studies for Coals .....	29
2.5 Coal petrography .....	30
2.5.1 Macerals.....	34

# CONTENTS

---

2.5.1.1	Liptinite.....	35
2.5.1.2	Vitrinite .....	36
2.5.1.3	Inertinite.....	36
2.5.2	Microlithotypes.....	38
2.5.3	Mineral Matter.....	40
2.6	Coal Conversion .....	40
<b>Chapter 3 .....</b>		<b>45</b>
3.	EXPERIMENTAL METHOD .....	45
3.1	Origin of the feed coal samples.....	45
3.2	Char Preparation .....	45
3.2.1	Description of Pilot scale Packed-bed reactor .....	46
3.3	Sample Analysis .....	47
3.4	<b>Phase 1: Chemical Analysis .....</b>	<b>48</b>
3.4.1	Proximate Analysis.....	48
3.4.2	Coal char CO <sub>2</sub> reactivity .....	48
3.5	<b>Phase 2: Physical Structural analysis .....</b>	<b>49</b>
3.5.1	Demineralization.....	49
3.5.2	Fourier Transform Infrared Spectroscopy (FTIR) analysis.....	49
3.5.3	BET Adsorption Analysis.....	50
3.5.4	X-ray diffraction analysis .....	52
3.5.5	<sup>13</sup> C Solid State Nuclear Magnetic Resonance Spectroscopy ( <sup>13</sup> C SSNMR) analysis.....	54
3.5.6	Conductivity analysis.....	57
3.6	<b>Phase 3: Petrographic analysis .....</b>	<b>61</b>



# CONTENTS

---

3.6.1	Maceral and Microlithotype analysis.....	61
3.6.2	Carbon Particle Type analysis.....	61
3.6.3	Total Reflectance analysis.....	65
3.6.4	Electron Microprobe on Oxidized Char .....	66
<b>Chapter 4</b>	.....	<b>67</b>
<b>4.</b>	<b>RESULTS AND DISCUSSION</b> .....	<b>67</b>
<b>4.1</b>	<b>PHASE 1: Chemical analysis results</b> .....	<b>70</b>
4.1.1	Proximate analysis results.....	70
4.1.1.1	Volatile matter profile .....	71
4.1.1.2	Fixed carbon profile .....	75
4.1.1.3	Ash profile.....	77
4.1.2	Coal char CO <sub>2</sub> reactivity analysis results.....	79
4.1.3	Summary of Phase 1 .....	83
<b>4.2</b>	<b>PHASE 2: Structural analysis results</b> .....	<b>85</b>
4.2.1	Demineralization results.....	85
4.2.2	Fourier Transform Infrared Spectroscopy (FTIR) analysis results.....	87
4.2.3	BET Adsorption analysis results .....	92
4.2.4	X-ray Diffraction (XRD) analysis results .....	97
4.2.4.1	Qualitative results of the X-ray diffraction analysis .....	99
4.2.4.2	Quantitative results of the X-ray diffraction analysis. ....	101
4.2.4.3	Comparison of Coal A and B packed-bed reactor generated samples. ....	105
4.2.5	<sup>13</sup> C Solid State Nuclear Magnetic Resonance Spectroscopy ( <sup>13</sup> C SSNMR) analysis results.....	108
4.2.5.1	Qualitative <sup>13</sup> C SSNMR analysis results of the parent coal samples and the packed-bed reactor generated samples. ....	110

# CONTENTS

---

4.2.5.2	Quantitative <sup>13</sup> C SSNMR analysis results for the parent coal and the packed-bed reactor generated samples.....	113
4.2.6	Summary of Phase 2.....	118
4.3	<b>PHASE 3: Petrographic results</b> .....	121
4.3.1	Maceral group analysis .....	122
4.3.2	Carbon particle type analysis .....	125
4.3.2.1	Devolatilization coal particles profile for Coal A and B packed-bed reactor generated samples.....	134
4.3.2.2	Porous char particles profile for the coal A and B packed-bed reactor generated samples.....	136
4.3.2.3	Inert char particles profile for the Coals, A and B packed-bed reactor generated samples.....	138
4.3.3	Total Reflectance analysis results.....	141
4.3.4	Electron Microprobe study on char particles.....	146
4.3.5	Comparative results of Coal A and B parent coal samples and packed-bed reactor generated samples.....	149
	<b>Chapter 5</b> .....	<b>153</b>
5.	<b>SUMMARY AND CONCLUSION</b> .....	153
6.	<b>RECOMMENDATIONS</b> .....	159
	<b>REFERENCES</b> .....	161
	<b>APPENDIX A: PROXIMATE ANALYSIS</b> .....	179
	<b>APPENDIX B: COAL CHAR CO<sub>2</sub> REACTIVITY RESULTS</b> .....	180
	<b>APPENDIX C: PROXIMATE ANALYSIS RESULTS AFTER DEMINERALIZATION</b> .....	181
	<b>APPENDIX D: BET ADSORPTION RESULTS (RAW DATA)</b> .....	182
	<b>APPENDIX E: X-RAY DIFFRACTION CALCULATIONS.</b> .....	186

---

# CONTENTS

---

<b>APPENDIX F: <math>^{13}\text{C}</math> SS NMR ANALYSIS RESULTS</b> .....	189
<b>APPENDIX G: CONDUCTIVITY RESULTS</b> .....	193
<b>APPENDIX H: PETROGRAPHY</b> .....	194
<b>APPENDIX I: TOTAL REFLECTANCE ANALYSIS RESULTS</b> .....	197

## LIST OF TABLES

---

### LIST OF FIGURES

Figure 2.1: Occurrence of Coal in South Africa (Schmidt, 2007).....	10
Figure 2.2: A hypothetical model of Coal Structure (Solum et al., 1988).....	16
Figure 2.3: A typical FTIR spectrum of coal (in this case Highveld (bottom) and Waterberg coals (top)) (Van Niekerk et al., 2008).....	20
Figure 2.4: Where N = number of aromatic crystallite in a unit cell, L – length of aromatic crystallite, La = average crystallite diameter in a unit cell.....	23
Figure 2.5: <sup>13</sup> C NMR of a typical high volatile bituminous coal showing different functional groups that can be distinguished from 13C NMR spectroscopy (Suggate and Dickson, 2004).....	28
Figure 2.6: Three analytical techniques used in Coal Petrography (Falcon and Snyman, 1986).....	33
Figure 2.7: Trigonal diagram showing microlithotype classification system across three maceral groups (Lester et al., 2003).....	39
Figure 3.1: A photograph showing the bed profile of the packed-bed reactor combustor unit (left =top of reactor, right = bottom of reactor).....	46
Figure 3.2: Micrometrics ASAP 2010 analyzer.....	51
Figure 3.3: Curve resolution of diffractogram for the Coal A packed-bed reactor generated sample no. 2.....	53
Figure 3.4: Varian Solid State NMR.....	54
Figure 3.5: Spectrum with defined integral reset points and referenced to 126.56ppm.....	57
Figure 3.6: Schematic representation of the laboratory made electrical resistivity equipment, excluding the electronic components.....	59

## LIST OF TABLES

---

Figure 4.1: Volatile matter (dry-basis) profile for the Coals, A and B packed-bed reactor generated samples as a function of reactor height.....	72
Figure 4.2: Volatile matter evolution of Coal A and B packed-bed reactor generated samples as a function of reactor height.....	74
Figure 4.3: Fixed carbon profile (dry basis) for the Coal A and B packed-bed reactor generated samples as a function of reactor height.....	75
Figure 4.4: Ash profile (dry basis) for the Coal A and B packed-bed reactor generated samples as a function of reactor height.....	78
Figure 4.5: CO <sub>2</sub> reactivity of Coal A and B parent coal samples and packed-bed reactor generated samples as a function of reactor height.....	80
Figure 4.6: Correlation of Coal Char CO <sub>2</sub> reactivity results with volatile matter evolution.....	82
Figure 4.7: FTIR spectrum of Coal A (left) and B (right) parent coal samples and the packed-bed reactor generated samples.....	88
Figure 4.8: Coal A and B packed-bed reactor generated samples showing reactor temperature against CO <sub>2</sub> BET surface area.....	95
Figure 4.9: XRD patterns for Coal A (left) and B (right) parent coal samples and the packed-bed reactor generated samples.....	100
Figure 4.10: Relationship between temperatures and the XRD structural parameters of Coal A and B parent coals and the packed-bed reactor generated samples.....	106
Figure 4.11: <sup>13</sup> C CP/MAS NMR spectra for the parent coal sample.....	109
Figure 4.12: <sup>13</sup> C CP/MAS NMR spectra for Coal A (left) and B (right) parent coals and the packed-bed reactor generated samples.....	111

## LIST OF TABLES

---

Figure 4.13: Correlation of volatile matter content of Coal A and B as a function of aromaticity value.....	116
Figure 4.14: Micrographs showing coal groups observed from the packed-bed reactor samples (magnification x500, oil immersion, reflected light).....	127
Figure 4.15: Micrographs showing devolatilizing coals observed from the packed-bed reactor samples (magnification x500, oil immersion, reflected light).....	128
Figure 4.16: Micrographs showing char particles observed from the packed-bed reactor samples (magnification x500, oil immersion, reflected-light).....	129
Figure 4.17: Carbon Particle Type Analysis results for Coal A packed-bed reactor generated samples.....	130
Figure 4.18: Carbon Particle Type Analysis results for the Coal B packed-bed reactor samples.....	131
Figure 4.19: Micrographs showing a char particle and coal particle within ash bed (magnification x500, oil immersion, reflected light).....	133
Figure 4.20: Devolatilization coal particles profile for the Coal A and B packed-bed reactor generated samples as a function of reactor height.....	135
Figure 4.21: Porous char particles (vol %) profile for the Coal A and B packed-bed reactor generated samples as a function of reactor height.....	137
Figure 4.22: Inert char particles (vol %) profile for the Coal A and B packed-bed reactor generated samples as a function of reactor height.....	139
Figure 4.23: Total reflectance analysis for Coal A and B parent coal samples and the packed-bed reactor generated samples.....	144
Figure 4.24: A photograph of inert char particle with both non-oxidized and oxidized sections.....	147

---

## LIST OF TABLES

---

Figure F-1: CP/MAS spectrum showing 8 integral values regarding to their structural parameters.....	189
Figure G-1: Graph showing resistivity of Coal A feed coal sample and the packed-bed reactor generated samples.....	193
Figure I-1: Total reflectance measurement of coal macerals for the Coal A feed coal sample.....	197
Figure I-2: Total reflectance measurement of coal macerals for the Coal A packed-bed reactor generated sample 1.....	198
Figure I-3: Total reflectance measurement of coal macerals for the Coal A packed-bed reactor generated sample 2.....	199
Figure I-4: Total reflectance measurement of coal macerals for the Coal A packed-bed reactor generated sample 3.....	200
Figure I-5: Total reflectance measurement of coal macerals for the Coal A packed-bed reactor generated sample 4.....	201
Figure I-6: Total reflectance measurement of coal macerals for the Coal A packed-bed reactor generated sample 5.....	202
Figure I-7: Total reflectance measurement of coal macerals for the Coal A packed-bed reactor generated sample 6.....	203
Figure I-8: Total reflectance measurement of coal macerals for the Coal B coal feed sample.....	204
Figure I-9: Total reflectance measurement of coal macerals for the Coal B packed-bed reactor generated sample 1.....	205
Figure I-10: Total reflectance measurement of coal macerals for the Coal B packed-bed reactor generated sample 2.....	206

## LIST OF TABLES

---

Figure I-11: Total reflectance measurement of coal macerals for the Coal B packed-bed reactor generated sample 3.....	207
Figure I-12: Total reflectance measurement of coal macerals for the Coal B packed-bed reactor generated sample 4.....	208
Figure I-13: Total reflectance measurement of coal macerals for the Coal B packed-bed reactor generated sample 5.....	209
Figure I-14: Total reflectance measurement of coal macerals for the Coal B packed-bed reactor generated sample 6.....	210



## LIST OF TABLES

---

### LIST OF TABLES

Table 2.1: Table of reactive and non-reactive macerals and their groups (Falcon and Snyman, 1986).....	35
Table 2.2: Char Morphology Classification (Bailey et al., 1990).....	42
Table 3.1: Gas adsorption experimental conditions.....	50
Table 3.2: List of integration regions and values.....	57
Table 4.1: Summary of the packed-bed reactor generated samples together with their reaction zones and temperature history.....	68
Table 4.2: Proximate analysis of parent coal samples (% dry basis).....	70
Table 4.3: Coal char CO <sub>2</sub> reactivity analysis results at 50% burn-off at 1000 0C (h- <sup>1</sup> ).....	79
Table 4.4: Summary of significant findings from chemical analysis results.....	84
Table 4.5: A summary of the ash contents for the packed-bed reactor generated samples before and after the demineralization process.....	86
Table 4.6: Tabulated FTIR wavenumbers and their annotations for the parent coal samples and the packed-bed reactor generated samples.....	89
Table 4.7: Tabulated results of CO <sub>2</sub> BET surface area for parent coal samples and the packed-bed reactor generated samples.....	94
Table 4.8: XRD structural parameters for the Coal A parent coal and the corresponding packed-bed reactor generated samples.....	103
Table 4.9: XRD structural parameters for the Coal B parent coal and its packed-bed reactor generated samples.....	103
Table 4.10: Summary of structural parameters for Coal A and the packed-bed reactor generated samples derived from <sup>13</sup> C Solid state NMR analysis.....	114

## LIST OF TABLES

---

Table 4.11: Summary of structural parameters for Coal B and its packed-bed reactor generated samples derived from <sup>13</sup> C Solid state NMR analysis.....	114
Table 4.12: Summary of significant findings obtained from FTIR, BET adsorption studies, XRD and <sup>13</sup> C SSNMR.....	120
Table 4.13: Maceral group analysis and rank value for the parent coal.....	122
Table 4.14: A summarized reactive and inert macerals for the parent coal samples.....	124
Table 4.15: Total reflectance analysis results for the Coal A and B reactor generated samples.....	142
Table 4.16: Elemental Composition in mass for sample 5 (Coal A packed-bed reactor) %.....	148
Table A-1: Table presenting proximate analysis data for the Coal A packed-bed reactor samples.....	179
Table A-2: Table presenting proximate analysis data for the Coal B packed-bed reactor samples.....	179
Table B-1: Summarized coal char CO <sub>2</sub> reactivity of Coal A and B packed-bed reactor samples.....	180
Table D-1: Summarized BET CO <sub>2</sub> isotherm pore volume results for both Coals, A and B packed-bed reactor generated samples.....	182
Table D-2: Summarized BET N <sub>2</sub> isotherm raw data for the Coal A packed-bed reactor generated samples.....	183
Table D-3: Summarized BET N <sub>2</sub> isotherm raw data for the Coal B packed-bed reactor generated samples.....	185

## LIST OF TABLES

---

Table E-1: XRD structural parameters for the Coal A feed coal and the corresponding packed-bed reactor generated samples.....	187
Table E-2: XRD structural parameters for the Coal B parent coal and its packed-bed reactor generated samples.....	188
Table F-1: List of integration regions and values.....	190
Table H-1: Summarized microlithotype analysis (vol %) for the Coals, A and B feed coal samples.....	194
Table H-2: Tabulated carbon particle type analysis results for the Coal A packed-bed reactor generated samples.....	195
Table H-3: Tabulated carbon particle type analysis results for the Coal B packed-bed reactor generated samples.....	196

# NOMENCLATURE

---

## NOMENCLATURE

FTIR	Fourier Transform Infrared Resonance
XRD	X-ray diffraction
NMR	Nuclear Magnetic Resonance
CP	Cross Polarization
MAS	Magic Angle Spinning
DD	Dipolar Dephasing
SPE	Single Pulse Excitation
BET	Brunauer Emmett Teller
TGA	Thermogravimetric analysis
$d_{002}$	Interlayer spacing of crystallites in a unit cell
$L_a$	Average crystallite diameter in a unit cell
$L_c$	Average crystallite height in a unit cell
$N$	Number of crystallite in a unit cell
$f_a$	Fraction of aromatic carbons
$f_{al}$	Fraction of aliphatic carbons
$f_a^{CO}$	Fraction of carbonyl carbons
$f_a^P$	fraction of phenolic carbons
$f_a^S$	Fraction of alkylated aromatic carbons
$f_a^N$	Fraction of non-protonated carbons and $CH_3$ in aromatic region
$f_a^H$	Fraction of protonated carbons in the aromatic region

## NOMENCLATURE

---

$f_a^B$	Fraction of bridgehead carbons
$f_a^{N^*}$	Fraction of non-protonated carbons and CH <sub>3</sub> in aliphatic region
$f_{al}^H$	Fraction of protonated carbons and CH <sub>3</sub> in aliphatic region
$f_{al}^O$	Fraction of aliphatic carbons bonded to oxygen
Å	Angstroms units
θ	Theta
λ	Lambda
γ	Gamma
β	Beta
ν	Frequency of wave
μm	Micrometre
°C	Degrees Celsius
m <sup>2</sup> /g	Square metre per gram
ppm	Parts per million
vol %	Volume percentage
m <sup>3</sup> /h	Cubic metre per hour
g.cm <sup>-3</sup>	Gram per cubic centimetre
Rot	Total reflectance
Std dev	Standard deviation
h <sup>-1</sup>	Per hour

## CHAPTER 1

### 1 INTRODUCTION

This chapter will focus firstly on the motivation behind the initiation of this study. Secondly, an introduction to coal structure and the structural changes occurring during the coal conversion process will be given. This chapter will also address the study hypothesis, what is aimed to be achieved, and the routes that will be taken to achieve the objectives of this project.

#### 1.1 Background and motivation of the study

South Africa is the fifth largest coal country in the world, producing 244 million tons of marketable coal annually (World Coal Institute, Coal Facts, 2008 edition). This country exports 25 % of its coal production making it the third largest coal exporting country in the world (Eskom, Coal Power, 2009). It was estimated in the year 2000 that there were 33.8 billion tons of South African coal reserves (consisting of hard coal with no lignite), which constitutes to 5.4 % of the world's coal reserves. Prevost (2004) determined that this amount should be able to supply South Africa up until around 2050.

South Africa produces high quality steam coal for the export markets and generally utilizes the lower quality for domestic consumption. The high quality steam coal is beneficiated before it is exported and the lower quality coal which is rich in ash (30 – 35 %) (Kruger and Krueger, 2005), is used for domestic power generation and for the production of synfuels and other petrochemical products. Dempers (2009) claimed that in

## CHAPTER 1: INTRODUCTION

---

2008, South Africa consumed 270 million tons of thermal coal and estimated that by 2018, there will be a 40 % increase in coal consumption. This estimation includes coal exports, power generation and synfuels production.

This brings us to a conclusion that South Africa will continue to benefit economically by exporting coal and domestically by using it for industrial purposes. Considering the limited amount of South African coal reserves, and the continuous reliance on coal, there is an essential need to better understand the chemical and physical structural changes of coal during the coal utilization processes.

### **1.1.1 Coal Structure**

Coal structure is made up of a macromolecular aromatic network. This macromolecular network consists of aromatic carbon structures of different functionalities, and is connected to each other by bridge-head carbons. These bridge-head carbons are aliphatic in nature. There are other attachments connected to the aromatic clusters and are known as side-chain carbons. These side-chain carbons are believed to be made up of aliphatic and carbonyl functional groups (Hambly, 1998).

During the coal conversion processes, covalent bonds throughout the coal matrix are broken. This is known as a depolymerization process (Van Krevelen, 1961). When these bonds are broken, fragments of coal molecules are formed. Tar and light gases will be released if these are small; and if not, the large fragments will remain in the solid phase and recombine with the coal macromolecule to form large aromatic clusters/fragments (Hambly, 1998). If the heating process continues, the char particles will further react

## CHAPTER 1: INTRODUCTION

---

with the reactant gases to form product gases and a residual ash. More still needs to be learned about the coal structure and the products of coal conversion processes, so that these processes can be well understood and managed.

Extensive research work on coal structural analysis has been conducted on pulverized high vitrinite-rich and low ash content coal (Solum et al., 1988 and 1989; Cartz and Hirsch, 1959; Wilson et al., 1984; Genetti et al., 1999). Little structural research work has been conducted on inertinite-rich and high ash content coals such as South African coals. The difference between vitrinite-rich coals and inertinite-rich coals has been based on their burning behaviour, i.e. vitrinite-rich coals burn much faster than inertinite-rich coals (Crelling et al, 1988; Jones et al, 1985; Choudhury et al., 2007). This implies that these coals have a different chemical structure so they tend to behave differently during the coal utilization process.

The current investigation aims at deepening the current level of understanding of the inertinite-rich lump coal structural properties and its structural behaviour during the lump coal conversion process. Since coal structural studies are new in the South African coal chemistry, special attention has been given to the characterization techniques that determine the coal structural properties and its products during coal conversion. Secondly, this study aims at bringing more insight into the char morphology produced from inertinite-rich Highveld lump coals.

This study was initiated after Koekemoer's (2009) studies revealed that two Highveld lump coals behave differently during heat treatment. Their study showed that Coal B had low calorific value when considering the amount of fixed carbon contained in this



## CHAPTER 1: INTRODUCTION

---

coal when compared to Coal G (in our case this coal is termed Coal A). According to this study, this was due to the fact that Coal B yielded more high density fractions (low energy fractions,  $SG > 2.0 \text{ g.cm}^{-3}$ ) and less of the low density fractions (higher energy fractions,  $SG < 1.6 \text{ g.cm}^{-3}$ ) during the density separation process when compared to Coal G. During evaluation of the pyrolysis gases, it was found that the total gas yield of these two lump coals varied significantly, and this could not be linked to any of the coal properties.

Since there was no significant variation in the coal properties and rank, this motivated the initiation of the current project, whereby chemical and physical structural changes of these coals was needed in order to obtain a deeper understanding as to why these coals with similar properties behave differently during coal conversion process. This will be achieved by utilization of advanced as well as conventional characterization techniques.

### 1.2 Research Questions

Research questions to be dealt with during the course of this thesis are:

- Does the structural difference of the feed lump coal samples influence the thermoplastic nature of two coals having similar properties during their transformation in packed-bed reactor?
- Can the carbon particle type analysis have an influence in the reactivity or burning behaviour of lump coals during the conversion process?

### 1.3 Aim and Objectives of the study

The main aim of this study is to fully understand the chemical and physical structural differences of the two Highveld feed coal samples (Coal A and B) during the coal conversion of lump coals in a packed-bed reactor combustor unit. This will enhance the understanding of reactivity development of these two Highveld coals.

The objectives that will be addressed during the course of the thesis are:

- Two feed coal samples from the Highveld coalfields are thermally treated utilizing a packed-bed reactor combustor unit and reaction zones are identified.
- Chemical and physical structural analysis of the resultant packed-bed reactor samples are characterized by various analytical techniques.
- Chemical structural changes are determined by proximate analysis and coal char CO<sub>2</sub> reactivity (50 % burn-off at 1000 °C) for the various packed-bed reactor combustor unit samples.
- Physical structural changes are determined by the utilization of FTIR analysis, BET adsorption methods, XRD and <sup>13</sup>C SSNMR analysis.
- Physical changes at a microscopic level are determined by petrographic analysis.

It is anticipated that by following the above mentioned objectives that the differences in the reactivity of the two Highveld coals will be better understood. The use of advanced analytical techniques in the utilization of lump coals during their transformation is needed for a detailed characterization of coals to fully determine their conversion performance; detailed coal petrography is one such tool that its value is frequently under-

## CHAPTER 1: INTRODUCTION

---

played. This study will clearly show the importance of coal petrography in the coal conversion process.

### **1.4 Scope of the thesis**

This thesis is divided into six chapters which include:

1. Chapter 1: Introduction – introduction, background of the study and motivation, hypothesis, aims and objectives.
2. Chapter 2: Literature review.
3. Chapter 3: Experimental methodology
4. Chapter 4: Results and discussion
5. Chapter 5: Summary of the thesis
6. Chapter 6: Conclusion and future work

### CHAPTER 2

#### 2 LITERATURE REVIEW

The following review will firstly survey the origins and formation of coal in Southern Africa as well as the geological occurrences and uses of coal in South Africa. Secondly the review provides information relating to petrographic composition and classification. Thirdly, the macromolecular structure of coal and the different characterization techniques used to determine the macromolecular structure will be addressed. The survey continues by reviewing coal conversion processes including the different stages such as: devolatilization, char formation, and burnout. The formation of the different char morphologies will also be addressed.

##### 2.1 Origins and Formation of Coal

The greatest coal forming time in the geological history was during the Carboniferous era (280 to 345 million years ago), more particularly in Europe, Asia and North America. The Carboniferous coal was formed from tropical swamp forests. Southern Hemisphere Permian coal (in South Africa, China, India and Australia) was formed from the *Glossopteris* flora, which grew in cold periglacial tundra when the South Pole was inland in Gondwanaland (Falcon, 1986a).

Coal is formed from plant remains that have been compacted, hardened, chemically transformed, and metamorphosed by heat and pressure over geological time from peat forming environments. These peat environments may be swamps and/or marsh. Coal

## CHAPTER 2: LITERATURE REVIEW

---

formed in swamp ecosystems persists in lowland sedimentary basins. These swamp environments were formed during slow subsidence of passive continental margins and most likely to have formed adjacent to estuarine and marine sediments, suggesting that they may have been in tidal delta environments (Stach et al., 1982).

As plant died in these peat environments, their biomass was deposited in anaerobic aquatic environments where the low oxygen levels prevented their complete decay by bacteria and oxidation. For these peat environments to form economically, valuable coal, masses of undecayed organic matter must be preserved and remain steady for prolonged periods of time. In addition the water feeding these peat swamps must remain essentially free of sediment. This required minimal erosion occurred in the uplands of the rivers which fed the coal swamps and efficient trapping of the sediments (Bend et al., 1991 and 1992). Usually due to the occurrence of tectonic events, the coal forming environment stopped. In many cases this is unexpected, with the majority of coal seams having a knife-sharp upper contact with the overlying sediments. This suggests that the early beginning of further sedimentation quickly destroyed the peat swamp environment and replaced it with indirect stream and river environments during subsidence (Falcon, 1986a).

Generally, to form a coal seam of 1 metre thick, between 10 and 30 metres of peat is required (Stach et al., 1982). Peat has a moisture content of up to 90%, so loss of water is of prime importance in the conversion of peat to lignite which is the lowest rank of coal. Lignite is then converted by dehydration and methanogenesis to sub-bituminous coal. Further dehydration reactions, progressively removing more methane and higher hydrocarbon gases such as ethane, propane, e.t.c leads to the formation of bituminous coal.

## CHAPTER 2: LITERATURE REVIEW

---

When the process is complete at sub-metamorphic conditions, lignite is formed (Coal fossil fuel, 2009).

Conditions for the formation of coal facies differ with palaeoecological environment. For example, in conditions with low ground water level, high aerobic oxidation of the plant matter occurs, resulting in a high degree of fusinitization and carbon enrichment, and the production of volatile-poor inertinitic organic components. In water-logged conditions which may be found in protected back swamps, the organic matter undergoes a process of gelification with extensive tissue conversion and volatile matter enrichment. This leads to production of volatile rich vitrinic organic matter (Falcon, 1986a).

The Permian swamps in the Southern Hemisphere (in this case South Africa) existed under cold to cool temperature conditions associated with warming of a massive ice age compared to the Northern Hemisphere Carboniferous swamps. South African coal is known to have a distinctive variation of organic and inorganic nature. South African coals are also known to have high inertinite content and low vitrinite content. Inertinite is variable in South Africa. Some inertinite subgroups show characteristics comparable to vitrinite in behaviour, and they are termed semi-reactive inertinite. This shows that coal in South Africa was formed in low ground water level and water-logged environments (Falcon, 1986a).

### **2.2 Geological Occurrence and uses of Coal in South Africa**

This section focuses on South African coal mining areas and their resources. The coal mining sector has become the second largest component of the South African mining sector with annual coal sales higher than gold (SAinfo reporter, 2008). This is due to the

## CHAPTER 2: LITERATURE REVIEW

fact that coal is the primary fuel produced and consumed in South Africa, and is one of the country's largest sources of foreign exchange.

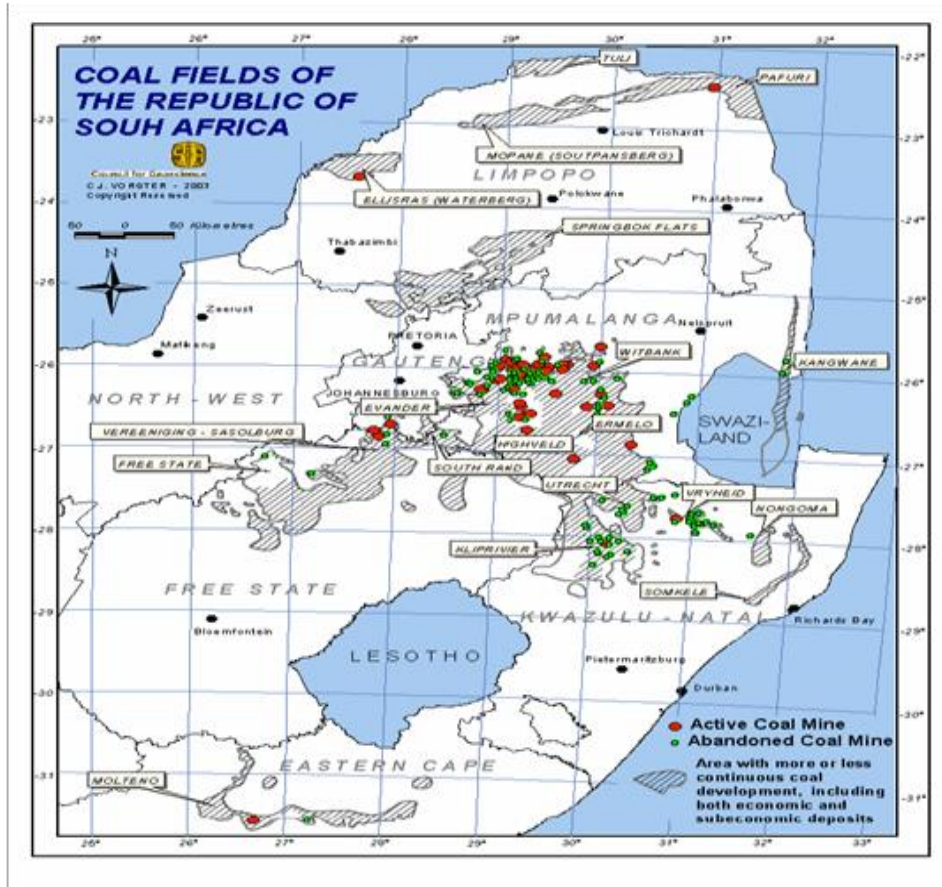


**Figure 2.1:** Occurrence of Coal in South Africa (Schmidt, 2007).

Figure 2.1 shows the main extractable South African coal deposits, starting from the Northern Province down to the Eastern Province. Most coal in South Africa is found in the Mpumalanga province which constitutes to the Highveld, Ermelo and Witbank coal-fields (as shown in Figure 2.1). Geological studies have currently determined that the Witbank coalfield which extends into Botswana is by far the most important source of South African's mined coal. The Waterberg deposits which extend into Botswana, are expected to be the country's principal future coal resource. South Africa has 11 coal fields extended across 19 regions, with 83% of the reserves concentrated in the mining

## CHAPTER 2: LITERATURE REVIEW

---

areas of Witbank, Highveld, Vereeniging/Sasolburg, Ermelo and Waterberg (Schmidt, 2007).

South Africa is known to export its best coal and uses the low-grade coals (high mineral content and low calorific value) in power stations specifically designed to handle them. More than 100 million tons of mined coal in South Africa is used for electricity generation, 40 million tons is used by Sasol for generation of petrochemical products, 15 million tons is used by small consumers, and the metallurgical industries use 5 million tons (Keaton Energy Holdings, 2008).

### **2.2.1 South African Coalfields**

South Africa's coal provinces are divided into distinct coalfields. As mentioned earlier the Waterberg coalfield is expected to be this country's future coal resource and is located on the borders of Botswana. A study conducted by De Jager (1982) on coal reserves and resources allocated 43% of South African coal to the Waterberg.

It is believed that there are 33 billion tons of coal resources, but this coalfield lacks infrastructure and water resources. The 33 billion tons are in 11 zones, which consist of bright coal with inter-bedded shale and dull coal, sandstone and carbonaceous shale. The Waterberg coal reserves constitute 11% of this country's reserves and have more than 40% of this country's coal resources. The Waterberg can become this country's future mining focus if given the right infrastructure and coal markets (Prevost, 2009).



## CHAPTER 2: LITERATURE REVIEW

---

The Soutpansberg Coalfield is situated to the north of the Soutpansberg Mountains in the Limpopo province. Soutpansberg is rich in bright vitrinite-rich coal that is tectonically highly disturbed and intruded by dolerite sills. It has only 258 Mt of reserves. There is one small mine that is currently operating and yields a high grade of coking coal. There will never be large scale mining in this coalfield due to the difficult nature of the deposits (Wilson, 2009).

The Highveld Coalfield has the largest reserves (9.6 billion tons) and hosts the largest colliery (Secunda 41.6 million tons per annum in 2007). Only one of the Highveld coalfield's five coal seams is laterally continuous and economically important. Furthermore, the coal measures tend to be adversely affected by dolerite sills and dykes, that can make mining difficult, and that may have affected the quality of the coal which has low calorific value. This coalfield is rich in low grade bituminous coal that is best suited for synfuels and power generation (Ward, 2009). This coalfield also hosts the world largest coal-to-liquids complex, producing fuels and petrochemicals (Prevost 2009).

Most of South Africa's coal exports emanate from the Witbank Coalfield, mainly from the No. 2 coal seam. The Witbank Coalfield is situated 6 km west of the town of Ogies in the Mpumalanga province extending to KwaZulu Natal. This coalfield has been mined for over a century, and in 40 to 50 years to come this coalfield would be exhausted. This coalfield is the main coal producing area in South Africa. It contains the second largest reserves (8.8 billion tons), and a large number of small blocks of reserves are presently being used by junior miners to establish new mines. The Witbank coalfield has diverse coal characteristics, resulting in a range of potential markets/utilization in power-generation, export, domestic, metallurgical, liquefaction and chemical sectors. The No. 2

## CHAPTER 2: LITERATURE REVIEW

---

seam is the critical source of high yield export quality steam coal, while the No. 5 seam is the source of metallurgical coal for the local steel industry (Jeffrey, 2005)

The Ermelo coalfield contains 4.4 billion tons of reserves. This coalfield is less productive than the Highveld and Witbank coalfields because most of the operating mines have been exhausted. Coal seam thickness and quality decreases from west to east and most of the high quality steam coal is of export quality. The Ermelo coalfield is attractive as the major junction of the export rail lines linking the inland coalfields to Richards Bay is in the town of Ermelo (Keaton Energy Holdings, 2008).

Lastly, the KwaZulu Natal coalfields contain leftover reserves of low quality coal and were once successful anthracite and coking coal mining area. Ten collieries are currently operational – four each in the Klip River and Vryheid collieries, and single operational in each of the Utrecht and Nongoma coalfields. The only colliery that produces bituminous coal is the Welgedacht Colliery. The coalfields in KwaZulu Natal are set to remain South Africa's major source of anthracite, bituminous and high quality metallurgical coal for local industry (Jeffrey, 2005).

### **2.3 Classification of Coal**

Owing to the worldwide occurrence of coal, its great variety, and different potential applications, a great deal of effort has been made over the years into the development of classification systems. The purpose of these classification systems is to group similar features together and to distinguish those that are not similar. Some workers (Van-Krevelen, 1993; Carpenter, 1988) have identified two kinds of classification of coals which serve different purposes: "scientific" and "commercial". Scientific systems deal

## CHAPTER 2: LITERATURE REVIEW

---

with genetic, constitution and basic or fundamental properties of coal. Commercial systems are concerned with aspects such as: market value, utilisation, technological properties, and suitability for particular end uses. The majority of the classification systems of coal comprise both scientific and commercial features, but either of them may be used for classification of any world coal. Coal classification systems are based on two main chemical analyses namely: (i) Ultimate analysis and

(ii) Proximate analysis,

which provide the percentage of the main chemical elements present in coal (carbon, hydrogen, nitrogen, oxygen, total sulphur and chlorine), and the relative amounts of moisture, volatile matter, ash and fixed carbon respectively. A number of technological properties of coal such as the calorific value, fusibility of coal ash, free swelling index and plasticity of coal have also been introduced as second classification parameters to characterise coal in the different fields of utilisation (Menendez, 2007).

The most reliable parameters that are used to classify coal is rank, grade, and type. Rank refers to the degree of maturity undergone by a coal seam, usually in response to time, pressure, and/or temperature. A parameter that is used to define rank is the reflectance of vitrinite, which is measured petrographically under the microscope (Falcon and Falcon, 1987). Grade is defined by means of the dry ash free content of coal. This parameter influences most properties of coal. For example, an increase in ash content results in a decrease of the calorific value, coking capacity, combustion behaviour, char reactivity and many other factors (Falcon, 1986b).

### 2.4 Coal Structure

Coal structural models have been developed by many researchers (Shinn, 1984; Solomon et al., 1988; Serio et al., 1987). These models have been developed to portray the properties and behaviour of coal during the conversion process. These models were developed such that they can be useful in the determination and management of the potential problems that might arise during the coal conversion processes. Generally, research shows that coal has a complex macromolecular structure (as illustrated in Figure 2.2). This complexity evolves from the fact that it is believed that coal is made up of large aromatic ring clusters which are believed to form a primary network structure. These aromatic clusters are linked to each other by bridges and they form part of the secondary network of coal structure. These bridges are formed from a variety of structures, made up of different kinds of bonding (covalent, donor-acceptor or hydrogen bonds, poly-conjugated delocalizing electrons, van der Waals forces etc) (Krichko and Gagarin, 1990). Most of these bridges are believed to be aliphatic in nature, but may contain oxygen and sulfur functionality, depending on the origin of the coal (Spiro and Kosky, 1982). Bridges that contain oxygen as ethers are thought to have relatively weak bond strength. Other bridges are believed to be single bonds between the aromatic clusters, and these are known as bi-aryl linkages.

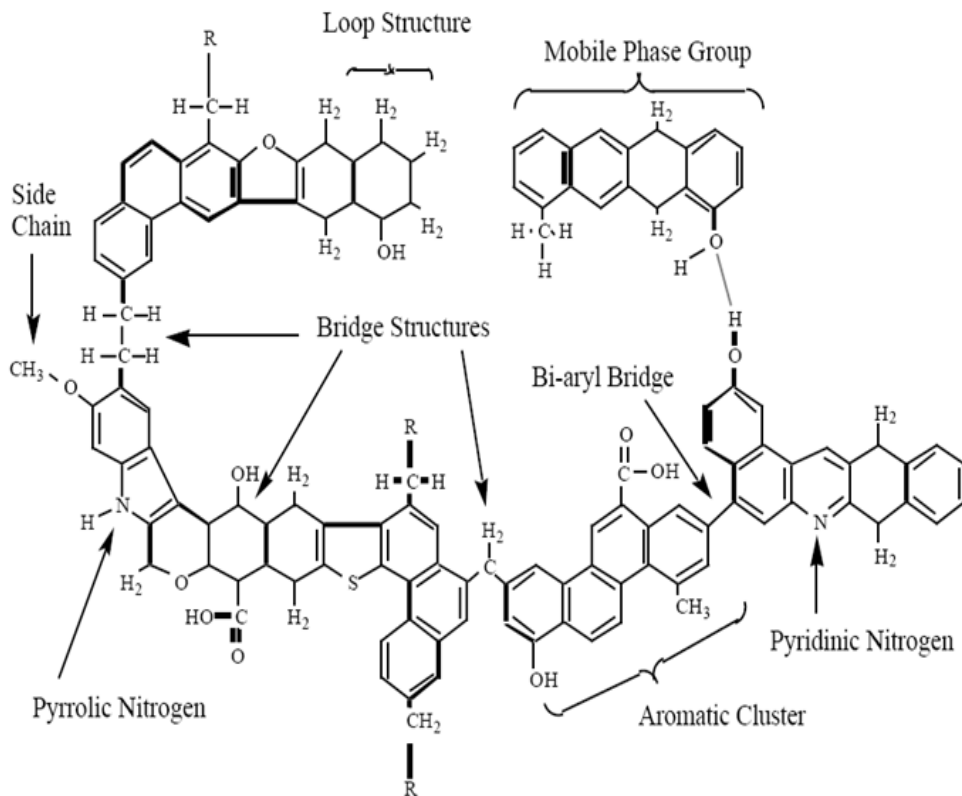


**Figure 2.2:** A hypothetical model of Coal Structure (Solum et al., 1988).

In all, there is large variety of functional groups that make up bridge structures of coal, and the bridge structures largely contribute to bond strength of coal structures (Kidena et al., 2008). Aromatic clusters have attachments that are known as side chains. Side chain structures are mainly composed of aliphatic and carbonyl functional groups. Coal structure is also made up of aromatic clusters that are known as mobile phase. Mobile phase is believed to consist of smaller molecular structures that are not strongly bonded to the coal macromolecule (Marzec and Schulten, 1989; Given et al., 1986). The mobile phase is thought to be either trapped in the molecular structure of coal, or weakly bonded to the coal macromolecule by hydrogen bonds or van der Waals type interactions.

## CHAPTER 2: LITERATURE REVIEW

---

The determination of macromolecular structural properties of coal expands and gives a clear understanding of coal structure. In the following section, analytical methods such as Fourier Transform Infra-Red Spectroscopy, X-ray diffraction,  $^{13}\text{C}$  solid-state Nuclear Magnetic Resonance Spectroscopy and Brunauer-Emmett-Teller (BET) adsorption methods will be reviewed.

### **2.4.1 Analytical methods utilized for the Coal Structural Studies.**

A better understanding of chemical composition and structural characteristics is essential in coal conversion. Understanding how the composition and structural changes influence the burning behavior of coal is important when assessing a coal's potential for utilization. This section will enhance the understanding of coal structure by means of Fourier Transform Infrared Spectroscopy (FTIR), X-ray powder diffractometry (XRD),  $^{13}\text{C}$  Solid State Nuclear Magnetic Resonance ( $^{13}\text{C}$  SSNMR) and Adsorption methods, by reviewing some of the work that has been published by different authors using different coals. The FTIR and  $^{13}\text{C}$  SSNMR only identifies the atomic groupings and inter-atomic linkages at the periphery, while XRD studies provide information about the bulk structure. Adsorption methods are utilized to determine of the gas capacity of coal sample by means of surface area and porosity. A combination of these techniques could be used to determine the whole structure of coal. Little published work has been conducted on South African coals with regard to structural analysis (Van Niekerk et al., 2008).

### 4.2.1.1 Fourier Transform Infrared Spectroscopy (FTIR) studies for Coals

FTIR can be used to characterize functional groups in a particular substance. Cannon and Sutherland (1945) were the first to characterize coal structure with this technique. It was determined that coal contains functional groups such as OH (with hydrogen bonded) and CH (aliphatic and aromatic), C=O (in humic acids) and  $-C-C=C-C-$  of aromatic rings (Cannon and Sutherland, 1945). Some researchers have used this technique to characterize different maceral groups (Fujii et al., 1970; Kuehn et al., 1982; Dyrkacz et al., 1984b). The functional groups that exist in coals were found to vary in their aromatic and aliphatic nature due to their degree of maturation. This analysis is essential in determining the structural changes during coal conversion because it can show which functional groups evaporate as the temperature increases.

Further investigations revealed that coal contains aliphatic CH, CH<sub>2</sub> and CH<sub>3</sub> groups; while on the other hand; aromatic ring systems,  $-C-O-$  or  $C-O-C$  bonds, and associated OH and NH bonds can be detected by this technique. It can also show the presence of C=O groups and isolated C=C bonds (Van Vutch et al., 1955). A typical spectrum that shows the presence of functional groups in coal is illustrated in Figure 2.3.

Cooke et al. (1986) have proved that the aromaticity of coal increases with increasing rank using FTIR. They compared bituminous, sub-bituminous and lignite coals. In the sub-bituminous coal, a weak aromatic hydrogen band at 3040 cm<sup>-1</sup> was observed, while in other coals this band was absent. A strong intensity band at 2930 to 2850 cm<sup>-1</sup> was obtained for the sub-bituminous coals and lignite, whereas for the bituminous coals, this intensity band was weak. This suggests that the ratio of aromatic hydrogen for sub-

## CHAPTER 2: LITERATURE REVIEW

---

bituminous and lignite is higher than that of bituminous coal. Another intensity band at  $1600\text{ cm}^{-1}$  which resembles the presence of hydroxyls or phenols was found to be stronger for sub-bituminous and lignite compared to bituminous coal (Cooke et al., 1986).

A recent study conducted on some South African coals by Van Niekerk et al. (2008) shows that the inertinite rich coals are more aromatic than the vitrinite rich coals, which are more aliphatic. This was evident by a strong aliphatic C-H band (at  $3000$  to  $2800\text{ cm}^{-1}$ ) on the vitrinite rich coal compared to inertinite rich coal (as illustrated on Figure 2.3). A Strong intensity band at  $1450\text{ cm}^{-1}$  due to aliphatic  $\text{CH}_2$  and  $\text{CH}_3$  supports this finding (Van Niekerk et al., 2008).



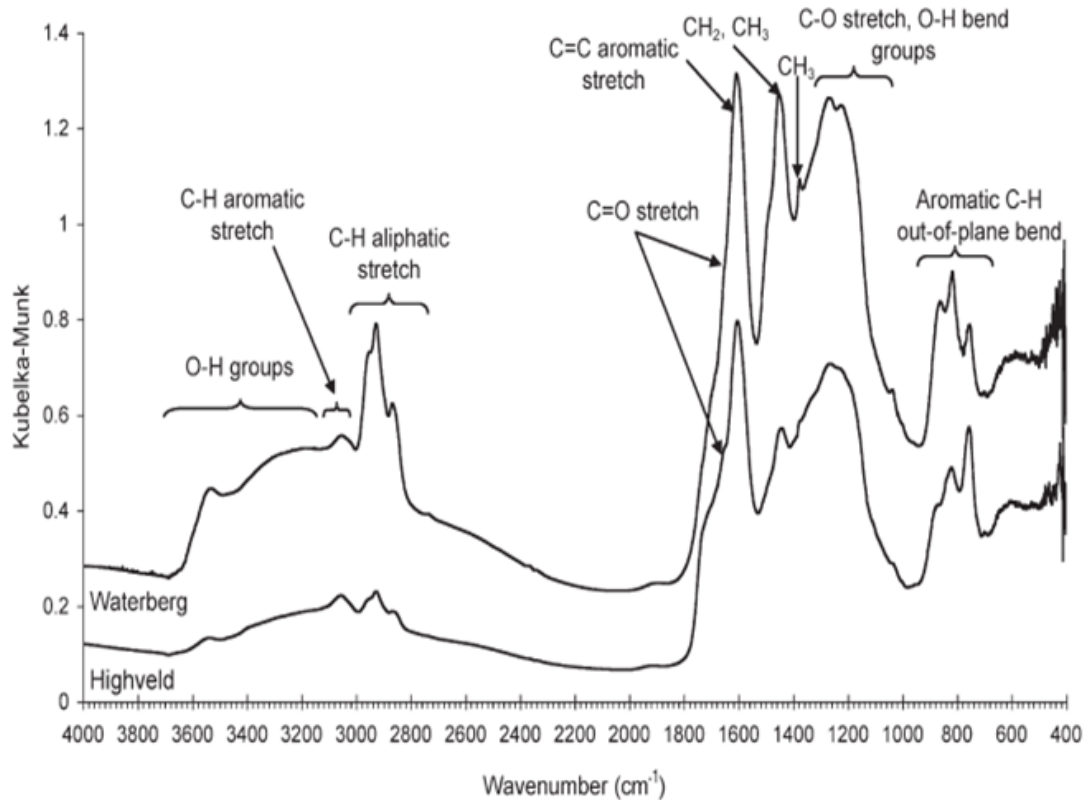


**Figure 2.3:** A typical FTIR spectrum of coal (in this case Highveld (bottom) and Waterberg coals (top)) (Van Niekerk et al., 2008).

Xuguang (2005) has reported on the chemical structure of barkinite, vitrinite, fusinite and sporinite. Compared to other maceral groups, barkinite was found to have strong aliphatic intensity bands ( $\text{CH}_x$ ) at  $3000 - 2800 \text{ cm}^{-1}$ , and less aromatic intensity bands at  $1610 - 1600 \text{ cm}^{-1}$ . The OH intensity bands were found to be weak at  $3600$  to  $3200 \text{ cm}^{-1}$ , and rare C=O at  $1740 - 1700 \text{ cm}^{-1}$  compared to other maceral groups. The aliphatic side chains of barkinite were found to be longer and less branched compared to other maceral groups. In conclusion, barkinite was found to be composed of long chained aliphatic groups, fewer aromatic rings and lesser oxygenates (Xuguang, 2005).

### 4.2.2.1 X-ray powder diffraction studies for Coals

X-rays were discovered by Wilhelm Roentgen in 1895 for medical diagnostic purposes. Following a discovery of the diffraction of X-rays by Max von Laue in 1913, two major fields of materials analysis have been developed. One of them is XRD which involves characterization of materials by means of atomic arrangement in the crystal lattice (Jenkins, 2000). This is a non-destructive and well established technique with good reproducibility. It uses a relatively large amount of sample and collects most of the intensities scattered from the examined sample.

Therefore the properties yielded represent an average for the sample rather than the local properties. XRD analysis of carbonaceous material was first conducted by Warren in 1941. In this work, Warren suggested a structural model, random layer lattices for the non-ideal layer materials like carbon black, and the derived intensity equations for the line profiles of diffraction bands due to these random layer lattices (Warren, 1941; Franklin, 1950).

Coal has a complex structure that is organically rich in carbon material and is also known to be highly disordered. As it is known, coal structure is made up of repeatedly aromatic and aliphatic carbons. The coal structure is determined by the presence of three Miller indices namely: (i) 002, (ii) 110 and (iii) 100. The Miller indices are the reciprocals of the intersection distances in a unit cell. XRD studies use these Miller indices to determine the regular arrangement of atoms in crystals and the symmetry of their arrangement in a unit cell (Atkins and De Paula, 2006).

## CHAPTER 2: LITERATURE REVIEW

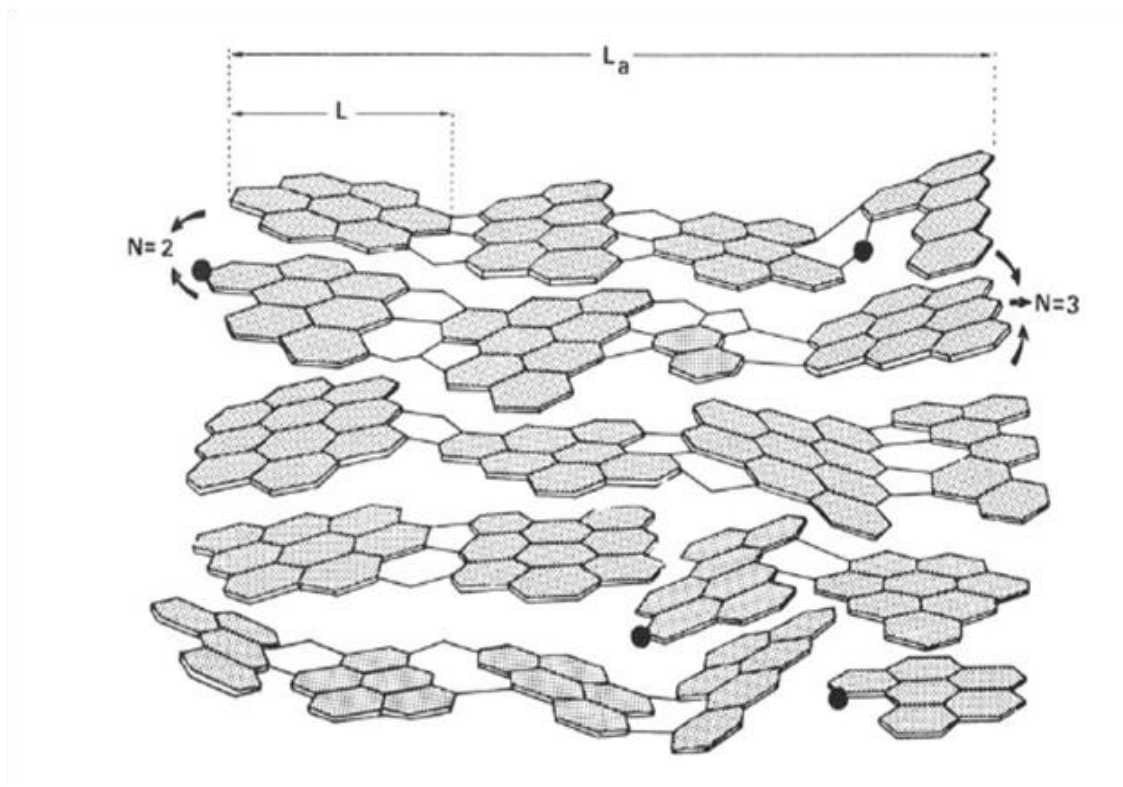
---

Hirsch (1954) studied the carbonization products from various coals. It was determined that coals contain aromatic layers about 20 to 30 Å in diameter, aligned parallel to their near neighbours at distances of about 3.5 Å, thus forming stacks of 14 to 17 Å in height. A special feature of this work was the interpretation of the (002) band (as illustrated in Figure 2.4) which arises from the stacking of planar aromatic ring clusters. An adjacent band at a spacing of 4 to 5 Å was attributed to the presence of aliphatic side chains (Hirsch, 1954; Cartz and Hirsch, 1959).

The ordering of the carbon atoms in the aromatic rings and parallel packing of these ring systems are associated with the maxima indexed (10) and (11), whereas the parallel ordering of the aromatic layers is associated with the (002) and (004) peaks (Lowry, 1963).

The most prominent band in an XRD diffractogram pattern of coal is the (002) band. As mentioned earlier that this band arises from the presence of stacked aromatic clusters (Ergun and Tiensuu, 1959). In some coal analysis, the (002) band has a folder band known as  $\gamma$  band. Nelson (1954) showed that the (002) peak position changes progressively with carbon content. This band also coincides with the peak position corresponding to the inter-layer spacing ( $d_{002}$ ) of graphite (Nelson, 1954).

The degree of ordering, interlayer spacing ( $d_{002}$ ) and crystallite size and its distribution ( $L_a$ ,  $L_c$ ,  $N$ ) can be used to obtain the stacking structure of coal (these parameters are shown in Figure 2.4).



Where  $N$  = number of aromatic crystallite in a unit cell,  $L$  - length of aromatic crystallite,  $L_a$  = average crystallite diameter in a unit cell.

**Figure 2.4:** Where  $N$  = number of aromatic crystallite in a unit cell,  $L$  - length of aromatic crystallite,  $L_a$  = average crystallite diameter in a unit cell.

Another useful parameter proposed by Yen et al. (1961) is the percentage of aromatic carbon atoms in coal (aromaticity). The aromatic nature of coal can be described by three parameters:

- The carbon aromaticity ( $f_a$ ) - this is the fraction of the carbon atoms belonging to aromatic ring systems.
- The hydrogen aromaticity ( $f_a$ ) - the fraction of the hydrogen atoms directly bonded to aromatic C-atoms.
- The average size of aromatic clusters, expressed as the average number of aromatic C-atoms per cluster.

## CHAPTER 2: LITERATURE REVIEW

---

The aromaticity can be distinguished by the use of the  $\gamma$  band next to the (002), and the (002) band. This can be calculated by taking the areas under the  $\pi$ - and  $\gamma$ -peaks which is equal to the number of aromatic atoms and saturated carbon atoms (as illustrated in equation 1) (Yen et al., 1961).

$$f_a = C_{ar}/C_{ar} + C_{al} = A_{002}/A_{002} + A_{\gamma} \quad (1)$$

The XRD studies can only reveal the average size of aromatic clusters. It does so by assuming that the carbon skeleton of coals is made up of a practically regular aromatic ring clusters and completely amorphous matter (Diamond, 1958). The other two parameters of aromaticity can be distinguished by  $^{13}\text{C}$  Solid State NMR.

Recently, extensive work has been done by Wertz et al. (1994, 1998) to quantitatively characterize eight Argonne premium coals. In Wertz's work, a radial distribution function (RDF), obtained from Fourier transform of molecular level scattering was used to examine the molecular level structuring of coals. The RDF is a type of XRD analysis technique that Wertz and his group developed more recently. An extensive study was recently conducted by Lu et al. (2001) where they focused on quantitative analysis of four Australian black coals ranging in rank from semi anthracite to high volatile bituminous coal. The quantitative XRD analysis yielded three structural parameters namely: fraction of amorphous carbon ( $x_a$ ), aromaticity ( $f_a$ ), and crystallite size and its distribution ( $L_a$ ,  $L_c$  and  $d_{002}$ ) respectively. Coal was found to contain a significant amount of highly disordered material, amorphous carbon, which gradually decreases during the coalification process. Coal crystallites were found to be around 6 Å in diameter and the

## CHAPTER 2: LITERATURE REVIEW

---

aromatic layers were piled up by 2 – 4 Å on average, with high rank coal being more condensed in terms of interlayer spacing (Lu et al., 2001).

XRD studies have also been conducted on some Indian coals. The study revealed that coal consists of a semi-crystalline turbostratic structure and has amorphous carbon structures. The  $d_{002}$  value of the Indian coals decreases and  $f_a$  increases with an increase in rank (Maity et al, 2006). Some researchers have used X-ray radial distribution analysis to determine the aryl and alkyl fractions in coal. They also determined the size of poly-cyclic aromatic unit of the Ledo coal. The X-ray scattering results indicated that in Ledo coal there is 74% of aromatic carbons and 26% of aliphatic carbons. The average stacking height of parallel aromatic layers ( $L_c$ ) and the average diameter of the aromatic layers of these coals were estimated to be 7.58 Å and 4.86 Å, respectively (Boruah et al., 2008).

Work conducted by Van Niekerk et al. (2008) on South African coals showed that they are well ordered compared to the American coals tested. In this study, it was claimed that this is due to the fact that South African coals are inertinite rich when compared to American coals (Van Niekerk et al., 2008). Schoening (1983) also did some X-ray studies of South African coal using radial distribution function. This work was based on heat treated coal. Some structural changes were observed after the coal was heated to 500 and 1000 °C in an argon atmosphere. It was observed that the fraction of atoms with graphitic surroundings increased as temperature increases (Schoening, 1983).

### 4.2.3.1 $^{13}\text{C}$ Solid State Nuclear Magnetic Resonance Spectroscopy studies for Coals.

Nuclear Magnetic Resonance (NMR) spectroscopy is a powerful instrument in chemical structure investigations. This instrument utilizes magnetic moment associated with spin of nuclei. It specializes in analyzing the various number of nuclei namely;  $^1\text{H}$ ,  $^{13}\text{C}$ ,  $^{15}\text{N}$ ,  $^{17}\text{O}$ ,  $^{19}\text{F}$ ,  $^{29}\text{Si}$ ,  $^{31}\text{P}$ .  $^{13}\text{C}$  NMR spectroscopy has been used for coal structure analysis since the 1970's, when it was initiated by Retcofsky and Friedel (1973). For all coals studied by Vander Hart et al. (1976), the position of the main peak was near the chemical shift of benzene, which proved the aromatic nature of coal. Since coal structure was thought to be mainly composed of aromatic and aliphatic carbons,  $^{13}\text{C}$  Solid state NMR became a useful technique to study the carbon structure of coal (Vander Hart et al., 1976).

The frequently derived value from  $^{13}\text{C}$  NMR spectra is the ratio  $C_{\text{ar}}/C_{\text{total}}$ , the carbon aromaticity ( $f_{\text{a}} \approx f_{\text{ac}}$ ) (Van Krevelen, 1961). The first "real coal spectra" were obtained in 1976; they appeared to consist of two overlapping resonance bands, representing aromatic and aliphatic carbons (as illustrated in Figure 2.5). The ratio of the surfaces of the two bands led to the first quantitative NMR estimation of carbon aromaticity. Basically four types of carbons can be recognized using this technique in coal analysis namely; poly-condensed aromatic (-C-C=C-C-), simple aromatic (C=C), oxygen bonded aliphatic (C-O), and simple aliphatic carbons ( $\text{CH}_x$ ) (Wemmer et al., 1981). The appearance of these carbons is also illustrated in Figure 2.5.

Various studies have been conducted to determine coal structure using different  $^{13}\text{C}$  solid state NMR spectroscopy techniques (Fletcher et al., 1993; Begon et al., 2003). Cross-polarization (CP), magic angle spinning (MAS) and dipolar dephasing techniques are the

## CHAPTER 2: LITERATURE REVIEW

---

famous techniques that permits direct measurements of the number, and diversity of aromatic and non-aromatic carbons present in a coal sample (Wilson et al., 1984; Vasallo et al., 1987). The studies conducted on structural characterization of coal have shown differences in the nature of coal, meaning the degree of maturation. Most of the NMR data obtained from these studies have been compared by the use of the van Krevelen diagram (axes of atomic O/C and H/C) and the changes of aromaticity with rank increase are illustrated by plotting aromaticity against rank (Maciel et al., 1979; Kalkreuth et al., 1991; Derrepe et al., 1985). Early NMR studies done on various maceral groups showed that in high and medium volatile bituminous coals, aromaticity ( $f_a$ ) decreases in the order of: fusinite > vitrinite > Sporinite > alginite (Zilm et al., 1981; Dyrkacz et al., 1984a).



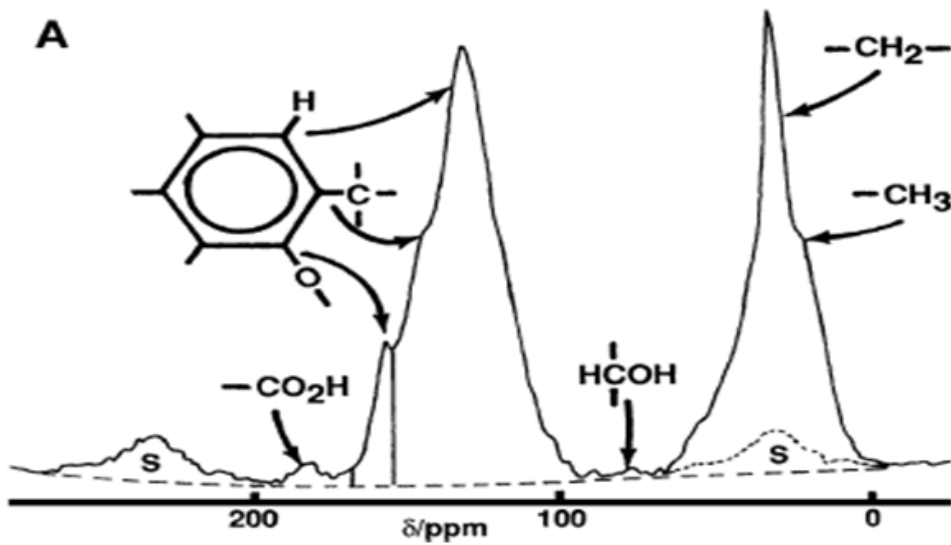


**Figure 2.5:**  $^{13}\text{C}$  NMR of a typical high volatile bituminous coal showing different functional groups that can be distinguished from  $^{13}\text{C}$  NMR spectroscopy (Suggate and Dickson, 2004).

In the mid 80's, Vasallo et al. (1987) studied five Australian coals and their flash pyrolysis products which were measured by  $^{13}\text{C}$  SSNMR. In all cases, the flash pyrolysis products contained the same or more aromatic carbon than the coals. The amount of aliphatic carbon converted to aromatic carbons varied from  $\approx 0 - 32\%$  (Vasallo et al., 1987).

Recent studies have shown that quantitative  $^{13}\text{C}$  SSNMR can reveal more than the aromatic and the aliphatic carbons. This analysis can reveal quantitative analysis on carbons bonded to phenolic groups (-OX), carboxylic groups (-CO<sub>2</sub>H), and alcohols (OH). Suggate and Dickson (2004) have conducted a  $^{13}\text{C}$  SSNMR study on New Zealand coals ranging from peat to semi-anthracite. The NMR spectra showed differences related to coal type and rank. Four NMR parameters were examined;  $-f_a$ ,  $S_{\text{OX}}$ ,  $f_{\text{CO}_2\text{H}}$  and  $f_{\text{OH}}$  (as shown in Figure 2.5). This study revealed that oxygenated functional groups to be ab-

## CHAPTER 2: LITERATURE REVIEW

---

undant, both within the peat and as the peat changes to the lowest rank lignite. It was also observed that as the rank increases, both  $f_{CO_2H}$  and  $f_{COH}$  progressively decline but neither  $f_a$  nor  $S_{Ox}$  shows a uniform change (Suggate and Dickson, 2004).

### 4.2.4.1 Brunauer-Emmett-Teller (BET) Adsorption studies for Coals

The word adsorption denotes the ability of gases to condensate on free solid surfaces. These free surfaces are made up of internal (also referred to as pore surface) and external surface and pore structure. In any surface of a solid structure, there are nearly always cracks and fissures present, some of which may penetrate very deeply and which contribute to the internal surface. On the other hand, there are superficial cracks and indentations which contribute towards the external surface (Gregg and Sing, 1967). Coal being a colloidal solid possesses certain porosity at any rank. It is due to this porosity that it has a capacity to adsorb gases and vapours (Van Krevelen, 1961). The pore system of any solid may vary greatly both in size and shape. Dubinin proposed a feature of special interest which can be used for many purposes, the pore width. A pore width is the diameter of a cylindrical pore, or the distance between the sides of the slit-shaped pore. Dubinin further classified the pores according to their average size widths. Pores of width below 20 Å are described as micropores, those pores with widths above 200 Å as macropores, and those pores in between the above mentioned classes are not regarded as purely arbitrary (Dubinin, 1960).

As mentioned, coals are highly porous materials with most of their surface areas enclosed in pores of molecular dimensions. Coal porosity and surface areas plays a vital role in coal utilization (Mahajan, 1991). Surface areas can be calculated from three ad-

## CHAPTER 2: LITERATURE REVIEW

---

sorption theories namely; BET, Langmuir and Dubinin-Polanyi. The BET surface area determination uses the amounts adsorbed between relative pressures of 0.02 to 0.35 and the Dubinin-Polanyi uses the amounts adsorbed between relative pressures of  $10^{-5}$  to 0.2. Comparisons of surface areas calculated from the three theories shows the Langmuir values to be greater relative to other theories. Langmuir theory requires all adsorbate to be distributed in mono-layers and as a result, would predict a larger surface area (Debelek and Schrodt, 1979a). The BET and Dubinin-Polanyi surface areas closely agree with each other and are a better explanation of adsorption process in coals. Since in fine pore structures adsorbate will condense to fill the pores rather than adsorb in layers (Marsh and Rand, 1970).

Coal surface areas can be measured by  $N_2$  and  $CO_2$  adsorption methods. The adsorption of  $N_2$  on coals at  $-196\text{ }^\circ\text{C}$  involves activated diffusion into the internal pore structure. Due to this activated diffusion, it was then decided and accepted that  $N_2$  adsorption at  $-196\text{ }^\circ\text{C}$  does not measure the total surface area of coals. Due to this limitation, it was decided that coal surface areas should be measured by adsorption gases that have small molecular sizes and high critical temperature.  $CO_2$  met these requirements and Marsh and Siemieniowska successfully used Dubinin-Polanyi equation to measure the surface area of microporous carbons from  $CO_2$  data.

### **2.5 Coal petrography**

Petrology is a study of rocks. Coal petrology is concerned with a microscopic description of coal aspects such as: the type of rock associations found in coal and the rock composition of coal (Stach et al., 1982). This information provides the physical foundations of the formation of coal. Petrographic microscopic examination is carried out in reflected

## CHAPTER 2: LITERATURE REVIEW

---

light. There are quite a few reasons that lead to the emphasis given to the microscopy in reflected light:

- The coal rank can only be determined with the necessary accuracy by measuring the reflectance of vitrinite on polished surfaces.
- Quantitative maceral analysis cannot be carried out on thin sections because the proportion of the not so easily visible inertinite is over-estimated, especially if the sample contains more inertodetrinite (Stach et al., 1982).

Usually the microscope is comprised of an immersion objective of magnification between  $\times 25$  and  $\times 60$  and an eyepiece of  $\times 8$  and  $\times 12$ . The eyepiece includes a fine crossline (cross hair) and a 20 crossline graticule. The fine crossline or cross hair is designed for point count analysis such as maceral analysis (ISO 7404/3, 1998). The 20 crossline graticule has an effective distance between extreme intersections in the  $x$  and a  $y$  direction respectively is  $50\mu\text{m}$ . this graticule is design for microlithotype analysis (ISO 7404/4, 1985). The microscope consist of a mechanical stage which is capable of advancing the specimen laterally by equal steps of such length that only a insignificant small proportion of the particles examined receives more than one count on the same particle. The counter of the microscope is capable of registering the counts in each category and the grand total of the petrographic components. After the completion of the analysis the results obtained are recorded as volumetric percentages.

Coal petrography on the other hand deals with a study, identification and characterization of organic and inorganic constituents of coal, and the degree of metamorphosis to which they have been subjected to their time of burial. Its main goal is to look backward

## CHAPTER 2: LITERATURE REVIEW

---

and attempt to understand fully how coal was formed. Petrography is of great importance as it is known that the different petrographic constituents of coal may behave differently under various processing conditions (Hessley et al., 1985).

There are three petrographic components of coal, namely;

- Macerals,
- Microlithotypes and
- Mineral matter

Figure 2.6 shows that maceral; microlithotype and reflectance analysis is done differently from each other. Figure demonstrates that with the maceral analysis, a point count analysis is conducted where the cross hair is seen. On the other hand, with the microlithotype analysis, a 50 $\mu$ m field of view area is of great importance because this is where the analysis is conducted.

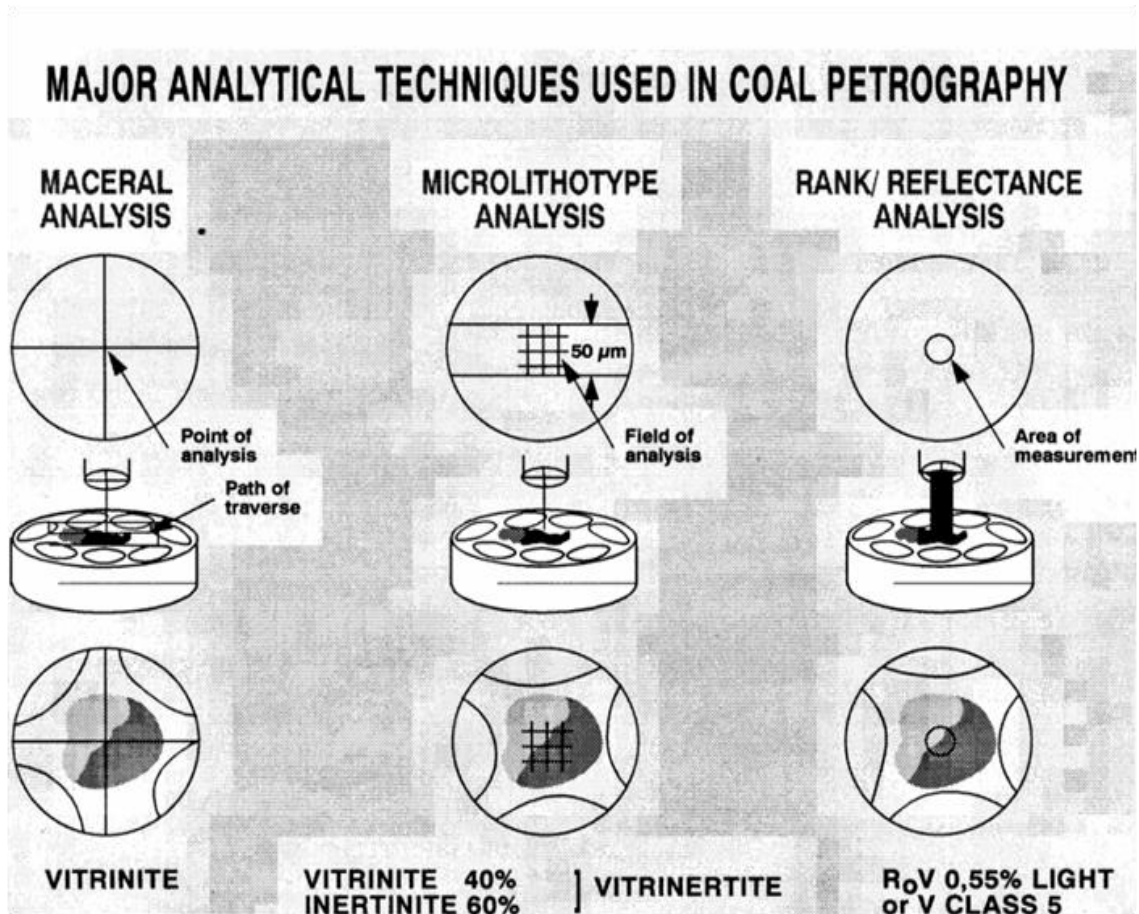


**Figure 2.6:** Three analytical techniques used in Coal Petrography (Falcon and Snyman, 1986).

When conducting reflectance analysis of coal, one is able to follow the historic structural reflectance of coal. The structure of carbon rich materials can vary from disordered isotropic optical texture to a well ordered graphitic-like texture. These transformations can be followed by the measurement of anisotropy. Optical microscopy uses light. Petrographic microscopes are the most advanced but the resolution is limited by photons. Hence Scanning Electron Microscopy (SEM) and other optical electron microscopy use electrons as the light source and have high resolution. Optical microscopy has less resolution but it has the possibility to account for sample heterogeneity which is very difficult to get with other microscopy techniques (Menendez and Borrego, 2007).

### 2.5.1 Macerals

Macerals are one of the three petrographic components of coal. Stopes considered macerals as distinct organic entities as analogous to rock minerals (Stopes, 1935). The word macerals is derived from a Latin verb 'macerate'; which means 'to soften', and it was Stopes (1935) who first used the term 'macerals' for the constituent of coal isolated by maceration (ICCP, 1971). Macerals originated from woody, plant material, cortical and vegetable tissues (Van Krevelen and Schuyer, 1957). Each maceral can be microscopically distinguished by its specific physical appearance and chemical properties. Each maceral type varies in composition, morphology, structure and reflectance. There are three macerals groups, namely;

(i) Liptinite

(ii) Vitrinite and

(iii) Inertinite

These maceral groups are either reactive or non reactive (as shown in Table 2.1) and differ in carbon to hydrogen ratios. The reactive macerals have lower carbon to hydrogen ratio than the non reactive macerals. They also tend to react very quickly when heated at high temperatures in a closed retort (De Jager, 1976). The most common maceral group in South African run of mine (ROM) coal is inertinite, with moderate to low amounts of vitrinite and lesser liptinite. South African coal is largely beneficiated to increase the vitrinite content and decrease the ash content for export purposes.

## CHAPTER 2: LITERATURE REVIEW

**Table 2.1:** Table of reactive and non-reactive macerals and their groups (Falcon and Snyman, 1986).

Maceral Sub-group		Maceral group name
Reactive	Sporinite, Cutinite, Resinite Alginite	Liptinite
	Collinite Tellinite	Vitrinite
	Reactive-Semifusinite	Inertinite
Non-Reactive	Inert Semi-fusinite Fusinite Macrinite Scleronite Micrinite Inertodetrinite	Inertinite

### 5.2.1.1 Liptinite

Stopes, (1935) introduced the term *exinite* (which is now known as liptinite) to describe the microscopic constituent of coal, rich in volatiles, and relatively rich in hydrogen. Liptinites are considered to be produced from decayed leaf matter, spores, pollen and algal matter. This maceral group tends to retain its original plant form (Stopes, 1935). This maceral group is usually less in coal when compared to vitrinite and inertinite. Liptinite is comprised of the maceral subgroups of sporinite, cutinite, suberinite, resinite, alginate and liptodetrinite (Stach et al., 1982).



### 5.2.2.1 Vitrinite

Vitrinite is derived from cell wall materials and cell fillings of the woody tissue of plants. Vitrinite is typically shiny and glass-like in appearance. Under transmitted light it is clear and of a light or dark orange colour, whereas under reflected light it is grey to yellowish white, depending on the coal rank (ICCP, 1998). In bituminous coals, the vitrinitic macerals show fissures and appear medium grey in reflected light under oil immersion lens (ICCP, 1971). Subdivision of vitrinite is based on botanical features and the degree of post-depositional alteration (Bend et al., 1992). The subgroups are: tellinite, collinite and pseudovitrinite (Stach et al., 1982).

The reflectance of vitrinite is intermediate compared with the other maceral groups and provides an excellent indication of the coal rank since it increases as coalification advances. Accordingly, the measurement of the vitrinite reflectance on a polished coal surface has been selected as the parameter to determine the rank of a coal. Vitrinite within low rank coals exhibit a marked variation in reflectance, although such variation diminishes with increasing rank (Melendez, 2001).

### 5.2.3.1 Inertinite

The term inertinite was chosen to describe the infusible nature of certain highly reflecting macerals during carbonization (Stach et al., 1982). This term was proposed to simplify the nomenclature of coal petrography by combining, in a single term, the macerals such as fusinite, semifusinite, inertodetrinite, scleronite, funginite, secretinite, macrinite and micrinite. This grouping is based on similarities in the optical and technological

## CHAPTER 2: LITERATURE REVIEW

---

properties under the microscope. The term inertinite implies that the constituents are more inert than the other maceral groups (vitrinite and liptinite).

Inertinite comprises a group of macerals derived from plant remains similar to vitrinite. However, oxygen has usually played a stronger role during the first stage of deposition and has been incorporated into the macerals. Depending upon the extent of the oxidation process (as discussed in section 2.1), part of the cell structure of the woody material may appear to be preserved retaining the original well-defined plant tissue structures, whilst in others they are not clearly perceived (Menendez and Borrego, 2007).

Compared with the other macerals, inertinite has the highest carbon and oxygen content, is the densest, and is the least volatile with lowest H/C ratio (Stach et al., 1982; Van Krevelen, 1993.). Generally, inertinite has a higher reflectance than that of vitrinite, although the differences become less evident with increasing rank (International Committee for Coal and Organic Petrology (ICCP, 2001). Inertinite is common in most coals especially in South Africa, although some coals may be poor in inertinite (Goodarzi, 1985.). Fusinite is always the highest reflecting inertinite maceral and is distinguished by cell-texture. It is normally broken into small shards and fragments. Semifusinite has the largest range of reflectance among the coal macerals going from the upper end of the vitrinite range to fusinite. Semifusinite is normally the most abundant of the inertinite submacerals. Inertodetrinite is a mixture of reactive semifusinite and non reactive semifusinite in discrete broken small fragments that vary in shape (ICCP, 2001).

### 2.5.2 Microlithotypes

Microlithotypes can be regarded as genetic units that occur in relatively large units if:

- the nature and quantitative distribution of their macerals, maceral types and maceral varieties,
- the type and quantity of mineral inclusion, and
- the texture (microlayering) are also considered (Stach et al, 1992).

In a simpler way, microlithotypes are known to be associations of macerals within coal, their names terminating with the suffix -ite (Bend et al., 1992). Microlithotypes are determined by assessing the proportion of maceral association present within a specified minimum area (50 $\mu$ m) using a 20 point graticule.

The triangle in Figure 2.7 represents the terminology and specific criteria for microlithotype classification according to the proportion of the three maceral groups. Each apex of the triangular plot represents a volumetric proportion of 0 to 100% of a given maceral group. Trimacerites contain equivalent content of maceral groups in a 50 $\mu$ m area. Bimacerals contain 50% of each maceral group in a 50 $\mu$ m area, whereas unimacerals contain 95% of one maceral group, and the other 5% will be the other maceral group. The central region within the triangular region represents trimacerites, formed from association of three maceral groups, whereas those classes around the perimeter indicate bimaceral or unimaceral associations (Lester et al., 2003).

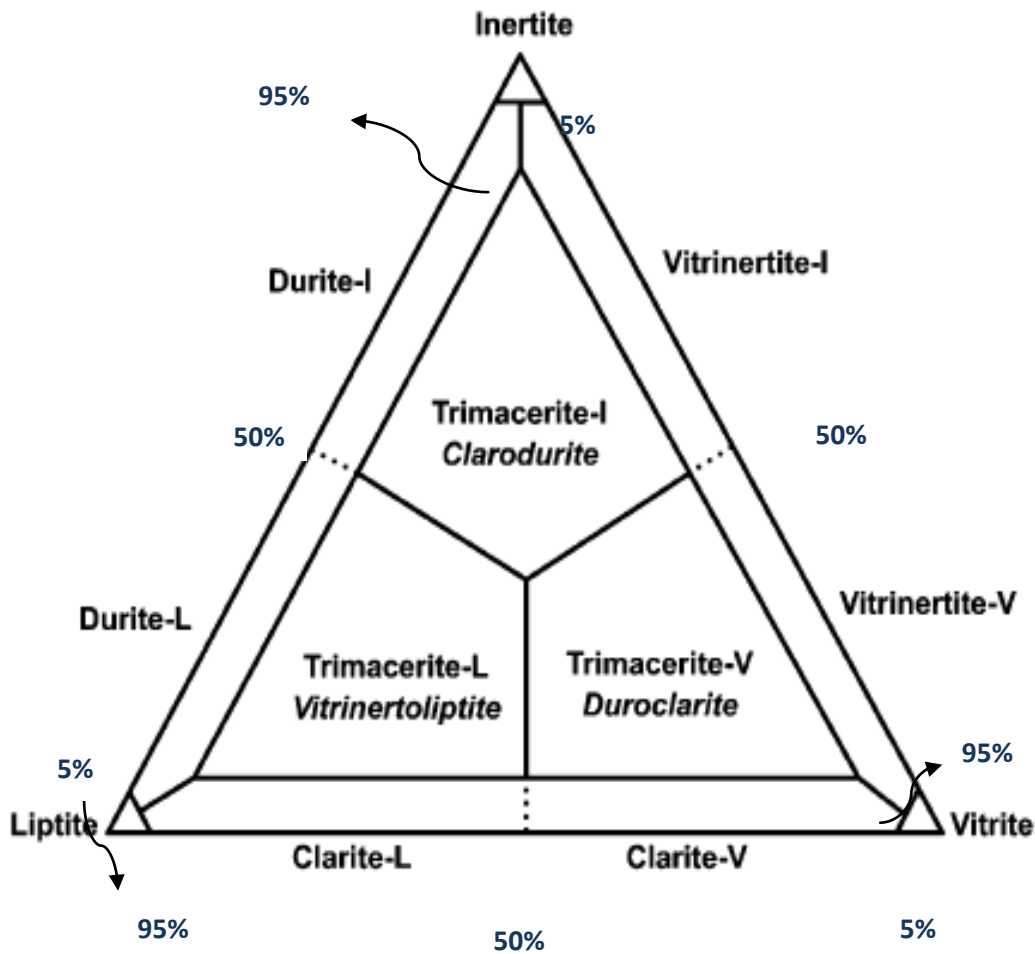


**Figure 2.7:** Trigonal diagram showing microlithotype classification system across three maceral groups (Lester et al., 2003).

Microlithotype analysis can be more useful than maceral analysis in the technological application field (Bunt et al., 2009). This classification system does not only identify maceral composition, it also classifies the associations of different maceral groups within each particle.

### 2.5.3 Mineral Matter

Mineral matter is the inorganic constituent which is intimately bound within coal. Minerals can be classified according to their origin, either as syngenetic or epigenetic. Syngenetic minerals are those that were introduced into the peat during the biochemical stage. Epigenetic minerals are those that were introduced into the coal during the maturing process following the biochemical change (Lowry, 1963). Gumz et al. (1958) reported that carbonate, sulphide and quartz minerals may be from both origins, whereas clay minerals are of syngenetic origin and the salt minerals of epigenetic origin.

South African coals are very rich in mineral matter (15 - 35%). This makes South African coal to be of low grade (Blauvelt, 2008).

### 2.6 Coal Conversion

Coal can be converted to various organic gases and liquids. When coal is heated, it undergoes physical and chemical changes. These changes are important in both the science and technology of coal utilization. Generally, the coal conversion process occurs as a two stage process. The initial stage is the thermal decomposition of coal (pyrolysis), which consists of a sudden release of volatiles (devolatilization) accompanied by drastic changes in morphology and molecular structure of the remaining solid to form char. The char particle formed can depend on: the maceral and microlithotypes present, the rank of the coal, the particle size (physical properties), and the temperature of char formation (Bailey et al., 1990; Solomon et al., 1988). Pyrolysis is very important in the coal conversion process since analysis of pyrolysis products gives some important clues as to the structure of the parent coal (Solomon and Beer, 1987).

## CHAPTER 2: LITERATURE REVIEW

---

The char structure is formed during the initial stage of devolatilization, where the pore openings of the softening coal will become blocked due to the high fluidity contributed by the softening coal. Due to this blockage, the volatile matter will be trapped in this fluid to form bubbles. When a large number of bubbles exist in the coal fluid, they will overcome the force balance and burst to release volatile matter. Then the release of volatile matter and the ultimate char structure will be determined more so by the bubble's behavior than the original pore structure of the feed coal (Yu et al., 2007). Thus, the devolatilization process and combustion of volatiles has an influence on the physical structure of char.

The char structure is highly heterogeneous and usually affects the char combustion reactions and ash formation (Sadhukhan et al., 2009). The diffusion of oxygen to and within the char particle influences the rate of char burning, and therefore the char morphology becomes important (Alonso et al., 1999; Alexander and Sommer, 1956). Also the complexity of the char formed lies in the heterogeneity of the structure within the individual particles, and between different particles. The chemistry of char is strongly dependent on the raw coal properties, and a char structure depends on heating conditions such as temperature, heating rate and pressure (Everson et al., 2006; Chunhua et al., 2001).

Optical microscopy (Coal Petrography) is a tool to determine the structural transformation of coal during coal conversion. There are many char morphology classifications that have been brought forward in the coal research field. Many research workers have created these classification systems according to their particular needs. Some of them have classified these char morphologies using qualitative differences such as isotropy

## CHAPTER 2: LITERATURE REVIEW

---

and anisotropy (Bailey et al., 1990), high and low reflectance, inclusion of minerals (Crelling, 1992; Bailey et al., 1990) and density of the network. In these classification systems the char types seems to be the same but the terminology varies (Crelling, 1992; Bailey et al., 1990; Shibaoka et al., 1985; Oka et al., 1987; Jones et al., 1985).

**Table 2.2:** Char Morphology Classification (Bailey et al., 1990).

Particle name	Shape	Pore Volume	Char Origin
Tenuisphere	<b>Spheroidal</b>	<b>&gt;80%</b>	<b>Vitrite, Clarite</b>
Crassisphere	<b>Spheroidal</b>	<b>60-90%</b>	<b>Vitrinertite-V, Duroclirite, Clarodurite</b>
Tenuinetwork	<b>Spheroidal, irregular or elongated</b>	<b>60-95%</b>	<b>Vitrite, Clarite</b>
Mesosphere Fragment	<b>As above Particle or group of particles &lt;10µm</b>	<b>40-60%</b>	<b>Vitrinertite-I Vitrite, Clarite</b>
Inertoid	<b>Subspheroidal, rectangular</b>	<b>5-40%</b>	<b>Durite, Inertite</b>
Solid	<b>Rectangular to irregular</b>	<b>&lt;5%</b>	<b>Durite, Inertite</b>
Fusinoid	<b>Irregular</b>	<b>&lt;5%</b>	<b>Durite, Inertite</b>
Mixed porous	<b>Spheroidal to irregular</b>	<b>&gt;50%</b>	<b>Vitrinertite-I, Duroclirite, Clarodurite</b>
Mixed Dense	<b>Rectangular to irregular</b>	<b>&lt;50%</b>	<b>Durite, Inertite</b>
Mineroid	<b>Spheroidal</b>	<b>-</b>	<b>&gt;50% Minerals</b>

Bailey et al. (1990) have used petrography to quantify and classify 11 different chars from inertinite rich pulverized coals (as illustrated in Table 2.2). They based their classification system on the physical and optical characteristics known to influence the burning behaviour of pulverized coal, the pore size and distribution, wall thickness and anisotropy. Their classification was actually describing the particle morphotypes that relate to different maceral types (Bailey et al., 1990).

## CHAPTER 2: LITERATURE REVIEW

---

There is less detailed published work that has been conducted on chars produced from inertinite rich lump coals. Lump coals are utilized in coal conversion processes for the production of synfuels and other petrochemical products. Bunt et al. (2009) have conducted a study on carbon particle type characterization of lump coal carbon behaviour impacting on a commercial scale Sasol® FBDB (™) gasifier. In their studies they have included microlithotype group analysis, devolatilized coal analysis, and considered the variety of chars formed. They determined that by using the microlithotype analysis in lump coals, vitrinite bands tended to devolatilize quicker, showing an equal degree of porosity when compared to the inertinite band, followed by reactive inertinites (Bunt et al., 2009). Wagner et al. (2008) noted that the swelling of a particle depends on the degree of heating, pressure, particle size and organic and inorganic interactions between and within the particles.

Microlithotypes consisting of reactive macerals (vitrinites and liptinites) are generally more able to form porous chars with large surface areas when compared to microlithotypes that consist of inert macerals (inertinites), which form closed chars with high density and low porosity (Oka et al., 1987; Bengtsson, 1987; Gupta, 2005). An increase in porosity of char is a result of higher vitrite content in coal char (Falcon and Sandman, 1986). Vitrite in larger inertinite fragments tend not to react so quickly because the vitrinite band is restricted from heat by the inertite bodies. Some inertite forms can be more reactive than vitrite, depending on rank, maceral type and degree of oxidation.



## CHAPTER 2: LITERATURE REVIEW

---

### Summary of Literature Review

This chapter revealed an in depth information on how Gondwana coal were formed. This chapter revealed that these coals were formed in cold periglacial tundra conditions in the in inland regions of Gondwanaland. This is reason why these coals are inertinite-rich (Falcon, 1986a). It was revealed that South Africa has 11 coalfields extended across 19 regions. Coal classification was reviewed in terms of ultimate and proximate analysis as the chemical methods that are widely used for coal classification. This chapter also reflected at the structure of coal proposed by Solum et al., (1988). Several methods such as FTIR, X-ray diffraction, <sup>13</sup>C Solid State NMR and adsorption methods were reviewed as analytical methods that have been utilized to determine the structure of coal. Coal petrography was introduced as an analytical tool that deals with a study, identification and characterization of organic and inorganic constituents of coal, and the degree of metamorphosis to which they have been subjected to their time of burial. The use of coal petrography in coal conversion processes and the char analysis were also reviewed.

### CHAPTER 3

#### 3 EXPERIMENTAL METHOD

This chapter will discuss the origin of the feed coal samples, the description of the packed-bed pilot scale combustion reactor, and how the chars were formed using this reactor. The methods used to analyze the parent coals and the packed-bed reactor samples are presented.

##### 3.1 Origin of the feed coal samples

Two feed coal samples, namely: (i) Coal A and (ii) Coal B were utilized during the course of this research. These coal samples originated from the Highveld coalfield, and were supplied by Sasol Research and Development (R & D). Sample preparation such as sampling screening was conducted at Sasol R & D laboratories in Sasolburg. Coal char samples were prepared from these feed coal samples using a pilot scale combustor unit known as the packed-bed reactor. There was limited control of sample generation since it was conducted by technicians at Sasol Research and Development (R & D).

##### 3.2 Char Preparation

The preparation of chars was conducted at Sasol R & D. Each feed coal sample was used in a fractional size of - 75mm +5mm (hence lump coals as no fine material included). Following combustion, seven equal size samples were collected from the top to the bottom of the packed-bed reactor. The top of the reactor is labelled sample 1, and the bottom of the reactor (the ash bed) is labelled sample 7 (as illustrated in Figure 3.1). Thus a

---

## CHAPTER 3: EXPERIMENTAL METHOD

---

total of 14 samples were collected from the packed-bed reactor combustor unit from both Coal A and B.



**Figure 3.1:** A photograph showing the bed profile of the packed-bed reactor combustor unit (left =top of reactor, right = bottom of reactor).

### 3.2.1 Description of Pilot scale Packed-bed reactor

The packed-bed reactor consists of a lined steel jacket with an outside diameter (OD) of 0.8 m and an inside diameter (ID) of 0.4 m, and is 3 m in length. The material specification of the refractory lining is high strength, abrasive resistant alumina lining with maximum operating temperature of 1700 °C. The reactor is designed to burn coal particles in an air atmosphere at atmospheric pressure, and reaction temperature is controlled with nitrogen. The reactor is equipped with thermocouples for temperature measurements, pressure transmitters for pressure measurements, and rota meters to control the air and nitrogen flow to the reactor (as illustrated in Figure3.1).

## CHAPTER 3: EXPERIMENTAL METHOD

---

The required amount of coal was homogenized and loaded using buckets into the pipe reactor to minimise segregation of the packed coal bed. The packed coal bed was heated with a gas burner to get the coal to a temperature where it will burn in an air atmosphere. After an hour the gas burner was turned off and the air flow was introduced to allow the coal to ignite. Upon reaching a bottom temperature of 600 °C, the air flow was increased to flow until the required temperature of 1250 °C was reached.

The bed temperature was controlled by adjusting the air and nitrogen flow through the bed. The ash bed temperature was controlled at 1250 °C (maximum) and the temperature, pressure and flow to the reactor were logged with a Delta V data logging system. The reactor was left to burn for approximately 18 hours before it was cooled down with nitrogen to 25 °C.

After cooling, the reactor was tilted onto its side and opened up like a coffin to allow visual inspection and sample taking of the bed profile (as illustrated in Figure 3.1). Seven equal sized fractions were dissected from the entire bed (as illustrated in Figure 3.1) and represent the samples that will be discussed in this thesis. The ash bed included the material below the flame front in the combustion zone.

### 3.3 Sample Analysis

The feed lump coals and the packed-bed reactor samples were analyzed using standard techniques such as proximate and coal char CO<sub>2</sub> reactivity analysis (TGA method). Chemical and physical structural analysis of coal samples was determined by Fourier Transform Infrared Spectroscopy (FTIR), BET adsorption analysis, X-ray diffraction, and <sup>13</sup>C Solid State Nuclear Magnetic Resonance Spectroscopy (<sup>13</sup>C SSNMR). The determina-

tion of structural analysis was conducted on demineralized parent coals and their subsequent packed-bed reactor generated samples. The demineralization was conducted to reduce mineral matter interference when determining the coal structural properties. Coal petrography was performed to determine the maceral content of the feed lump coal samples, and carbon particle type was performed on the packed-bed reactor generated samples.

### **3.4 Phase 1: Chemical Analysis**

#### **3.4.1 Proximate Analysis**

Proximate analysis was conducted to determine the amount of moisture, volatile matter, fixed carbon and ash in the lump coal samples and packed-bed reactor generated samples. This analysis was conducted at the Sasol R&D laboratories.

The analysis was performed following standard methods to measure the percentage of moisture (SABS 924, 1978), ash content (ISO 1171, 1997) and volatile matter. The difference between these three percentages and the mass of the original sample (100 %) is referred to as fixed carbon. To calculate the surface moisture, the percentage mass loss between the initial sample mass and the stable mass at 110 °C is measured. This can be reported as mass percent or mass.

#### **3.4.2 Coal char CO<sub>2</sub> reactivity**

There is no internationally accepted method of determining the reactivity of a given coal char sample. This analysis was conducted at Sasol Technology Research and Develop-

## CHAPTER 3: EXPERIMENTAL METHOD

---

ment using their method. This method determines the rate of mass loss using a thermogravimetric analyser (TGA).

### **3.5 Phase 2: Physical Structural analysis**

Due to high ash content of these coal and packed-bed reactor generated samples, demineralization was conducted to reduce the amount of ash in these samples.

#### **3.5.1 Demineralization**

The removal of mineral matter in the coal samples was conducted following a paper written by Schoening (1983). 150 ml of 5M HCl was added to 25 g of coal and the acid mixture was heated at 60 °C in a water bath for an hour before the mixture was filtered using a Buchner funnel and washed with 200 ml of distilled water and filtered again. The solid coal sample was heated again in 150 ml of 40 % HF for an hour at 60 °C then the acid coal mixture was filtered using Buchner funnel and washed with 200 ml of distilled water and the wet coal was allowed to dry under atmospheric temperature. After drying, the coal samples were weighed and TGA analysis was conducted to determine the amount of ash left in the samples.

#### **3.5.2 Fourier Transform Infrared Spectroscopy (FTIR) analysis**

FTIR studies were conducted to determine the functional groups present in the parent coal samples and packed-bed reactor generated samples. The analysis was conducted using a Bruker Tensor 27 with a diamond crystal located at the University of the Wit-

## CHAPTER 3: EXPERIMENTAL METHOD

---

watersrand in the School of Chemistry. The analysis was conducted at wavenumbers of 4000  $\text{cm}^{-1}$  to 600  $\text{cm}^{-1}$ .

### 3.5.3 BET Adsorption Analysis

BET adsorption analysis was conducted to obtain information regarding the structural properties such as pore size and surface area of the feed coal samples and the packed-bed reactor derived samples. The analyses were conducted at the North West University, Chemical Engineering laboratories. A Micrometrics ASAP 2010 Analyzer was used to perform the analysis (as illustrated in Figure 3.2). Both carbon dioxide and nitrogen were used as adsorbent gases in the analyzer.

The coal samples were degassed at 25  $^{\circ}\text{C}$  for a period of 48 hours. After degassing, the coal was analyzed by means of gas adsorption to determine the specific surface area, pore volume and pore diameter of the given coal samples and the packed-bed reactor samples. The saturation pressure used in the adsorption experiments was 660 mm Hg. Table 3.1 gives a summary of the experimental conditions used in the gas adsorption experiments.

**Table 3.1:** Gas adsorption experimental conditions.

$T_{\text{degas}}$ ( $^{\circ}\text{C}$ )	$P_{\text{final}}$ ( $\mu\text{m Hg}$ )	Coal sample	Analysis gas	$T_{\text{analysis}}$ ( $^{\circ}\text{C}$ )	Cooling medium
25	< 4	Raw coal	$\text{CO}_2$	0	Ice water
25	< 4	Raw coal	$\text{N}_2$	-197	Liquid $\text{N}_2$

( $T_{\text{degas}}$ : Degassing temperature,  $P_{\text{final}}$ : Final degassing pressure,  $T_{\text{analysis}}$ : Analysis temperature.)



**Figure 3.2:** Micrometrics ASAP 2010 analyzer.



### 3.5.4 X-ray diffraction analysis

X-ray diffraction (XRD) studies were conducted to determine the physical structure of the coal samples such as size distribution of the aromatic ring systems, average diameter of the aromatic lamellae, average thickness of the aromatic lamellae, and the aromaticity of the coals. This analysis was also conducted on the parent coals and the packed-bed reactor samples in order to determine the changes occurring on the above mentioned XRD parameters with regard to heat effect on the coal samples. The experimental method utilized followed that of Hirsch (1954). XRD was performed using Philips PW 1710 generator operating at 40 kV and 20 mA located at the University of the Witwatersrand in the School of Metallurgical and Chemical Engineering. Radiation of copper  $K\alpha_1$  monochromatic with a wavelength of  $1.54186 \text{ \AA}$  was used. A powdered coal sample was run from  $10^\circ$  to  $80^\circ 2\theta$  with a step size of  $0.02^\circ 2\theta$  and step time of 1 second. The obtained spectrum was corrected for polarization using techniques described in literature by Franklin, 1950. The obtained peaks were corrected by curve fitting using a Gaussian fit in the region of the study (as shown in Figure 3.3).

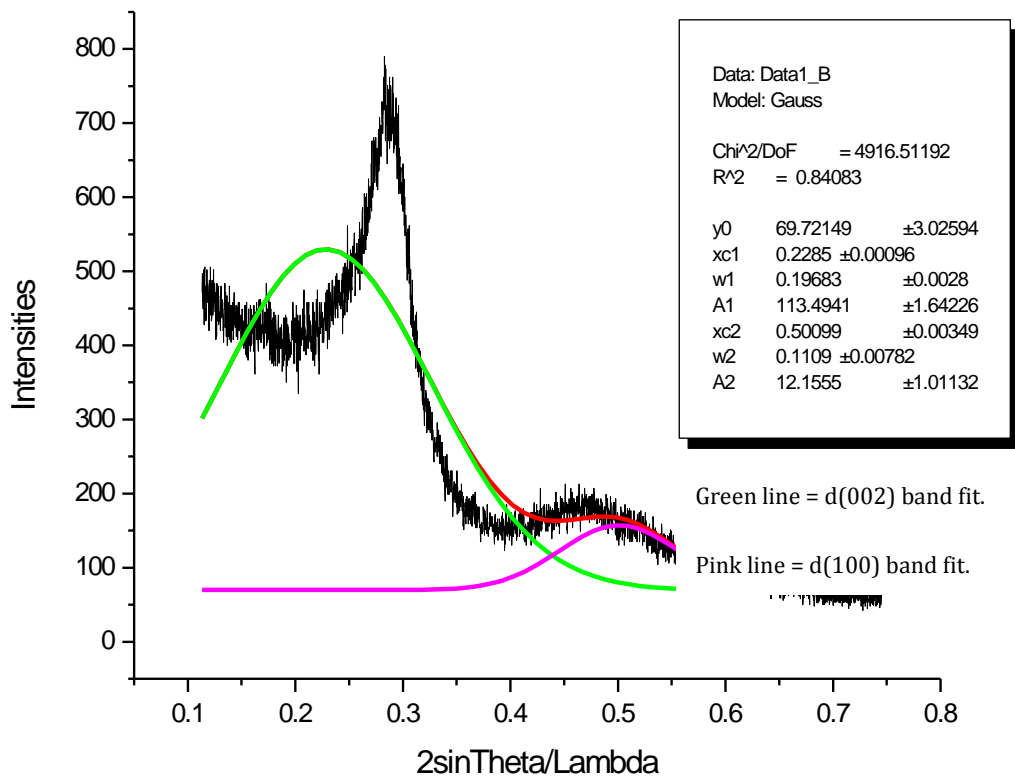


**Figure 3.3:** Curve resolution of diffractogram for the Coal A packed-bed reactor generated sample no. 2.

The quantitative analysis was based on the curve fitted peaks rather than the peaks obtained directly from the XRD. The curve fitting technique was described in literature (Maity and Mukherjee, 2006; Lu et al. 2001). The d (002) and d (100) band were taken around 3° and 5°, respectively. The corrected Gaussian peak width were used to calculate the average stacking height ( $L_c$ ), the average stacking diameter of the aromatic rings ( $L_a$ ) and  $d_{002}$ . The areas obtained from the corrected Gaussian fit were used to determine the aromaticity of the parent coal samples as well as for the packed-bed reactor generated samples. The equations used to calculate these parameters are fully discussed in Appendix E.

### 3.5.5 $^{13}\text{C}$ Solid State Nuclear Magnetic Resonance Spectroscopy ( $^{13}\text{C}$ SSNMR) analysis.

$^{13}\text{C}$  SSNMR analysis was conducted to quantify the structural functional groups of the coal samples and the packed-bed reactor derived samples. This analysis is able to give six structural parameters namely: (i) the aromatic carbons, (ii) the aliphatic carbons, (iii) the carbons bonded to phenolic groups, (iv) carbons bonded to carboxylic groups and (vi) those carbons bonded to alcohols. This analysis was conducted at the Stellenbosch University by the Central Analytical Facility.



**Figure 3.4:** Varian Solid State NMR.

## CHAPTER 3: EXPERIMENTAL METHOD

---

### **Instrument Setup**

The solid state NMR spectra were acquired on a Varian VNMRS 500 MHz two-channel spectrometer using 3.2 mm zirconia rotors and a 3.2 mm Chemagnetics™ T3 HXY MAS probe (as shown in Figure 3.4). All cross-polarization (CP) spectra were recorded at ambient temperature with proton decoupling and a relaxation delay of 3 s. The power parameters were optimised for the Hartmann-Hahn match; the radio frequency fields were  $\gamma_{\text{C}}B_{1\text{C}} = \gamma_{\text{H}}B_{1\text{H}} \approx 55$  kHz. The contact time for cross-polarization was 2 ms. The free induction decay was 852 points, Fourier transformed with 1704 points and 50 Hz line broadening. Magic-angle-spinning (MAS) was performed at 15 kHz and Adamantane was used as an external chemical shift standard where the downfield peak referenced to 38.3 ppm. The dipolar dephasing experiments were carried out under similar conditions, with the interrupted decoupling time constant,  $t_{1\text{Xidref}}$  set to 40  $\mu\text{s}$  after evaluating an array of time constants.

### **Data Processing**

The integration reset points were taken from the publications of Solomon et al., (1989) and Suggate and Dickson (2004). The aromatic peak was referenced to 126.56 ppm to ensure reproducible integration of all spectra. A macro (Coal\_int) was created in order to ensure that exactly the same regions were integrated every time. The integral values were transferred to a Microsoft Excel spreadsheet (Coal\_DataProcessing.xlsx) for calculation of the Coal structural parameters as per the above-mentioned publications.

## CHAPTER 3: EXPERIMENTAL METHOD

---

### Notes:

- No Variable Contact Time (VCT) experiments were performed on the samples; hence the fraction of aromaticity was calculated from the CP-MAS experiments. The reason for this can mainly be ascribed to the long acquisition times for VCT experiments. The aromaticity determined from VCT will be more accurate since it compensates for cross-polarization inefficiencies within the matrix. However, since all the other parameters are calculated from the CP-MAS experiment anyway, it was thought to do the same for the aromaticity. The logic behind this is that a consistent error should still allow for meaningful comparisons between samples of the same kind.
- For the dipolar dephasing experiments, an array of interrupted decoupling time constants were evaluated and 40  $\mu\text{s}$  were found to be suitable to saturate the signals of the protonated carbons.
- The dipolar dephasing peak areas were normalised to the spinning sideband area (region F) of the CP-MAS spectrum based on the assumption that the spinning sideband intensity is not affected to a great extent by the interrupted decoupling. This was also verified by inspection of the arrayed dipolar dephasing experiment (10-100  $\mu\text{s}$ ). This allows for the comparison of the CP-MAS peak areas with that of the normalised dipolar dephasing peak areas to determine the fraction of protonated and non-protonated carbons in the aromatic and aliphatic regions.
- An example of the spectrum (Figure 3.5) and the output data is shown below (Table 3.2).

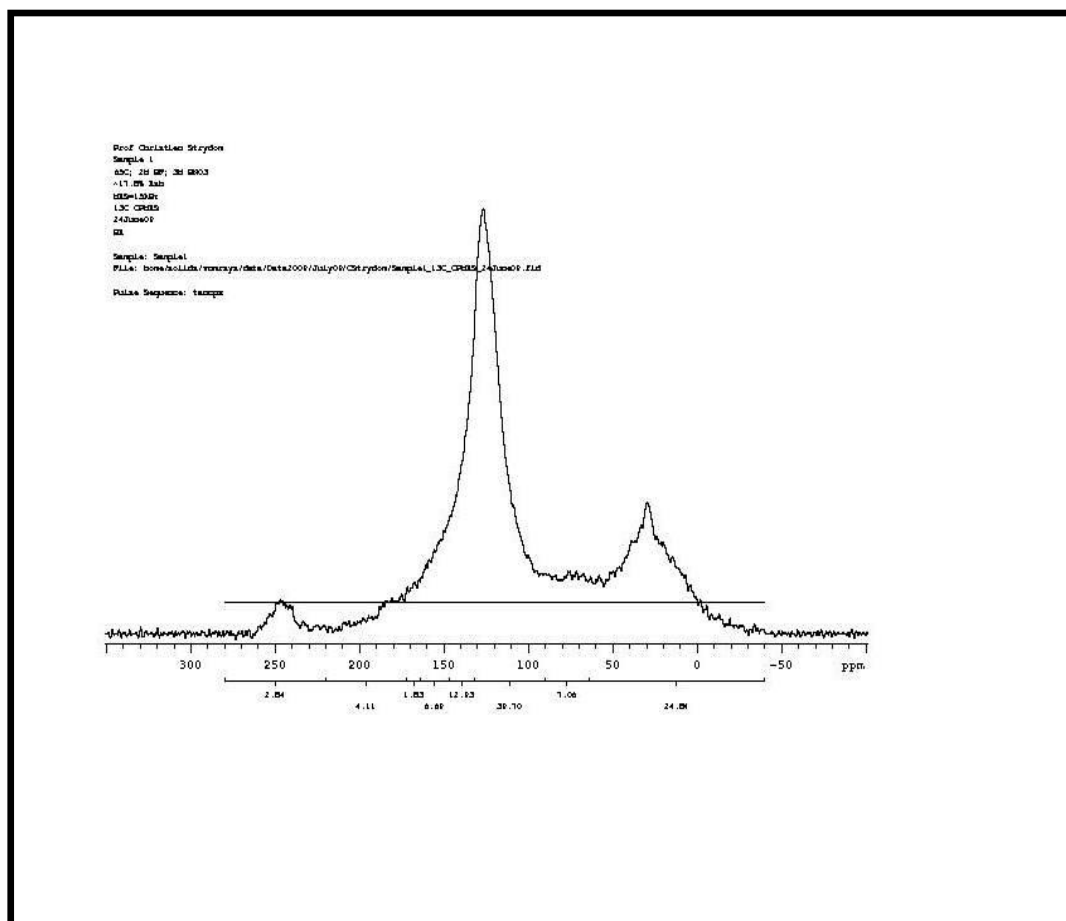


**Figure 3.5:** Spectrum with defined integral reset points and referenced to 126.56ppm.

**Table 3.2:** List of integration regions and values.

Region	Start (ppm)	End (ppm)	Integral
F	280	220	2.83
E	220	172	4.11
C	172	164	1.83
D	164	147	6.69
G	147	132	12.93
C	132	90	39.69
B	90	64	7.06
A	64	-40	24.84

### 3.5.6 Conductivity analysis

Conductivity is a measure of material's ability to conduct an electrical current. Conductivity is the reciprocal of electrical resistivity,  $\rho$ .

$$\sigma = 1/\rho \quad (2)$$

Since this is the case, the conductivity of the coal sample was measured using electrical resistivity. A sample that appeared to have low electrical resistivity was considered to have high electrical conductivity. The method and equipment used to measure electrical resistivity is discussed below.

**Electrical resistivity:** Electrical measurements were made in a special apparatus shown in Figure 3.6.

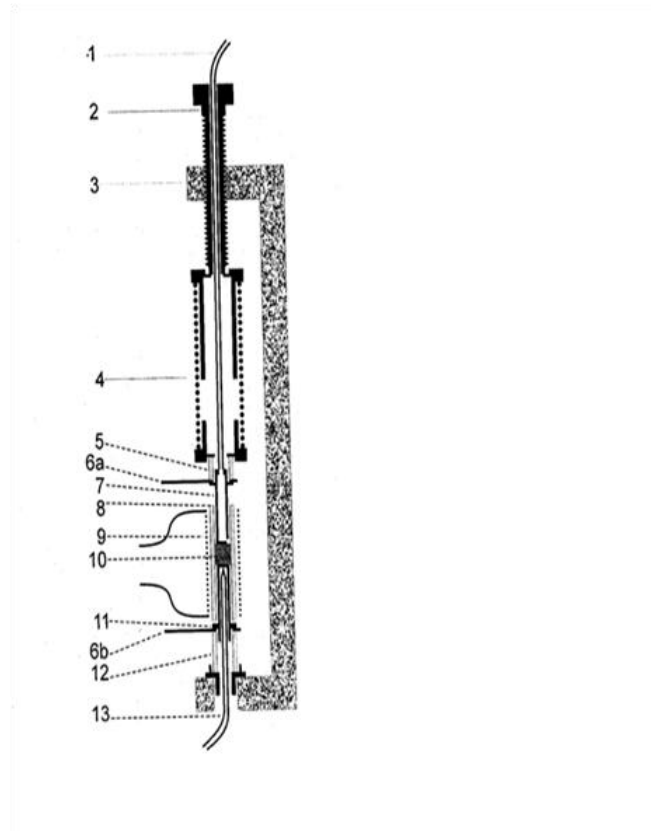


**Figure 3.6:** Schematic representation of the laboratory made electrical resistivity equipment, excluding the electronic components.

A continuous steady flow of nitrogen 156ml/min (plant purity) was introduced through pipe (1) to provide an inert atmosphere at the same time not interfering with the resistivity measurements. The apparatus is such that the nut (2) can be adjusted to press the spring (4) which in-turn applies constant pressure on the upper electrode(7). Thus the sample is pressed/sandwiched at a constant pressure between the two electrodes ensuring maximum contact points throughout the temperature range. The upper electrode (7) was drilled having a tiny hole on the side to allow for the flow of nitrogen into the measurement chamber (electrodes and all contact points are of stainless steel material, ensuring that in the case of material oxidation there is still appreciable contact between



## CHAPTER 3: EXPERIMENTAL METHOD

---

the sample and contact points). A type K double barrel thermocouple (13) was fitted through the bottom electrode (11) such that it touches the surface on which the sample is placed. This provided an accurate reading of the temperature of the sample. The thermocouple was held into position by Teflon which further isolated it from contact to other points of the instrument. To ensure even temperature distribution in the measuring chamber, the element wire (9) was coiled very closely around the non porous alumina tube. A heat insulator blanket was used to cover the whole assembly of electrodes and element wire during the course of the experiment.

### **Electronic devices used:**

- The element wire was connected to a 24V ac transformer through a variance controlled by a programmable temperature control box of the type K thermocouple.
- The thermocouple was connected to the temperature control box, and simultaneously the temperature control wire was also connected to a ADVANTECH data acquisition lab card (USB-4718). The USB device permitted the recording of the temperature profiles on a personal computer system.
- The leading contact points on the electrodes were connected tightly through a special cable to a micro Ohm meter (Agilent 34420A, 7½ Digit Nano Volt/micro Ohm meter). This multimeter was then connected to a personal computer with its inbuilt data acquisition card using a RS 232 cable allowing the recording of the resistance data.

### 3.6 Phase 3: Petrographic analysis

#### 3.6.1 Maceral and Microlithotype analysis

The parent coals and the packed-bed reactor generated samples were crushed and sieved to -1mm following the standard petrography procedure ISO 7404/2 (1985). Coal blocks for point count and image analysis were produced by mounting the coal in an epoxy resin. After setting, the blocks were polished using a Struers TegraForce-1 polisher machine located at the University of the Witwatersrand, in the School of Metallurgical and Chemical Engineering.

The polished blocks were examined under a Leica DM4500P petrographic microscope located at the University of the Witwatersrand, in the School of Metallurgical and Chemical Engineering. Maceral group analysis was conducted on the parent coals following ISO 7404/3 (1985) and microlithotype analysis was carried out on the parent coals following ISO 7404/4 (1985). The analysis was conducted at a magnification of x500 with oil immersion in polarized light.

#### 3.6.2 Carbon Particle Type analysis

A carbon particle type analysis applying petrographic techniques was conducted on the packed-bed reactor generated samples. This analysis was established by Wagner (2005); Bunt and Waanders, 2009). For the purpose of this study few modifications to this analysis were made and the results were recorded on a volume percentage basis.

The packed-bed reactor generated samples were analyzed over a 50  $\mu\text{m}$  field of view and the classification categories used included: (i) coal, (ii) devolatilizing coal, (iii) chars

## CHAPTER 3: EXPERIMENTAL METHOD

---

and (iv) minerals; and these were divided into different subgroups. The classification method was thus conducted in the following manner;

**1) Monomacerite** – Vitrite, where more than 95 vol % of the maceral is vitrinite.

- Liptite, where more than 95 vol % of the maceral is liptinite.
- Inertite, where more than 95 vol % of the maceral is inertite.
- The inertite was further divided into semifusite, fusite (including fusite, secretite and micrite) and inertodetrinite. This subdivision was made because the parent coal is rich in inertinite.

**2) Intermediate coal:** comprised of bimacerite, trimacerite, and banded coal (where more than three macerals are observed).

**3) Carbominerite:** where both maceral and minerals are present in excess of 50 vol %.

**4) Minerals:** where there is more than 70 vol % of minerals.

**5) Devolatilizing coal:** where coal particles that are partially heated, and under the reflected light microscope, a colour change, cracks and pores are observed. These particles are still grey compared to white chars. This type was divided into four subdivisions and is as follows;

**(i) Colour change devolatilized coal:** This is a coal that is starting to change colour from grey to white, the white parts are usually observed at the edges of the particle, and sometimes along the cracks. The colour change is likely to be on

## CHAPTER 3: EXPERIMENTAL METHOD

---

vitritite particles because they contain a high content of aliphatic groups which have a high potential to experience heat earlier leading to a release of volatile matter content. This colour change should be 70 % distributed on the coal particle at a 50µm grid line area.

**(ii) Cracked devolatilized coal:** Cracks are observed in coal particles, especially on vitrite particles. These cracks are either passing through the coal particle (big crack), or they are finely distributed all over the coal particle (fissures). The cracks should be 70 vol % distributed on the coal particle at a 50 µm grid line area.

**(iii) Porous devolatilized coal:** Pores are observed in the field of view in the coal due to heat, especially on vitrites and reactive semifusites. The pores are distributed all over the coal particle, or one or two pores will be seen on a coal particle. The pores should be 70 vol % distributed on the coal particle at a 50 µm grid line area.

**(iv) Mixed devolatilized coal:** This comprises of a mixture of the above mentioned features examined in the devolatilizing coal particle. The mixture is made up of two or more of these features. The examined mixed features should be 60/40, or 50/50 vol % distributed on the 50 µm grid line of the devolatilizing coal particle.

**5) Chars:** Char is a carbonaceous rich material that is produced during pyrolysis. The char particles can be divided into four subgroups depending on their physical appear-

## CHAPTER 3: EXPERIMENTAL METHOD

---

ance under the microscope. Chars are white in appearance compared to devolatilizing coal particles. The following subgroups were distinguished for the packed-bed reactor generated samples.

**(i) Porous chars:** Chars are comprised of pores moderately or largely distributed in the char particle. Some of the porous chars had thick walls or thin walls depending on the initial maceral. The porous with thin walls are believed to have formed from vitrite since they are easily heated relative to inertodetrinite. Porous with thick walls appears to be formed from reactive semifusite, or where there was a banded coal with vitrinite in the middle and inert semifusite.

**(ii) Inert chars:** Chars that are inert and appear white in colour; they don't have pores, or have less than 20 vol % of pores and seems not to be affected by heat treatment. These chars may originate from inert semifusinite and a banded coal, where there was inertodetrinite (20 % or less) and inert semifusinite.

**(iii) Fusinoids:** Chars that have retained their parent coal structure (fusites), or seem not to have reacted or been affected by heat treatment.

**(iv) Oxidized chars:** Inert chars that appear to have a brown layer on the edges of chars, whereas the middle is white and sometimes will have cracks along the char particle. Oxidation may form cracks as well.

**6) Intermediate/Mixed Chars:** Chars that are both porous and inert in a 60/40 vol % ratio.

**7) Carbominerite chars:** are made up of both minerals and chars in a 60/40 vol % ratio.

**8) Ash:** are particles that appear to be glassy amorphous material under the field of view. They might as well be heat altered minerals.

### 3.6.3 Total Reflectance analysis

Total reflectance analysis was conducted using a Leica DMP 4500 reflected light polarising microscope equipped with an oil objective lens of X50 magnification. The microscope is interfaced with a J & M spectroscopic system whereby reflectance values are obtained via a fibre optic cable. A computer collects and processes the data via MSP software. The spectroscopic system is calibrated using glass reflectance standards with known reflectance reading (0.431, 0.906, 1.728, 3.240 and 5.370 %  $R_o$ ). Rank determination was conducted through total maceral reflectance measurements in order to establish the feed coal samples and the packed-bed reactor generated samples maturity. This was carried out in accordance with ISO Standard 7404-5, (1985). 250 readings were taken on the vitrinite and semifusinite particles. These were averaged to obtain a mean total reflectance value, and ranges of readings and standard deviations were recorded. Total reflectance was conducted for only the pipe-reactor generated samples (sample 1-6) because it provides more information about the whole coal sample. Also since the pipe-reactor generated samples were heated to temperatures of 1250 °C, the total reflectance analysis can provide results for the coal maturity at these temperatures.

### 3.6.4 Electron Microprobe on Oxidized Char

Electron Microprobe was used to determine the elemental composition difference between the oxidized and non-oxidized sections on chars. This analysis was conducted using a Cameca SX 100 electron microprobe at 10 kV accelerating voltage, 15 nA beam current, and with a 10  $\mu\text{m}$  diameter electron beam and 5  $\mu\text{m}$  with small surfaces especially for the non-oxidized sections. Al was determined by EDS, other elements by WDS. The calibration standards are listed below. This setup, typically, has detection limits for N, O, and Fe of roughly 1.6, 0.5, and 0.8 mass %, respectively, and detection limits for Si, S, Ca, and Ti of about 0.06 mass % (or better).

The reference materials that were used for calibration are as follows;  
C: Anthracite + "calibration curve" to account for carbon coating.

### CHAPTER 4

#### 4 RESULTS AND DISCUSSION

This chapter presents experimental results obtained from the various analytical techniques discussed in Chapter 3. The coals used in this study were lump coals and originated from the Highveld coalfield, and were labelled as “Coal A” and “Coal B” for the purpose of this study. The two lump coals were selected since Coal B is claimed to convert at a slower rate in commercial conversion process when compared to Coal A (Koekemoer, 2009).

The two Highveld lump coals were converted using a packed-bed reactor combustor unit at temperatures of up to 1250 °C. Lump coal with a fraction size of -75mm +5mm was used as feed coal for both coal types, A and B. In total, 14 samples were generated in the packed-bed reactor combustor unit from both Coal A and B. The 14 resultant packed-bed reactor samples were taken from the various reaction zones (as shown in Table 4.1).

In this chapter the word mineral matter clearly refers to all forms of inorganic material associated with coal. The word ash clearly refers to all non-combustible residues of gasification of combustion reactions.



## CHAPTER 4: RESULTS AND DISCUSSION

---

**Table 4.1:** Summary of the packed-bed reactor generated samples together with their reaction zones and temperature history.

Sample number	Coal A, Temp °C	Coal B, Temp °C	Reaction zone
1	111	93	Drying zone
2	200	183	Drying zone
3	289	342	Pyrolysis zone
4	419	693	Pyrolysis zone
5	671	980	Pyrolysis zone
6	1160	1225	Reduction zone
7	1250	1260	Combustion and ash

The four reaction zones were determined from the previous study conducted by Bunt 2006 and therefore this study aims to expand more into the findings obtained from Bunt's (2006) and Koekemoer's (2009) studies. It is interesting to note that from Table 4.1, that Coal B ran cooler in the drying zone (sample 1-2) when compared to Coal A and that higher temperatures are reflected in the hotter regions of the reactor; sample 5-7 (from the end of the pyrolysis zone to the ash bed zone) for Coal B when compared to Coal A. This may be due to differences in the chemical and physical structural properties of these coals. It may also be possible that this is due to mineralogical differences of these two coal types. It is hoped that this chapter will reveal why this happens.

This chapter is divided into three phases. The first phase presents the results for the chemical analysis which includes the proximate analysis and the coal char CO<sub>2</sub> reactivity results of the coal feed samples and their packed-bed reactor generated samples.

## CHAPTER 4: RESULTS AND DISCUSSION

---

In the second phase of this chapter, structural analysis results of the parent coal samples and the packed-bed reactor generated samples are compared and discussed. Structural analysis results were obtained by the use of Fourier Transform Infrared Spectroscopy (FTIR), BET Adsorption analysis, X-ray diffraction Spectroscopy (XRD), and  $^{13}\text{C}$  Solid State Nuclear Magnetic Resonance Spectroscopy ( $^{13}\text{C}$  SSNMR). Structural analysis experiments were used in attempt to investigate the differences in structural properties, or behaviour of Coal A and B within the various reaction zones of the packed-bed reactor.

The third phase of this chapter presents the petrographic analysis results obtained by the use of maceral count for the parent coal samples, and carbon particle type analysis for the packed-bed reactor generated samples. Petrographic analysis experiments were used to determine the physical changes of the packed-bed reactor generated samples at a microscopic level. Carbon particle type analysis was undertaken to investigate the char morphologies of Coal A and B within the various reaction zones identified. Total reflectance analysis results of the parent coal samples and the packed-bed reactor generated samples are also discussed in this phase. This experiment was conducted to compare the increase in reflectance behaviour of Coal A and B with regard to reaction zones.

It is hoped and aimed that by linking the various techniques used and discussed in this chapter, an explanation as to why Coal B converts at a slower rate in commercial conversion process when compared to Coal A can be given.

### 4.1 PHASE 1: Chemical analysis results

The standard chemical analysis technique used worldwide for coal characterization is proximate analysis. This technique is used to obtain the broad chemical composition of coal samples. In this section, the chemical behaviour of Coals A and B (-75mm +5mm) will be compared by the use of the packed-bed reactor generated samples. Coal char CO<sub>2</sub> reactivity will be utilized to compare the reactivity for Coal A and B at 50 % burn-off at 1000 °C.

#### 4.1.1 Proximate analysis results

Proximate analysis determines the moisture, volatile matter, fixed carbon and ash content of coals. Since the combustible part of coal is mainly composed of volatile matter and fixed carbon, this part of the study will mainly focus on these aspects. The proximate analysis for Coal A and B was conducted on a dry basis using the thermogravimetric analysis (TGA) method as outlined in Chapter 3, Section 3.3.1.1. These results are reported on a dry basis and are tabulated in Table 4.2.

**Table 4.2:** Proximate analysis of parent coal samples (% dry basis).

---

	<b>Coal A</b>	<b>Coal B</b>
<b>Volatile matter</b>	26.1	29.0
<b>Fixed Carbon</b>	47.0	49.0
<b>Ash</b>	26.5	22.0

---

## CHAPTER 4: RESULTS AND DISCUSSION

---

The proximate analysis results for the parent coal samples are typical of those obtained on Highveld coal. It can also clearly be observed that Coal B has a higher volatile matter and fixed carbon content when compared to Coal A. It is expected that during the coal conversion process, that Coal B will release volatile matter at a higher rate and will experience internal heat transfer faster relative to Coal A which is contrary to what is observed in practise (Koekemoer, 2009). The detailed proximate analysis raw data results is attached in Appendix A, Table A1 and A2.

### **1.4.1.1 Volatile matter profile**

Volatile matter consists of a complex mixture of gaseous and liquid products resulting from the thermal decomposition of the coal substance. The volatile matter profile is presented in Figures 4.1 for both Coals, A and B packed-bed reactor generated samples.

At the beginning of the drying zone (sample 1) for Coal A and B, the volatile matter content decreased from 26.1 % and 29.0 % (parent coal samples) to 21.9 % and 23.5 % (sample 1 within the drying zone of the reactor). This can be related to the fact that the coals have been exposed to temperatures which lead to a loss of certain light volatiles such as carboxylic carbons, methane etc. (Solomon et al., 1989).

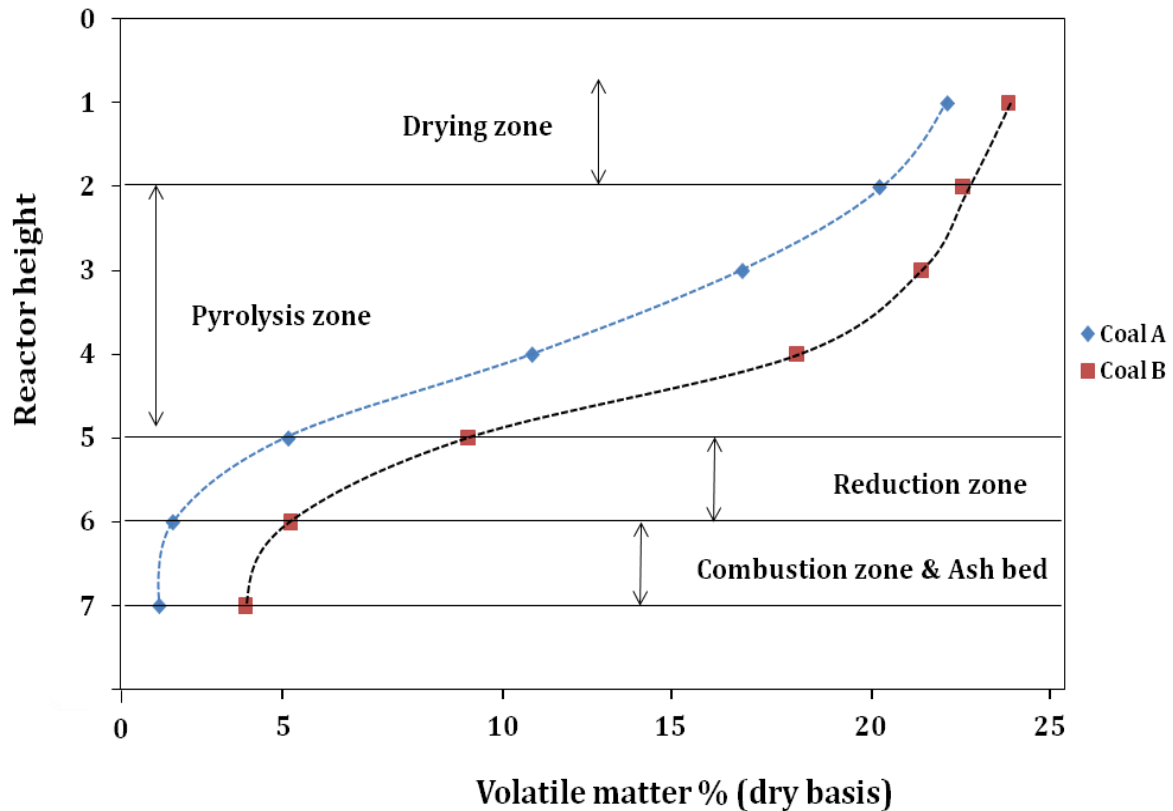


**Figure 4.1:** Volatile matter (dry-basis) profile for the Coals, A and B packed-bed reactor generated samples as a function of reactor height.

Expectedly, it was observed that the volatile matter of both coals decreases from the drying zone to the base of the reactor (ash bed). This is due to the higher reaction temperatures existing from the drying zone to the ash bed (as illustrated in Table 4.1). From the beginning of the pyrolysis zone to the end of pyrolysis zone (samples 3-5), the volatile matter content decreases from 16.4 % to 4.4 % for Coal A; and from 21.2 % to 9.2 % for Coal B. This showed that volatile matter evolution for Coal A is faster when compared to that of Coal B. The decrease in volatile matter content within the pyrolysis zone is due to breakage of weak carbon bonds within the coal particle, resulting in a release of volatiles (Solomon, 1989).

## CHAPTER 4: RESULTS AND DISCUSSION

---

Small quantities of volatile matter were still observed within the ash bed in both Coal A and B; Coal B having the higher amount of volatile matter content (3.3 %) left when compared to Coal A which had 1.0 % volatile matter. The difference in the volatile matter content left in the ash bed for both coals might be attributed to their different coal structural properties, which will be discussed in Phase 2. The remaining volatile matter content within the ash bed means that there is an incomplete conversion of coal. This was attributed to high reaction temperatures existing within the reduction and combustion zones leading to collapsing of the char pores. In addition the inorganic ash chemistry playing a great role resulted in glass encapsulation of the char matrix, thus trapping volatile matter. Figure 4.2 shows the volatile matter evolution within the four reaction zones identified.

It can be seen that the volatile matter evolution in the drying zone is less than 10 % for both Coal A and B. This is due to the temperature values that are less than 200 °C, and at these temperatures the coal is starting to soften, so it is expected that some volatile matter will be released at this stage. In the pyrolysis zone, there is high evolution of volatile matter for both coals. The volatile matter evolution in the pyrolysis zone ranged from 24.7 to 79.7 % for Coal A; and from 9.7 to 60.9 % for Coal B, Coal A releasing 10% more volatile matter when compared to Coal B in the pyrolysis zone. It can be observed that at higher reactor temperatures (900 - 1260 °C), Coal A still has 10 % more volatile matter (95.3 %) yield when compared to Coal B (85.9 %). This clearly showed that Coal A experienced better heat transfer when compared to Coal B.

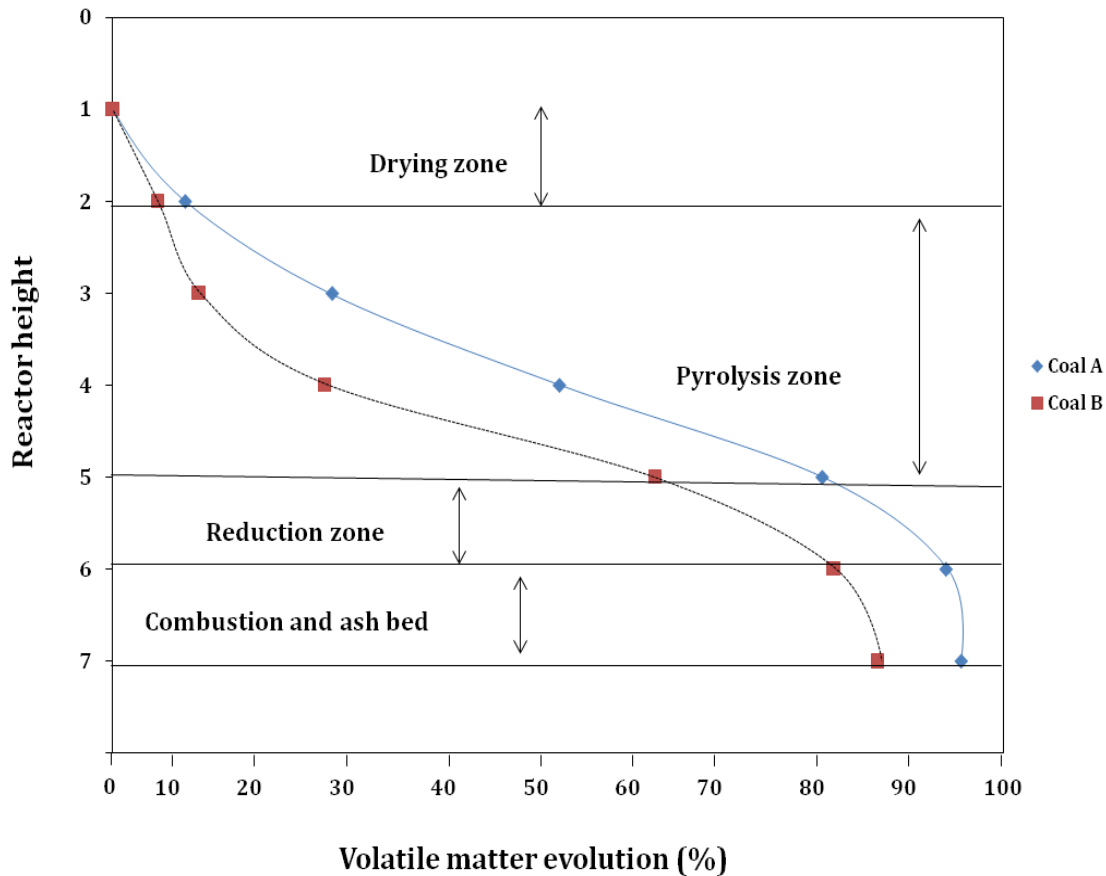


**Figure 4.2:** Volatile matter evolution of Coal A and B packed-bed reactor generated samples as a function of reactor height.

It was clearly observed that within the ash bed region of both Coals A and B packed-bed reactor generated samples, there is less than 5 % of the volatile matter content left within Char A and 10 % more of the residual volatile matter content for Char B. This might be attributed to the difference in reactivity and structural orientation of these coals, and this will be further explored in the following phases.

1.4.2.1 Fixed carbon profile

Fixed carbon is the solid residue remaining when the volatile matter has been driven off, and it contains all the mineral matter originally present in the coal, together with the non-volatile part of the coal substance (Johns, 2008). The non-volatile part is called the fixed carbon. Fixed carbon is determined by subtracting the total of the percentages of moisture, volatile matter and ash from 100 %.

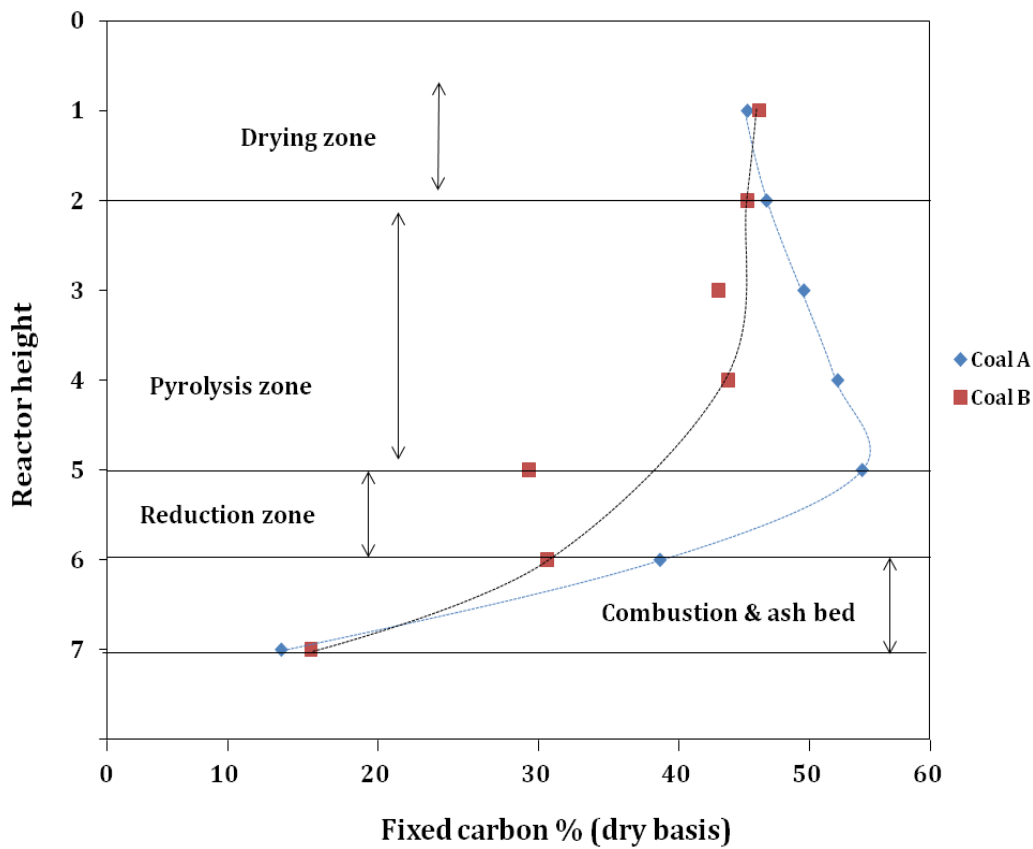


**Figure 4.3:** Fixed carbon profile (dry basis) for the Coal A and B packed-bed reactor generated samples as a function of reactor height.

Figure 4.3 shows the fixed carbon profile (dry basis) for Coal A and B as a function of reactor height. Initially both Coal A and B packed-bed reactor generated samples have 45 % and 47 % of fixed carbon content respectively within the drying zone (sample 1).



## CHAPTER 4: RESULTS AND DISCUSSION

---

The fixed carbon content for Coal A in the pyrolysis zone tends to increase (from 51 % to 55 %) to the end of pyrolysis, and then further decreases to the ash bed zone to 13 % fixed carbon. This increase may be associated with the correspondent decrease in volatile matter content (as shown in Figure 4.1), since fixed carbon is obtained from the TGA analysis by difference between the moisture, volatile and ash content and is mainly due to the slower rate of the volatile matter evolution at higher temperatures when compared to Coal A. On the contrary the fixed carbon content for Coal B seems to show a decrease in the pyrolysis zone. The decrease of fixed carbon for Coal A from 55 % to 40 % within the reduction zone indicates the beginning of carbon conversion at temperatures above 1000 °C of the reactor unit. Coal B shows a decrease in fixed carbon content from the drying zone to the middle of the pyrolysis, and before the end of pyrolysis a slight increase of fixed carbon is observed. Coal B, sample 5 experiences higher temperatures (980 °C) within the end of the pyrolysis zone, and this is shown by the presence of the out of line scatter in Figure 4.3. This is possibly due to hot spot formed at the end of the pyrolysis zone which is caused by high ash content. This is not observed for Coal A since sample 5 is at lower temperatures (671 °C). At this point the difference in temperature profile of these two coals, A and B, cannot be explained and it is hoped that the structural analysis and petrographic analysis will be able to reveal why these coals behave differently with regard to temperature. Thereafter, a decrease in fixed carbon content is observed to the ash bed region for Coal B. Fixed carbon is still observed within the ash bed for both Coal A and B, and again this indicates incomplete carbon conversion. The calculated fixed carbon conversion within the ash bed zone is 74 % for Coal A and 70 % for Coal B.

### 1.4.3.1 Ash profile

Ash is formed from the complete burning of coal, and it originally comes from the mineral matter in coal.

Figure 4.4 shows the ash profile (dry basis) for Coal A and B packed-bed reactor generated samples as a function of reactor height. The ash profile for both Coal A and B packed-bed reactor generated samples appear to be relatively constant from the drying zone to the middle of the pyrolysis zone, ranging from 31.4 % to 35.83 % for Coal A; and from 29 % to 37 % for Coal B.

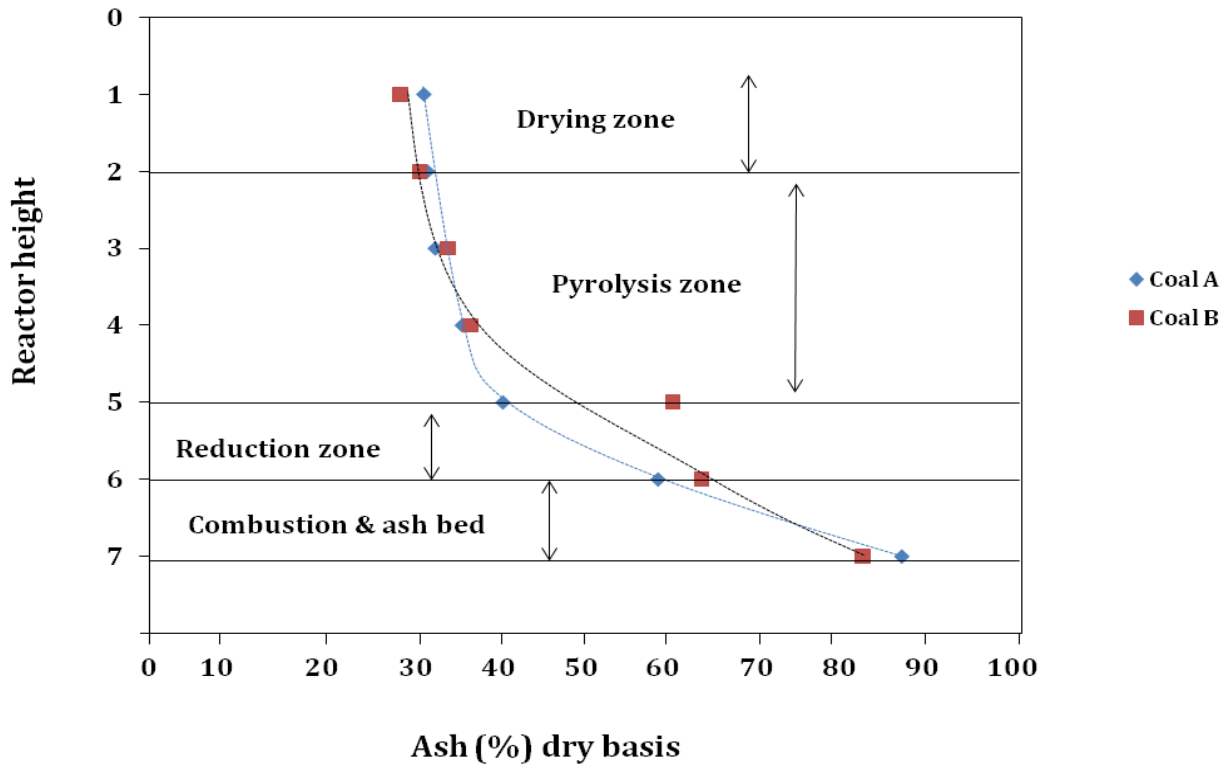


**Figure 4.4:** Ash profile (dry basis) for the Coal A and B packed-bed reactor generated samples as a function of reactor height.

Once more the hot spot for Coal B, sample 5 is observed within the end of pyrolysis zone. Thereafter, an increase in ash content of the packed-bed reactor generated samples is observed to the ash bed. The increase in ash content shows that the carbon conversion occurs at higher reaction temperatures (temperatures above 700 °C) of the reactor unit. This is expected since at these temperatures carbon reacts with the reactant gases leaving behind ash residue.

### 4.1.2 Coal char CO<sub>2</sub> reactivity analysis results

CO<sub>2</sub> reactivity analysis was performed to determine the reactivity difference of Coal A and B towards CO<sub>2</sub> at 50 % burn-off within the four reaction zones of the packed-bed reactor combustor unit. Coal char reactivity analysis is important because it influences the efficiency of the coal conversion processes (Tay and Li, 2009). The coal char CO<sub>2</sub> reactivity analysis results at 50 % burn-off at 1000 °C for the parent coal samples are summarized in Table 4.3, and the results for the packed-bed reactor samples are illustrated in Figure 4.4.

**Table 4.3:** Coal char CO<sub>2</sub> reactivity analysis results at 50% burn-off at 1000 °C (h<sup>-1</sup>).

Coal A	Coal B
3.50	3.20

From the results presented in Figure 4.5, it can be observed that the coal char reactivity results vary significantly within the reaction zones of the packed-bed reactor. Coal char CO<sub>2</sub> reactivity was not conducted on sample 7 (sample in the ash bed region) since this sample contains less carbon content. Both Coal A and B packed-bed reactor generated samples follow the same trend with regard to coal char CO<sub>2</sub> reactivity within the reaction zones, Coal A being more reactive when compared to Coal B. This is also supported by the volatile matter evolution findings, where Coal A released more than 10 % of volatiles within the pyrolysis zone to the ash bed region compared to Coal B.

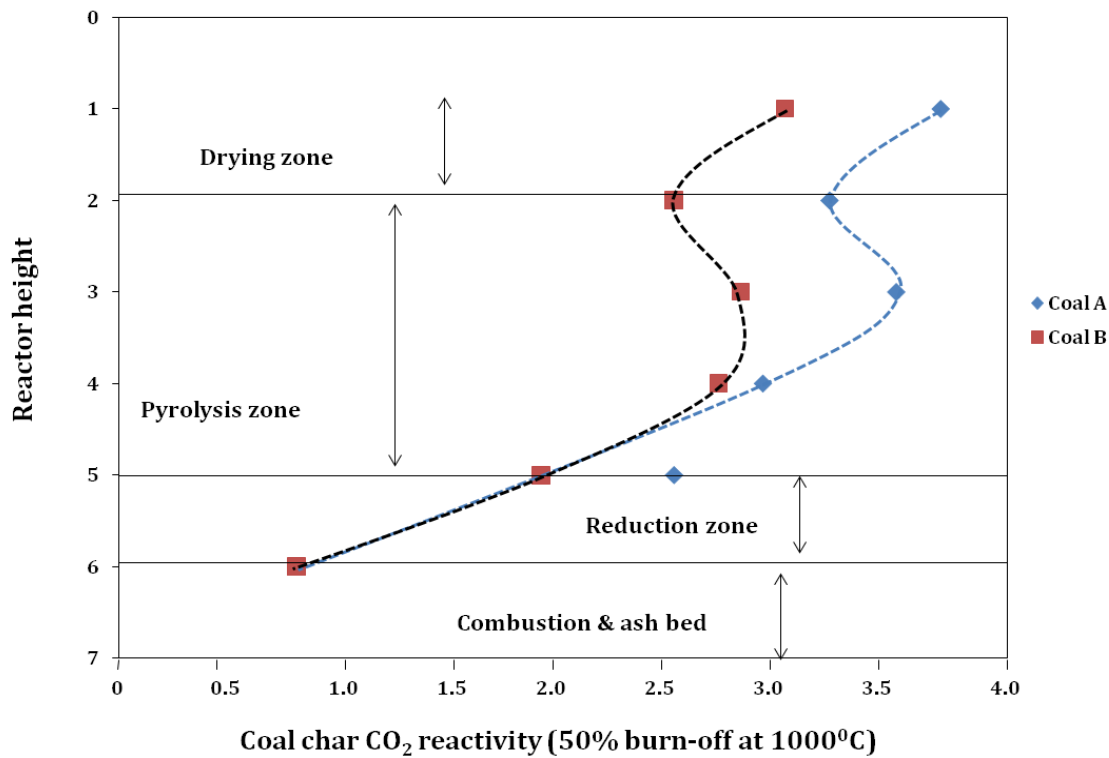


**Figure 4.5:** CO<sub>2</sub> reactivity of Coal A and B parent coal samples and packed-bed reactor generated samples as a function of reactor height.

Generally a decrease in reactivity from the parent coal samples to the drying zone is observed for both coals. This may be a result of re-arrangement of coal structure due to heat treatment. Within the pyrolysis zone, there is a slight increase in reactivity (from 3.2 h<sup>-1</sup> to 3.4 h<sup>-1</sup> at temperatures above 300 °C) to the middle of pyrolysis zone, and then a further decrease is observed at the end of pyrolysis zone to the reduction zone for both coals. The increase in reactivity in the pyrolysis zone is due to the opening of previously closed pores, resulting in an increase in surface area (Sadhukhan et al., 2009). This occurs at temperatures below 700 °C (as illustrated in Table 4.1) in the region of fast pyrolysis and its where char particles are formed. Coal B sample 5 shows to have a hot spot due to higher ash content at higher temperatures (980 °C) within the end of pyrolysis zone.

## CHAPTER 4: RESULTS AND DISCUSSION

---

The decrease in reactivity before the end of pyrolysis zone to the end of reduction zone is due to coalescence and pore collapsing of chars leading to reduction of active surface areas and thus a decrease in reactivity. Also at the reduction zone (at temperatures above 700 °C), carbon is being consumed and therefore there is less reactive carbon material remaining in the sample leading to a decrease in reactivity. Coal A appears to have a higher reactivity rate when compared to Coal B. This can be attributed to the higher surface area of Coal A (surface area results will be discussed in the following phase, section 4.2.3). In many cases, reactivity of coal is related to the surface area of the samples because it is believed that the pores of the particles determine its reactivity. Hurt et al. (1991) revealed that specific internal surface area monotonically increases with the carbon burn-off due to opening of new pores. However, the pore collapsing phenomenon occurs during the later part of the char combustion resulting in a decrease in surface area after critical burn-off.

Attempts were made to correlate coal char CO<sub>2</sub> reactivity results with the amount of volatile matter evolution from the drying zone to the end of pyrolysis zone (as illustrated in Figure 4.6)

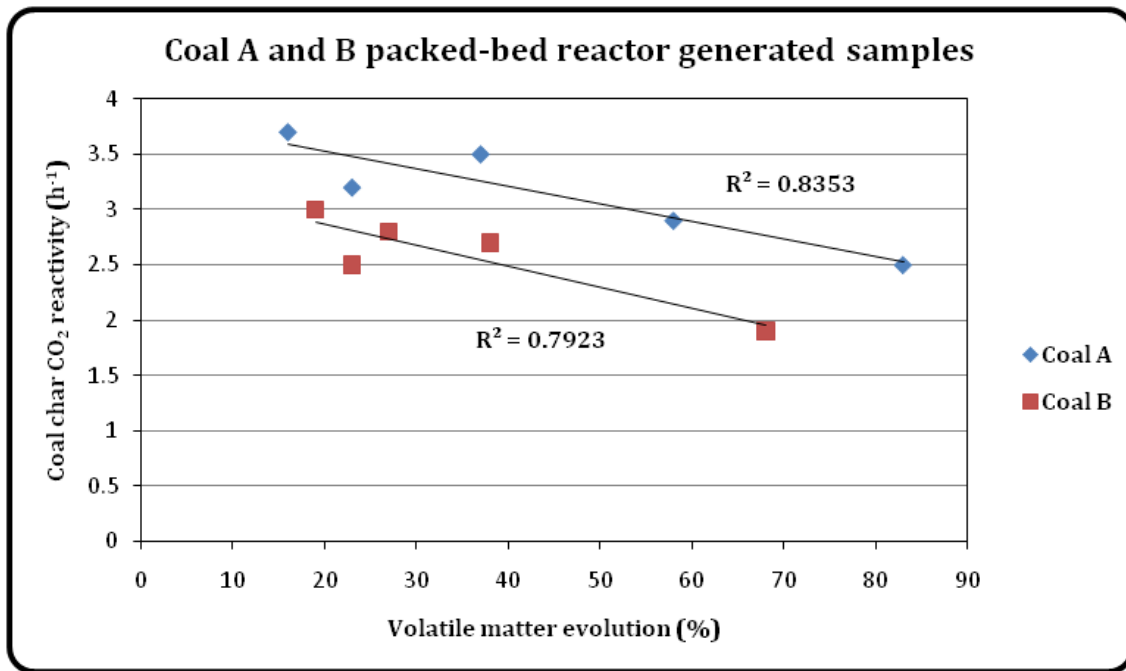


**Figure 4.6:** Correlation of Coal Char CO<sub>2</sub> reactivity results with volatile matter evolution.

Expectedly Figure 4.6 shows that the coal char CO<sub>2</sub> reactivity is decreasing with an increase in the volatile matter evolution for both coals, A and B packed-bed reactor generated samples from the drying zone to the pyrolysis zone (from sample 1 to 5). This means that as more volatile matter is released from coals, the reactivity of coals decreases because the carbon active sites are reduced. In other words reactivity of coal samples is governed by amount of volatile matter contained on that coal sample. This correlation appears not be a very good one because it ranges from 0.835 to 0.792 % and Coal A shows a better correlation when compared to Coal B.

### 4.1.3 Summary of Phase 1

Chemical analysis results were able to clearly show chemical structural properties variation of Coal A and B within the four distinct reaction zones occurring within the packed-bed reactor combustor unit; i.e. drying, pyrolysis, reduction, and combustion or ash bed zones. Temperature profile data results showed that Coal B runs cooler in the drying zone (sample 1-2) and higher temperatures were reflected in the hotter regions of the reactor (sample 5-7, end of the pyrolysis zone to the ash bed region) relative to Coal A. The reason for this is still not clear at this moment. The experimental results obtained from the proximate analysis confirmed that the pyrolysis zone is the largest zone in the reactor unit and major chemical properties variation of Coal A and B appear to occur within this zone as well as in the reduction zone. Coal A releases more volatile matter in the pyrolysis zone (at temperatures above 200 °C) when compared to Coal B. Coal B appears to have a higher volatile matter and fixed carbon content remaining in the ash bed when compared to Coal A, implying incomplete carbon conversion with 74 % and 70 % of carbon conversion for both Coal A and B respectively. Coal char CO<sub>2</sub> reactivity showed that Coal B has a lower reactivity when compared to Coal A possibly due to the lower surface area and given the fact that this coal was also found to have high amount of volatile matter and fixed carbon in the ash bed zone of the reactor when compared to Coal A.

At this point it cannot be explained as to why Coal B behaves differently from Coal A. It is hoped that the following phase (structural analysis) will reveal an explanation as to why Coal B has a lower reactivity when compared to Coal A. Table 4.4 below summarizes significant findings from chemical analysis results.



## CHAPTER 4: RESULTS AND DISCUSSION

**Table 4.4:** Summary of significant findings from chemical analysis results.

Analytical Technique	Coal A	Coal B
Temperature profile	<ul style="list-style-type: none"><li>➤ Higher temperature profile within the drying zone relative to Coal A.</li><li>➤ Lower temperature profile within the end of pyrolysis zone to the ash bed region</li></ul>	<ul style="list-style-type: none"><li>➤ Lower temperature profile within the drying zone relative to Coal A.</li><li>➤ Higher temperature profile within the end of pyrolysis zone to the ash bed region.</li></ul>
Proximate analysis	<ul style="list-style-type: none"><li>➤ Higher VM evolution relative to Coal B.</li><li>➤ Higher FC conversion within ash bed region relative to Coal B.</li><li>➤ Higher carbon conversion relative to Coal B.</li></ul>	<ul style="list-style-type: none"><li>➤ Lower VM evolution relative to Coal A.</li><li>➤ Lower FC conversion within ash bed region relative to Coal A.</li><li>➤ Lower carbon conversion relative to Coal A.</li></ul>
Coal Char CO <sub>2</sub> reactivity	<ul style="list-style-type: none"><li>➤ Higher CO<sub>2</sub> reactivity relative to Coal B</li></ul>	<ul style="list-style-type: none"><li>➤ Lower CO<sub>2</sub> reactivity relative to Coal A.</li></ul>

### 4.2 PHASE 2: Structural analysis results

This section will discuss results that were obtained using different analytical techniques to determine the structural components of the Coal A and B packed-bed reactor generated samples obtained within the four reaction zones identified. This section does not focus on the quantitative measurements of the following techniques but focuses rather on the variation of coal structural properties with regard to heat treatment occurring in the four packed-bed reactor zones. It also focuses on finding the structural differences between Coal A and B, if any. The following analytical techniques were carried out on the parent coal samples and the -75mm +5mm packed-bed reactor generated samples: FTIR, BET adsorption methods, X-ray diffraction, and  $^{13}\text{C}$  Solid state NMR. The background and relevance of these methods to this research has been discussed in Chapters 2 and 3.

The coal samples were demineralized before they were analyzed using the above mentioned techniques. This was performed to reduce the mineral matter interference when conducting structural analysis of the coal samples.

#### 4.2.1 Demineralization results

The demineralization process was performed to reduce the amount of mineral matter present in the Coal A and B parent coal samples and the packed-bed reactor generated samples. TGA analysis was conducted to determine the amount of ash left in the samples after demineralization process. The mineral matter content before and after the demi-

## CHAPTER 4: RESULTS AND DISCUSSION

neralization is summarized in Table 4.5. The TGA graphs and the calculations used to obtain the amount of ash content are attached in Appendix C.

**Table 4.5:** A summary of the ash contents for the packed-bed reactor generated samples before and after the demineralization process.

Sample	Coal A (%)	% Ash reduction	Coal B (%)	%Ash reduction
<b>1</b>	26.9		29.0	
<b>1 DM*</b>	3.9	86	3.6	88
<b>2</b>	29.4		29.0	
<b>2 DM*</b>	3.9	87	3.1	89
<b>3</b>	32.7		26.7	
<b>3 DM*</b>	2.7	92	1.8	93
<b>4</b>	34.7		33.5	
<b>4 DM*</b>	3.2	91	1.5	96
<b>5</b>	34.4		37.4	
<b>5 DM*</b>	3.5	90	2.4	94
<b>6</b>	54.6		70.5	
<b>6 DM*</b>	13.5	75	15.8	78

\*DM = demineralized

The use of HCl and HF was based in the literature findings which suggest that HCl removes ZnS, PbS and CuFeS<sub>2</sub> to form hydrogen sulphide and metal chloride, and HF removes silicates and clays (Klika et al., 2009). Seemingly, these acids were able to extract significant amount of mineral matter from parent coals and the packed-bed reactor generated samples. Unfortunately, XRD or XRF analyses were not conducted to determine which minerals were left after demineralization. Sample 6 for both Coal A and B packed-bed reactor generated samples retained a high quantity of ash after the demineralization process and these samples were unable to produce data of any value when it

## CHAPTER 4: RESULTS AND DISCUSSION

---

came to structural analysis. The extraction method used gave satisfactory results in terms of the amount of ash that was removed from samples 1 to 5. The % reduction of ash from samples 1 to 5 ranges from 85 % to 91 % for Coal A and from 87 % to 96 % for Coal B. Extraction of minerals and ash from sample 7 was not performed since this sample was taken from the ash bed zone, and it contains close to 90 % of ash for both Coal A and B packed-bed reactor samples, as shown in Figure 4.4.

### **4.2.2 Fourier Transform Infrared Spectroscopy (FTIR) analysis results**

FTIR analysis was performed to determine the functional groups that exist in the Coal A and B sample surfaces, and to understand the changes occurring in their composition with respect to heat treatment during coal conversion. It was decided that only qualitative analysis will be conducted since this study only concerns the behaviour of coal structural changes within the different reaction zones of the packed-bed reactor combustor unit, and not with the quantity of functional groups released within the four reaction zones. The FTIR results were reported from  $4000\text{ cm}^{-1}$  to  $750\text{ cm}^{-1}$  wavenumbers as discussed in Chapter 3, Section 3.3.2.2. The spectra of both Coal A and B parent coal samples and packed-bed reactor generated samples are illustrated in Figure 4.7.

## CHAPTER 4: RESULTS AND DISCUSSION

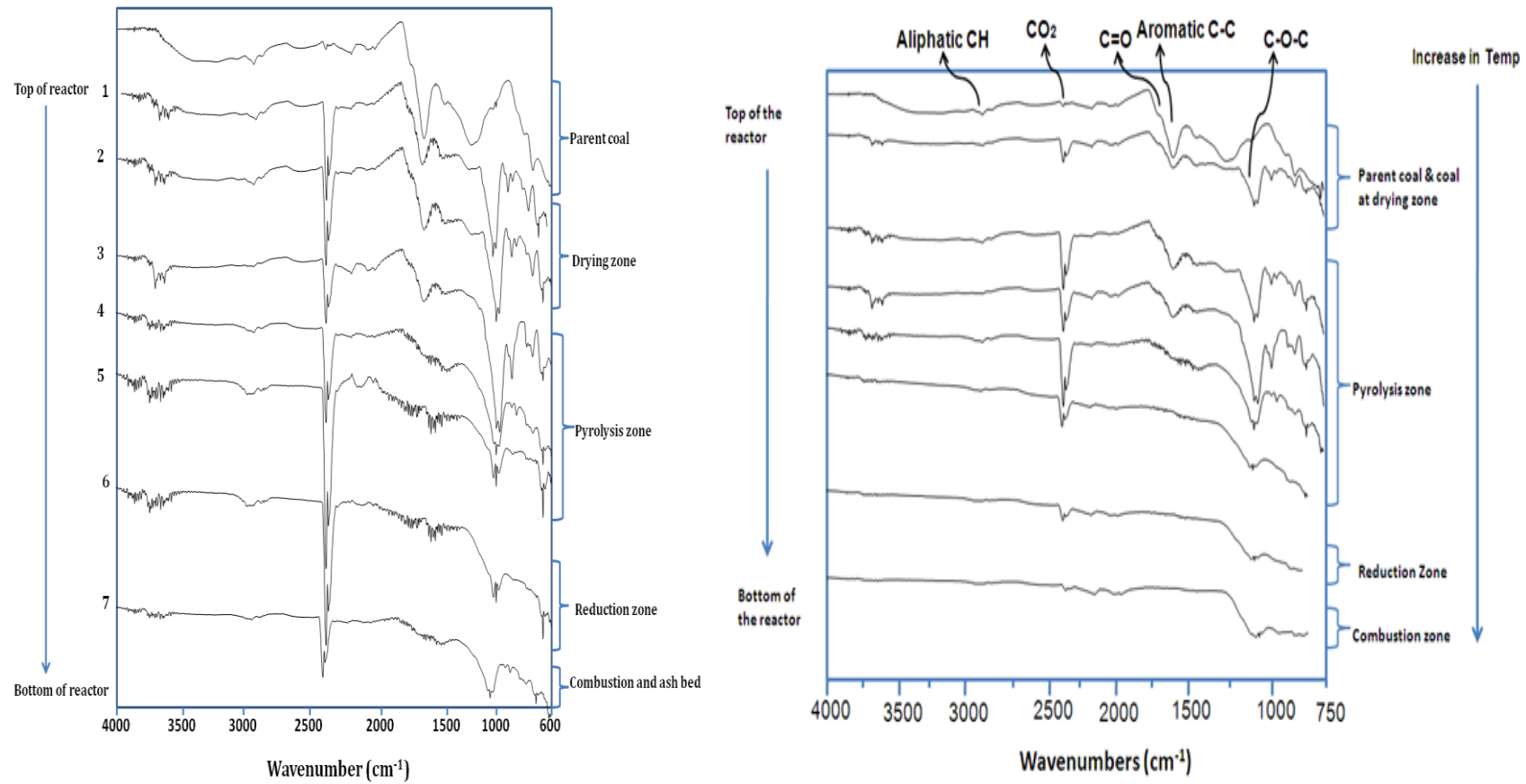


Figure 4.7: FTIR spectrum of Coal A (left) and B (right) parent coal samples and the packed-bed reactor generated samples.

## CHAPTER 4: RESULTS AND DISCUSSION

**Table 4.6:** Tabulated FTIR wavenumbers and their annotations for the parent coal samples and the packed-bed reactor generated samples.

Wavenumbers ( $\nu$ , $\text{cm}^{-1}$ )	Functional groups
3690 – 3620, b	-OH
3500 – 3200, b*	-OH, -H (terminal -OH & intermolecular H)
2918 with shoulder at 2859	$\text{CH}_2$ , $\text{CH}_3$ (Aliphatic and Aromatic)
2355 with shoulder at 2329, s*	-C-N (Pyridinic nitrogen) or $\text{CO}_2$
2167	-C-C=C-C (Aromatic rings)
2025	-C-C=C-CH (Aromatic rings)
1697	-C=O (ketone)
1600	-C=C (aromatic rings)
1439, b*	$-\text{CH}_2$ , $\text{CH}_3$ (aliphatics)
1221	-C-O
1020, s*	-C-O-C (from alcohols and aliphatics)
912, s*	$-\text{CH}=\text{CH}_2$
750, s*	$-\text{CH}=\text{CH}$ (cis & tans)

\*s = sharp band; \*b = broad

Sharp -OH bands at a frequency of  $3690 \text{ cm}^{-1}$  to  $3620 \text{ cm}^{-1}$  were observed in both Coal A and B packed-bed reactor generated samples. Big broad bands from  $3500 \text{ cm}^{-1}$  to  $3200 \text{ cm}^{-1}$  were observed for Coal A and B parent coal samples only. This band is caused by intermolecular H bonds and the -OH groups at the terminal of aromatic coal clusters (Solomon et al., 1988). The intermolecular H bonds and -OH groups tend to disappear in the drying zone, meaning that these functional groups are weakly bound to the coal structure and at temperatures below  $200 \text{ }^\circ\text{C}$  they had already been volatilized.

A band at  $2918 \text{ cm}^{-1}$  having a shoulder at  $2859 \text{ cm}^{-1}$  was observed in the parent coal and the packed-bed reactor generated samples for both coals. This absorption band is due to

## CHAPTER 4: RESULTS AND DISCUSSION

---

-CH<sub>3</sub> and -CH<sub>2</sub> moieties which are found at the edges of the aromatic rings (CH<sub>3</sub>) as side-chains, and the CH<sub>2</sub> of the symmetric aliphatic stretch (Xuguang, 2005). The -CH<sub>3</sub> and -CH<sub>2</sub> groups were also found at the bridge structure of coal (Solomon et al., 1988). Both Coal A and B packed-bed generated samples had a CO<sub>2</sub> absorption band was evident at 2358 cm<sup>-1</sup> due to breakage of weak aliphatic bonds that tend to release CO<sub>2</sub> as part of volatile matter during heat treatment. The CO<sub>2</sub> is formed by condensation after the CO radical is formed in the aromatic rings when the carboxyl is removed (Serio et al., 1987).

A band at 2157 to 2035 cm<sup>-1</sup> arises from C-C=C-C moieties of the aromatic rings of the coal structure. A band at 1600 cm<sup>-1</sup> was due to conjugated C=C stretching of the aromatic rings. The band at 1600 cm<sup>-1</sup> appeared to have a shoulder band at 1697 cm<sup>-1</sup> assigned to C=O (ketone) (Xuguang, 2005). These two functional groups are thought to be bonded (-C=C-C=O), when they appear at these frequencies (1697 cm<sup>-1</sup> and 1600 cm<sup>-1</sup>) (Banwell, 1972). A band at 1439 cm<sup>-1</sup> arises from CH<sub>3</sub> and CH<sub>2</sub> vibrations of aliphatic carbons. Absorption bands between 1300 and 1000 cm<sup>-1</sup> indicate the presence of ethers in the coal structure (Berkowitz, 1985). A band at 1221cm<sup>-1</sup> was due to the existence of C-O stretching vibrations that connects the aromatic clusters and the pyridinic nitrogen clusters of the parent coal molecular structure. Due to the breakage of weak aliphatic carbons by heat, a band at 1020 cm<sup>-1</sup> occurs in the packed-bed reactor samples due to the presence of aryether (C-O-C). Ibarra et al., attributed this band to the presence of aryether which are due to the presence of lignin-like structures present in coal structure. The bands observed at 912, 750 and at 674 cm<sup>-1</sup> were due to the vibration stretch of CH=CH<sub>2</sub>, CH=CH-(cis), CH=CH-(trans), and C=CH<sub>2</sub> of the aromatic rings. These aromatic absorption bands were sharper in the pyrolysis zone, becoming less sharp at the start of the reduction zone to the ash bed.

## CHAPTER 4: RESULTS AND DISCUSSION

---

It is evident from the spectra in Figures 4.7 and 4.8 that absorption bands are more visible and sharper for the packed-bed reactor generated samples in the drying and pyrolysis zone when compared to that of the parent coal samples. In the reduction zone to the ash bed some absorption bands tend to disappear for Coal A. Coal B showed visibility of functional groups in the reduction and combustion zone. This indicates that Coal B had some unreacted carbon left within these zones indicating that this coal has slower reactivity. Serio et al. (1987) conducted similar work where by coal was heated at temperatures of up to 900 °C. The disappearance of aliphatic hydrogen and -CH<sub>3</sub> were observed in the first stage of pyrolysis (at temperatures below 550 °C). They also observed that the appearance of additional bands such as CO<sub>2</sub> was observed throughout the pyrolysis stage.

The absorption bands that appear in the drying and pyrolysis zones were due to the weakening and breakage of aliphatic bonds producing molecular fragments, which is caused by an increase in temperature. The molecular fragments tend to abstract hydrogen from the hydro-aromatics or aliphatics, and thus increase the aromatic hydrogen concentration. In the reduction zone the absorption bands tend to disappear when the char particles react with gases forming an ash residue.

Thus, FTIR was able to confirm the presence of four reaction zones observed by proximate analysis, (Section 4.1.1) and was also able to demonstrate that during the coal conversion process that most of the chemical structural changes occur within the pyrolysis and reduction zones. Evidence of aliphatic bonds were observed by the appearance of the absorption bands at 2918 cm<sup>-1</sup> which are due to the presence of -CH<sub>3</sub> and -CH<sub>2</sub> groups that represents aliphatic groups (Van Niekerk et al., 2008). Further evidence



of aromatic bonds in the coal samples is observed by the presence of the most distinct absorption band at  $1600\text{ cm}^{-1}$  assigned to C=C stretching vibrations of the aromatic rings (Painter et al., 1983).

At low bed temperatures (drying and pyrolysis zone), the volatile matter functional groups were found to be more prominent than at high bed temperatures regions i.e. reduction and ash bed zones. This indicates that as temperature increases above  $200\text{ }^{\circ}\text{C}$ , the volatile matter is released from the coal structure and this was also observed in the proximate analysis results (section 4.1.1, Figure 4.1). As mentioned earlier, it should be noted that FTIR analysis was conducted to obtain the functional group behaviour of Coal A and B within the four reaction zones of the packed-bed reactor combustor unit, and not to quantify these functional groups so that one can generate a molecular structure of coal. The results are qualitative and do not appear to show any significant difference between the sets of samples. According to the discussion made above this was successfully achieved.

### **4.2.3 BET Adsorption analysis results**

BET analysis was conducted to determine the changes occurring in the surface areas of the packed-bed reactor generated samples with regard to heat treatment within the four reaction zones identified. The analysis was conducted using both  $\text{N}_2$  and  $\text{CO}_2$  as adsorbent gas as discussed in Chapter 3, Section 3.3.2.3. The choice of  $\text{CO}_2$  as adsorbent gas was based on the literature argument that states that the usage of  $\text{N}_2$  does not give accurate surface area and porosity results for coal samples. Gan et al. (1972) claimed that  $\text{N}_2$  gas does not penetrate all of the coal pores, nor does it cover the coal area, so it

## CHAPTER 4: RESULTS AND DISCUSSION

---

is difficult to obtain the total surface area and porosity when compared to CO<sub>2</sub> gas. Many researchers claimed that CO<sub>2</sub> surface area is associated with the micro-pore area of coals, while N<sub>2</sub> surface area has the limitation that it diffuses very slowly into the micro-pores below 5 Å, and therefore it does not cover all of the coal's surface area. This indicates that the N<sub>2</sub> surface area covers only the meso-pore area of coal particles (Nandi and Walker, 1964; Debelak and Schrodtr, 1979b; Hurt et al., 1991).

Coal A and B have CO<sub>2</sub> surface areas of 154.4 m<sup>2</sup>/g and 117.5 m<sup>2</sup>/g, respectively (as shown in Table 4.8). The surface area results for N<sub>2</sub> as adsorbent were less than 16 m<sup>2</sup>/g which is very low compared to CO<sub>2</sub> surface areas. Walker et al, (1968) also observed that surface area of coals conducted with CO<sub>2</sub> as adsorbent gas were higher than 100 m<sup>2</sup>/ g and when N<sub>2</sub> was used as adsorbent gas, the surface areas were less than 1 m<sup>2</sup>/ g.

## CHAPTER 4: RESULTS AND DISCUSSION

**Table 4.7:** Tabulated results of CO<sub>2</sub> BET surface area for parent coal samples and the packed-bed reactor generated samples.

Sample	Coal A		Coal B	
	Temp °C	Surface area, m <sup>2</sup> /g	Temp °C	Surface area, m <sup>2</sup> /g
Parent Coal	25	154.4	0	117.5
1	111	81.3	93	69.0
2	200	70.4	183	60.5
3	289	72.5	342	70.1
4	419	104.3	693	103.0
5	671	87.0	980	78.1
6	1160	25.0	1225	27.2
7	1250	21.2	1260	18.0

1 = drying zone, 2 = end of drying zone, 3 = pyrolysis, 4 = pyrolysis, 5 = end of pyrolysis, 6 = reduction zone, 7 = ash bed

This means that Coal A may have a higher probability of reacting faster with regard to heat treatment than Coal B, since the surface area determines the reactivity of a particle to heat treatment. From the results discussed in Section 4.1.2, this was demonstrated to be true. In the drying zone (at temperatures below 200 °C), a decrease of surface area to 81.29 m<sup>2</sup>/g and 68.90 m<sup>2</sup>/g was observed in both coals (as illustrated in Figure 4.8). This is the result of structural re-arrangement of coal upon heat treatment (Hurt et al., 1991). Thereafter the surface area increases rapidly in the beginning of pyrolysis zone to the middle of pyrolysis zone (from sample 3-4). This is caused by the release of volatile matter from the coals, resulting in the increase of the surface areas, which might be attributed to the structural ordering of aromatic clusters to form a more compact stack-

## CHAPTER 4: RESULTS AND DISCUSSION

ing arrangement as the heat treatment is increased (Zhu and Sheng, 2010). Also devolatilization and char formation occurs within this zone (pyrolysis zone). In the reduction zone, the surface area tends to decrease to the end of ash bed position due to coalescence and collapse of char structure (as illustrated in Figure 4.8).

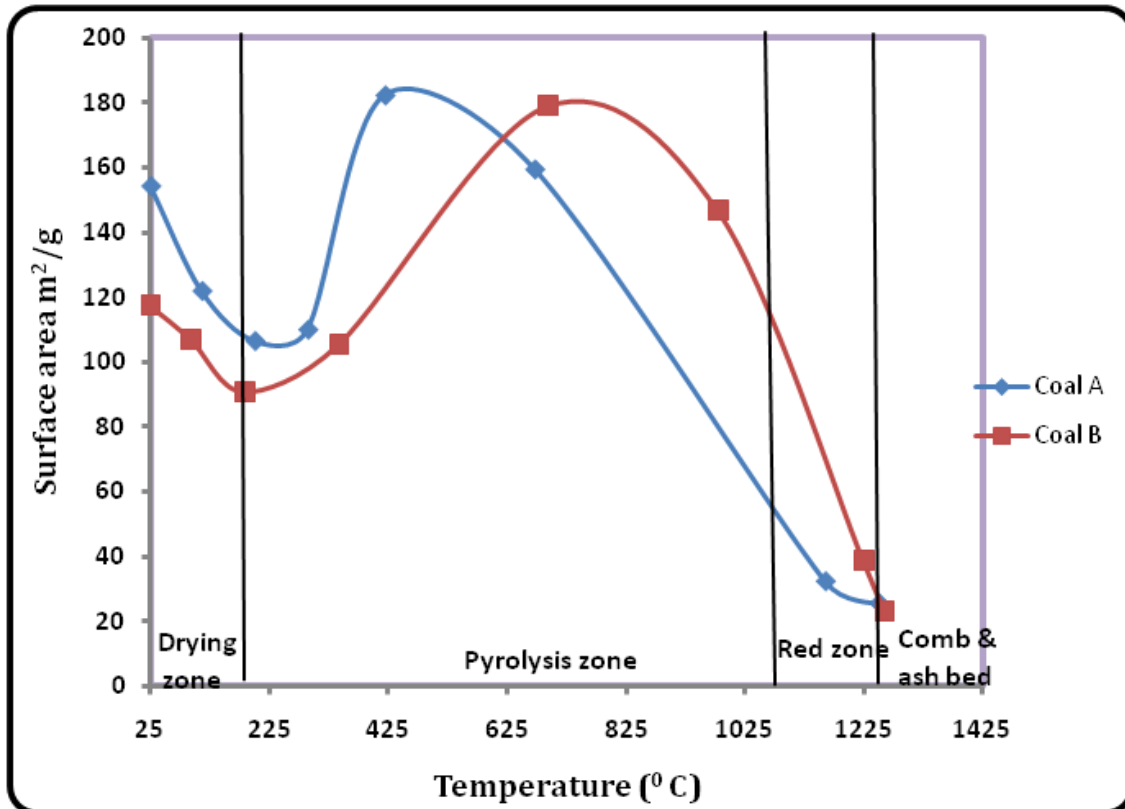


**Figure 4.8:** Coal A and B packed-bed reactor generated samples showing reactor temperature against CO<sub>2</sub> BET surface area.

At low bed temperatures, temperatures above 200 °C and below 650 °C (pyrolysis zone) for Coal A and B respectively, the reaction is believed to be controlled kinetically, but there is a mass transfer limitations due to the use of lump coal (Sadhukhan et al., 2009) and the feed reactant gases have enough time to diffuse through the coal particles creating more micropores which results in higher surface area. The rapid increase observed in the pyrolysis zone was due to the re-opening or creation of new pores of micropores

## CHAPTER 4: RESULTS AND DISCUSSION

---

during heat treatment (Feng and Bhatia, 2003). It can be observed in Figure 4.7 that for Coal B, that the re-opening of the micro-pores occurs at higher temperatures of 342 °C to 693 °C; and for the Coal A, it occurs at lower temperatures of 289 °C to 419 °C. This can possibly also be attributed to the lower surface areas of the Coal B parent coal sample leading to lower heat transfer within the particle. This explains the lower temperatures obtained in the drying zone for Coal B (as seen in Table 4.1).

At high bed temperatures, temperatures above 700 °C (reduction to ash bed position), the reaction possibly proceeds through a diffusion controlled regime, reactant gases are consumed by the reaction before it can diffuse into the inner micropores. Reaction occurs at fewer reaction sites leading to the formation of macropores which results in lower surface area. The micropores get transformed to mesopores and then to macropores towards the end of combustion zone (as the converted carbon is consumed), and this leads to a decrease in surface area (Sadhukhan et al., 2009). The transformation of micro-pores to meso-pores occurs at higher temperatures (980 °C) for Coal B and at lower temperatures (671 °C) for the Coal A.

Thus the BET surface area analysis was able to show the physical structural changes occurring within the four reaction zones identified. At the beginning of the drying zone, surface area tends to decrease due to drying and structural rearrangement of coal to temperatures below 200 °C. As the temperature increases through the pyrolysis zone, the reaction is controlled kinetically and the coal becomes more aligned and ordered leading to an increase in surface area. When the coal is more aligned, it reacts with reactant gases leading to coalescence and pore collapse of the char particles which result in a decrease in surface area. In the study of Sadhukhan et al. (2009), Indian coals with an

## CHAPTER 4: RESULTS AND DISCUSSION

---

average diameter of 6.0mm were used for char generation in the fluidised-bed combustor. Air was utilized as a source of oxygen. At low bed temperatures, the combustion proceeds by shrinking core model. However it was observed that near the end, the pore collapsing phenomenon decreases the surface area. The combustion follows the shrinking unreacted core model (Sadhukhan et al., 2009). This trend was also confirmed by Weisz and Goodwin (1963).

Coal A parent coal sample and the packed-bed reactor generated samples were shown to have a higher surface area when compared to the Coal B parent coal sample and its packed-bed reactor generated samples. This implies that the Coal A parent coal sample will react at a faster rate when compared to the Coal B parent coal sample, as also demonstrated in the coal char CO<sub>2</sub> reactivity results.

### **4.2.4 X-ray Diffraction (XRD) analysis results**

X-ray diffraction studies were conducted to understand the structural changes occurring in the parent coal samples and packed-bed reactor generated samples at a molecular or crystallite level within the four reaction zones identified. The XRD patterns for the parent coal samples and the packed-bed reactor samples examined in this work have almost the same graphitic features as those reported in literature (Franklin, 1950; Hirsch, 1954; Ergun, 1959). It should be noted that coal is not a graphitic material but it is known to contain crystalline domains of the order of nanometers, composed of graphite-like layers arranged turbostratically (Senneca et al., 1998). The graphitic resemblance of these coal samples was observed from the XRD diffractogram by the presence of the d (002) and d (100) bands. Three major bands were expected to be observed

## CHAPTER 4: RESULTS AND DISCUSSION

---

from the diffractogram;  $\gamma$ ,  $d(002)$  and  $d(100)$ . In this case two bands,  $d(002)$  and  $d(100)$  positioned at  $2\theta = 0.28 - 0.30^\circ$  and  $0.48 - 0.50^\circ$  were observed and used as initial estimates to calculate crystallite parameters. The 002 band corresponds to the spacing of the aromatic layers. The  $\gamma$  band corresponds to the aliphatic side chains that are attached to the aromatic carbons (aromatic crystallites) (Lu et al., 2001; Van Niekerk et al., 2008).

The  $\gamma$  band was expected to appear on the diffractogram since in Van Niekerk et al.'s (2008) study, the  $\gamma$  band was present for the Highveld inertinite-rich coal when compared to the Waterberg vitrinite-rich coal. As mentioned earlier, the  $\gamma$  band represents the aliphatic side-chains attached to the crystalline carbon (Lu et al., 2000). The reason behind the disappearance of the  $\gamma$  band might be: (i) In the study by Van Niekerk et al. (2008), only pure inertinite and vitrinite maceral components were examined, and (ii) the variability of XRD machines and programmes used might lead to the differences in the results obtained. In addition to this, a high amount of amorphous (non-crystalline) material will mask the  $\gamma$  band.

Senneca et al. (1998) also studied microstructural changes and loss of reactivity of chars upon heat treatment. Two coals and one coke were selected for this study, and one of them was an inertinite-rich South African coal. The  $\gamma$  band was not observed in this study but it was observed only for the coke samples. The coals used in this study had volatile matter that contributes to the amorphous content of the diffractogram. Therefore, it is difficult to see this signal. The XRD analysis results are discussed both qualitatively and quantitatively below.

### 2.4.1.4 Qualitative results of the X-ray diffraction analysis

Figure 4.9 show a typical diffractogram of Coal A and B parent coal and their respective packed-bed reactor generated samples within the four reaction zones identified.



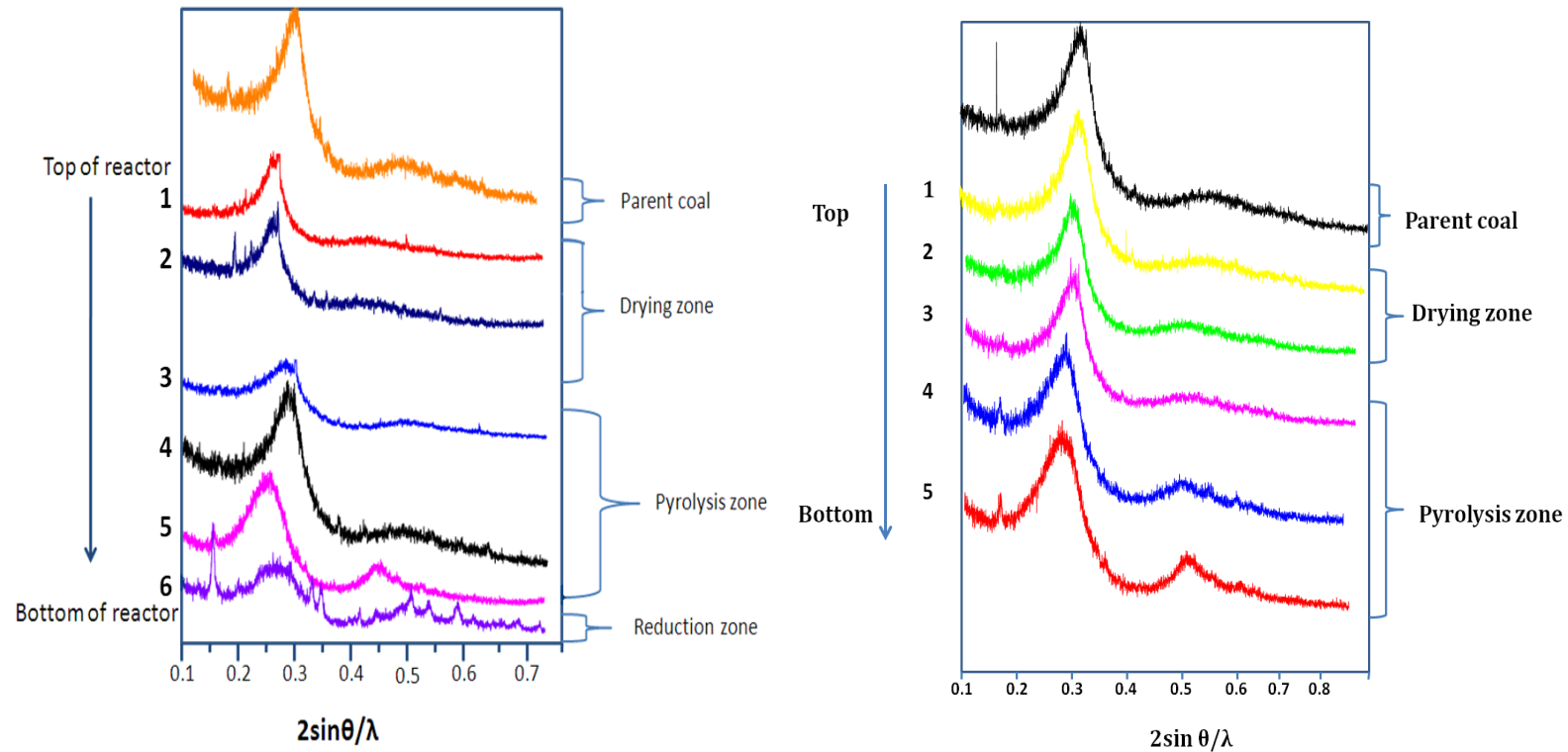


**Figure 4.9:** XRD patterns for Coal A (left) and B (right) parent coal samples and the packed-bed reactor generated samples.

This analysis shows that the crystallite ordering for both the Coal A and B parent coal samples and the packed-bed reactor generated samples, is more prominent within samples 4 to 5 in the packed-bed reactor generated samples. This is observed by the sharpness and broadening of the  $d_{002}$  peak, and the  $d_{100}$  peak becomes more visible at 419 to 671°C (samples 4 and 5). Since coal samples have crystallite domains, during heat treatment the crystallites tend to grow at higher temperatures forming a graphitic material like structure (Emmerich, 1995). The sharpness and broadening of the  $d_{002}$  peak during heat treatment was also observed by Lu et al. (2002) during pyrolysis and combustion of char samples.

Sample 6 for Coal B had retained a high ash content after the demineralization process (as shown in Table 4.5), and when XRD analysis was performed on this sample, the diffractogram still showed the presence of the ash content bands, which overlapped with the  $d_{002}$  band. This diffractogram was subsequently omitted because it was impossible to calculate XRD structural parameters due to the interference of the ash components.

#### **2.4.2.4 Quantitative results of the X-ray diffraction analysis.**

In order to obtain quantitative information from the diffractogram, curve fitting of the theoretical distribution was required. In this case, Gaussian fitting procedures were used by applying Origin Software as described in Section 3.3.2.4. XRD structural parameters were evaluated using an equation supplied by Lu et al. (2001), and are summarized in Tables 4.8 and 4.9, and the equations are attached in Appendix E.

## CHAPTER 4: RESULTS AND DISCUSSION

---

Walker (1971) has used different parameters for describing the deviations of the crystallite structure of carbon residues after heat treatment. This deviation can be easily described by the lattice constant in the  $c$  direction. The general meaning of this method is based on the experience that the lattice distance in the  $c$  direction increases greatly with decreasing crystalline order, whereas it does not change significantly in the  $a$  direction. The parameters describing the crystalline order are the mean crystallite sizes in the  $c$  and  $a$  directions ( $L_c$  and  $L_a$ ).

## CHAPTER 4: RESULTS AND DISCUSSION

**Table 4.8:** XRD structural parameters for the Coal A parent coal and the corresponding packed-bed reactor generated samples.

Sample	Temp (° C)	Reaction zone	$d_{002}$	Lc (Å)	N
Parent coal	25	-	3.44	7.49	3.08
1	111	Drying	3.38	7.17	3.21
2	200	Drying	3.45	6.78	2.88
3	289	Pyrolysis	3.50	6.50	2.98
4	419	Pyrolysis	3.57	6.94	2.91
5	671	Pyrolysis	3.64	7.26	3.51
6	1160	Reduction	3.64	9.19	3.00

$d_{002}$  = Interlayer spacing of crystallites in a unit cell, Lc = Average crystallite height in a unit cell, N = number of crystallite in a unit cell

**Table 4.9:** XRD structural parameters for the Coal B parent coal and its packed-bed reactor generated samples.

Sample	Temp (° C)	Reaction zone	$d_{002}$	Lc, (Å)	N
Parent	25	-	3.46	10.10	3.30
1	93	Drying	3.46	7.99	3.91
2	183	Drying	3.49	7.13	3.04
3	342	Pyrolysis	3.49	7.11	3.04
4	693	Pyrolysis	3.55	7.18	3.02
5	980	Pyrolysis	3.64	10.09	3.76
6	1225	Reduction	Na	Na	Na

$d_{002}$  = Interlayer spacing of crystallites in a unit cell, Lc = Average crystallite height in a unit cell, N = number of crystallite in a unit cell

## CHAPTER 4: RESULTS AND DISCUSSION

---

Petersen et al. (2004) have described a fully ordered graphite structure to have an interlayer spacing ( $d_{002}$ ) that ranges between 3.36 – 3.44 Å. The average interlayer spacing ( $d_{002}$ ) for Coal A and B parent coal samples studied were 3.44 and 3.46 Å respectively, which closely falls within the range of a graphitic material. However, from the end of the drying zone to the reduction zone (samples 3 – 6), there is a slight increase of the  $d_{002}$  (to 3.38 – 3.64 Å for Coal A, and 3.48 – 3.64 Å for Coal B). This increase shows some degree of ordering of the coal sample with an increase in temperature.

A decrease in the average stacking height of aromatic crystallites, ( $L_c$ ), is observed from the parent coal to the beginning of the pyrolysis zone at temperatures below 350 °C (sample 3). There is an increase in  $L_c$  from the middle of the pyrolysis zone (at temperatures above 400 °C) to the reduction zone for both Coal A and B packed-bed reactor generated samples. The decrease in  $L_c$  is due to the re-arrangement of aromatic crystallites caused by the drying and softening of the coal samples and release of the volatile matter species from the coal samples. The increase in  $L_c$  shows a growth in aromatic crystallite stacking leading to an increase in aromatic crystallite structural ordering resulting from re-hardening in the char particles. Wu et al. (2009) conducted a study on physical properties and CO<sub>2</sub> gasification reactivity between Chinese coal chars and petroleum cokes. According to the results obtained from the study, an increase in  $L_c$  was observed and it suggested that the increasing pyrolysis temperature result in a more ordered carbon crystalline structure of both the coal chars and the petroleum cokes. Petroleum cokes being more ordered than the coal chars.

Between samples 3 and 4 there is a change in the coal structure from softening to re-hardening in the char particles. This corresponds with the BET surface area analysis

## CHAPTER 4: RESULTS AND DISCUSSION

---

results whereby from samples 3 to 4 within the pyrolysis zone, a great increase in surface area was observed (Figure 4.8) for both Coal A and B packed-bed reactor generated samples.

The number of aromatic crystallites ( $N$ ) showed no apparent trend with regard to heat treatment from the parent coal samples to the end of the reduction zone. The number of aromatic crystallites remained between 2.88 - 3.51 and 3.02 - 3.91 (approximately 3 - 4) for Coals, A and B parent coal samples and packed-bed reactor generated samples. This implies that the crystallite stack of these coal samples increases by 1 during heat treatment within the four reaction zones. This is expected since the char particles generated become consumed within the reduction zone to form an ash residue.

The aromatic crystallite parameter variations imply that during pyrolysis that the rearrangement of aromatic carbons due to weakening and bond cleavage, accompanied by a release of weak carbon bonds is occurring, and thus leading to a decrease in  $L_c$ . When all of the weakly bound carbons have been released from the coal structure, the coal structure becomes more ordered and well aligned leading to an increase in  $L_c$ . Kidena et al. (1998) did similar work on semi-cokes, and reported similar conclusions regarding heat treatment and XRD structural parameters.

### **2.4.3.4 Comparison of Coal A and B packed-bed reactor generated samples.**

XRD structural parameters ( $L_c$ ,  $N$  and  $d_{002}$ ) for the Coal A and B packed-bed reactor generated samples follow the almost the same trend with regard to heat effect (as this is illustrated in Figure 4.10).

## CHAPTER 4: RESULTS AND DISCUSSION

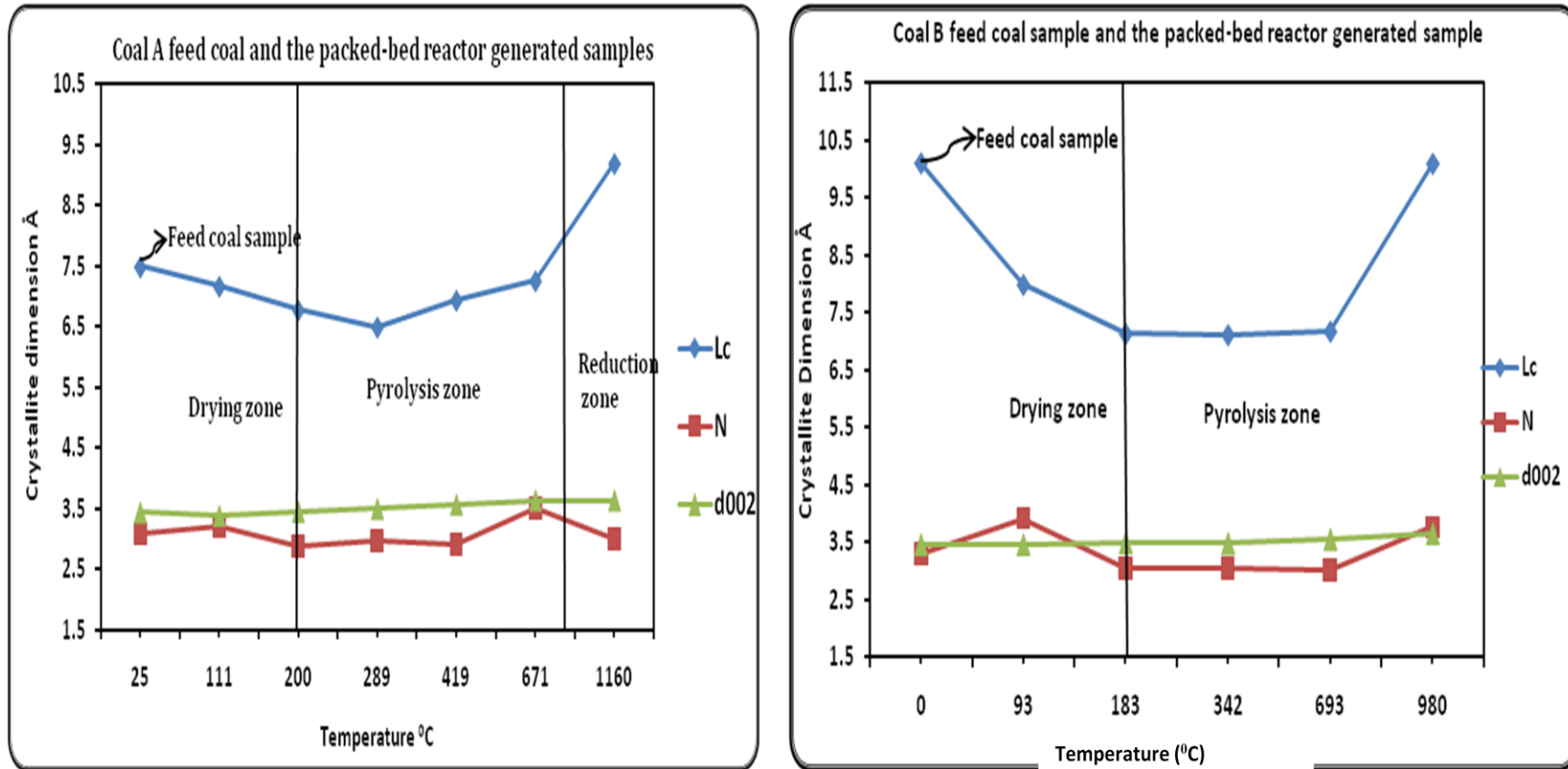


**Figure 4.10:** Relationship between temperatures and the XRD structural parameters of Coal A and B parent coals and the packed-bed reactor generated samples.

## CHAPTER 4: RESULTS AND DISCUSSION

---

One thing to note is that the Coal A packed-bed reactor generated samples start to become structurally more ordered at temperatures above 289 °C (between samples 3 and 4) whereas Coal B packed-bed reactor generated samples start to become structurally more ordered at temperatures above 693 °C (as shown in Figure 4.10) within the pyrolysis zone. When referring to structural ordering in this case, it is only  $L_c$  that is considered since this is the only structural parameter that appears to show variation between the Coal A and B packed-bed reactor generated samples. The  $L_c$  variation might be due to difference in surface area of these parent coal samples as observed earlier. Coal A parent coal sample had a higher surface area of 154 m<sup>2</sup>/g when compared to Coal B parent coal sample (117 m<sup>2</sup>/g).

When looking at other XRD structural parameters, both coals followed the same trend in terms of crystallite growth or structural ordering with regard to heat treatment within the four reaction zones.

In summary, it was noticed that it is important to demineralize coal samples prior to XRD analysis, so as to omit the mineral matter interference when calculating XRD parameters. When comparing the XRD parameters of the two different coal samples, they appeared to follow the same trend regarding to heat treatment, except for  $L_c$ . This parameter showed that Coal B is more ordered compared to Coal A. This is also supported by the results obtained from the BET surface area analysis which showed that Coal B has a lower surface area compared to Coal A. This may result to Coal B converting carbon at slower rates when compared to Coal A, because particles with a higher surface areas tend to have high reactivities with regard to heat treatment. Coal char CO<sub>2</sub> reactivity results reported earlier in Section 4.1.2 are in agreement with this statement. The



interlayer spacing  $d_{002}$  does not show a big change with regard to heat treatment. However, the packed-bed reactor generated samples were able to show structural variation within the four reaction zones of the packed-bed reactor combustor unit.

### **4.2.5 $^{13}\text{C}$ Solid State Nuclear Magnetic Resonance Spectroscopy ( $^{13}\text{C}$ SSNMR) analysis results.**

$^{13}\text{C}$  Solid state NMR is widely used to determine specific structural components and to obtain information pertaining to specific carbon functional group distributions in coal, as discussed in Chapter 3, Section 3.3.2.5. Cross-polarization (CP), magic angle spinning (MAS), and dipolar dephasing (DD) are the techniques that allow for the characterization of a variety of average chemical structural features in the coal samples. In this study, the former mentioned techniques were performed to obtain qualitative and quantitative data. Usually these techniques will all be performed on coals to determine all of the carbon structural features associated with aromatic and aliphatic bonding. These features include the carbon aromaticity, the number of bridges and loops per cluster, the number of side chains per cluster, the fraction of carbons that are bridge-heads, the average number of carbons per aromatic cluster, and the average number of aliphatic carbons (Perry et al., 2000). A more time-consuming DP/SPE experiments was not conducted in this study. This is because the study aims at studying the structural variation of the coals and its chars, not to actually quantify the parameters for structural elucidation.

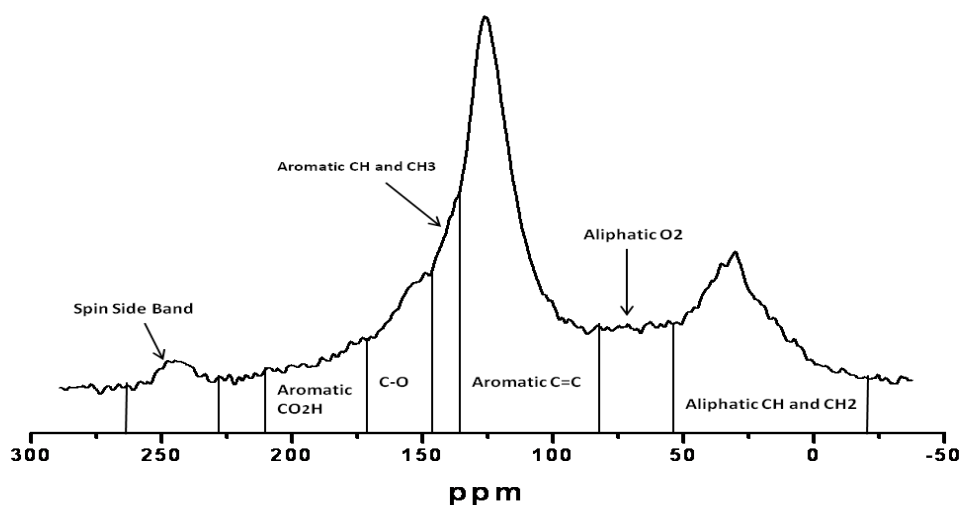


**Figure 4.11:**  $^{13}\text{C}$  CP/MAS NMR spectra for the parent coal sample.

A typical  $^{13}\text{C}$  CP/MAS NMR spectrum produced from the coal samples used in this study is illustrated in Figure 4.11. This spectrum shows two big broad bands representing aromatic and aliphatic carbons. A small spin side band with a low intensity was also observed, and it is believed that it corresponds to a central signal of the aromatic structure units (Straka et al., 2002). The non-protonated aromatic band ranges from 218 ppm to 96 ppm. This band overlaps that of the phenolic carbons band ( $f_a^P$ ) that ranges from 157 ppm to 146 ppm, alkylated carbons ( $f_a^S$ ) which range from 146 ppm to 131 ppm, and aromatic carbons at 131 ppm to 96 ppm. An additional band due to carbonyl carbons ( $f_a^{C=O}$ ) bonded to aromatic rings as side chains was observed at 218 ppm to 157 ppm. Aliphatic carbons such as  $-\text{CH}_2$  and  $\text{CH}_3$  are observed at 54 ppm to -10 ppm. The aliphatic carbons can be further sub-divided into those that are bonded to oxygen ( $f_{al}^O$ ), non-protonated ( $f_{al}^{N^*}$ ) and protonated aliphatic carbons ( $f_{al}^H$ ). A clearly demonstrated spectrum is attached in the Appendix F, Figure F1 and the integral values are in Table F1.

### 2.4.1.5 Qualitative $^{13}\text{C}$ SSNMR analysis results of the parent coal samples and the packed-bed reactor generated samples.

$^{13}\text{C}$  CP-MAS NMR spectra for the Coal A (left) and B (right) packed-bed reactor generated samples is illustrated in Figure 4.12. It is observed that at the top of drying zone, sample 1 (in both coals) is rich in aromatic rings when compared to the other packed-bed reactor samples i.e. this was confirmed by comparing the ratio of the aromatic peak intensity to that of the aliphatic peak. Upon heating, the aliphatic peak decreases with no distinct corresponding increase or decrease in the aromatic peak to the end of pyrolysis zone (sample 4 in Figures 4.12 on the left hand side and sample 5 in 4.12 on the right hand side). The disappearance of the aliphatic carbon band is clearly observed in sample 4 (Figure 4.12 on the left hand side) and sample 5 (Figure 4.15 on the right hand side). These are samples heated at temperatures above  $400\text{ }^{\circ}\text{C}$  for both coals and the disappearance of the aliphatic peak shows that at these temperatures there appears to be small quantity of aliphatic carbons remaining in the coal. This was also evident in XRD analysis results, where at temperatures above  $400\text{ }^{\circ}\text{C}$  (from sample 4) the crystallite structure of coal became more structurally ordered because the coal began to re-harden to form char particles and they tend to become more like a graphitic material.

## CHAPTER 4: RESULTS AND DISCUSSION

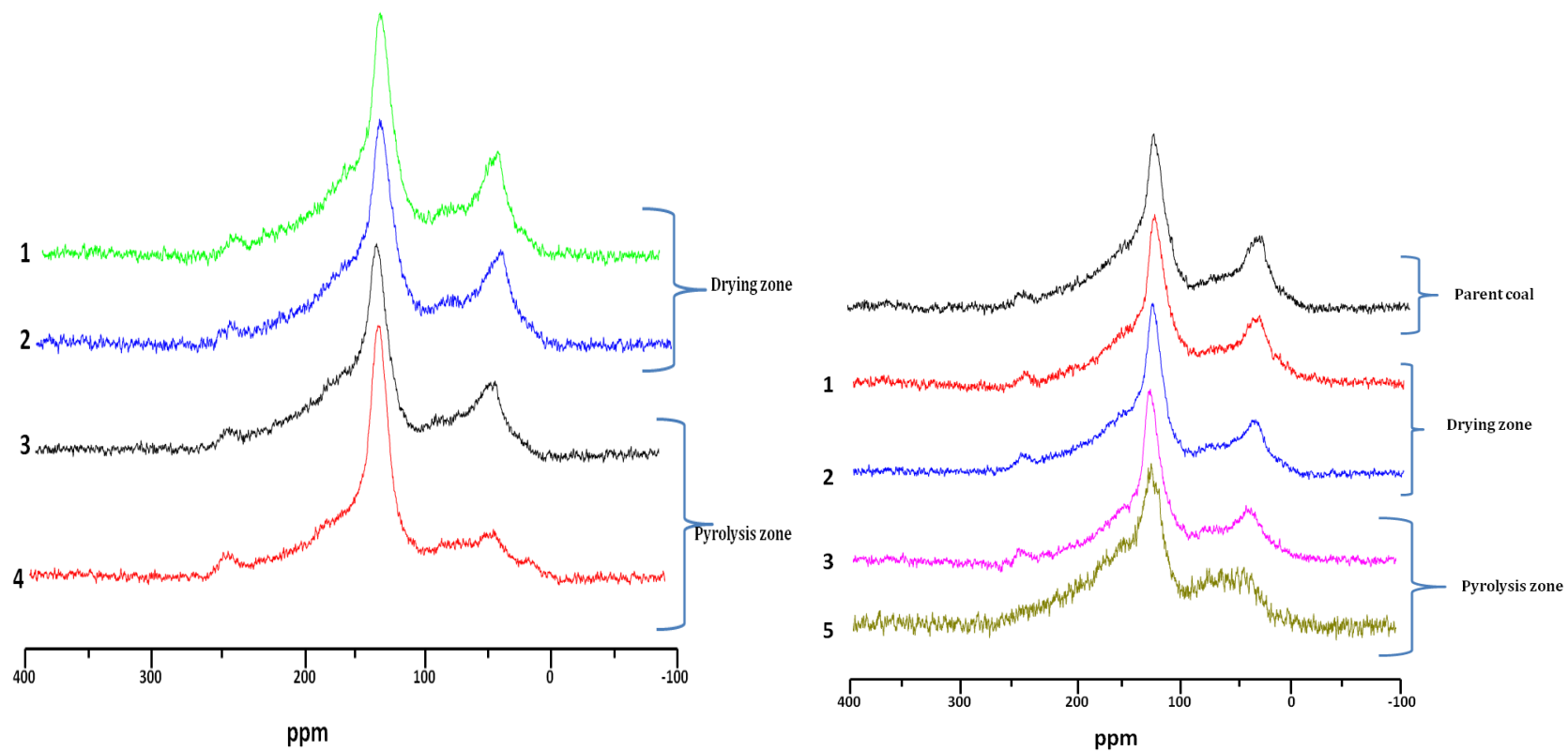


**Figure 4.12:**  $^{13}\text{C}$  CP/MAS NMR spectra for Coal A (left) and B (right) parent coals and the packed-bed reactor generated samples.

## CHAPTER 4: RESULTS AND DISCUSSION

---

When looking at the phenols and the carboxylic carbons (band ranges from 157 ppm to 146 ppm and from 218 ppm to 157 ppm respectively) within this zone (pyrolysis zone), the shoulder band of the phenols did not seem to be visible. The only shoulder band that was visible within this zone was the alkylated carbon shoulder band (ranging from 146 ppm – 131 ppm). This implies that only alkylated and aromatic carbons are present at the end of pyrolysis zone at temperatures above 400 °C. This implies then that these carbons are the ones that form the structure of char.

At the end of pyrolysis zone for Coal B (sample 5 in Figure 4.12 on the right hand side), the spectrum appeared to have two broad peaks with very high signal to noise ratio (as shown in Figure 4.12 on the right hand side). This was due to the high conductivity of chars and possibly due to the presence of paramagnetic species present in the coal sample. It was therefore decided not to quantify this spectrum. To confirm this, a conductivity test for all the packed-bed reactor generated samples was performed, and the above mentioned statement was confirmed to be true. The conductivity results are attached in the Appendix F, with further discussion. Samples 6 and 7 were omitted from the analysis since they contained high amount of mineral matter and ash content and the analysis requires only a very low mineral matter or ash free sample. The demineralization process utilized was not able to extract all of the mineral and ash content in these samples.

### **2.4.2.5 Quantitative $^{13}\text{C}$ SSNMR analysis results for the parent coal and the packed-bed reactor generated samples.**

The quantitative analysis results determined 11 structural parameters in the samples used in this study, with the aid of CP-MAS and  $^{13}\text{C}$ - $^1\text{H}$  dipolar dephasing experiments. The 11 structural parameters of coals were calculated using the aromatic peak as the reference peak at 126.56 ppm for all obtained spectra as discussed in Chapter 3, Section 3.3.2.5. Six structural parameters were calculated using  $^{13}\text{C}$  CP-MAS NMR and the other five were calculated using dipolar dephasing experimental data. The method used to determine these structural parameters is a combination of methods utilized by Solum et al. (1989) and Suggate and Dickson (2004), and the spin side band intensity was taken into consideration. The structural parameters are summarized in Tables 4.10 and 4.11 and the equations used to calculate these structural parameters are attached in Appendix E.

## CHAPTER 4: RESULTS AND DISCUSSION

**Table 4.10:** Summary of structural parameters for Coal A and the packed-bed reactor generated samples derived from  $^{13}\text{C}$  Solid state NMR analysis.

Coal	$f_a$	$f_{al}$	$f_a^{\text{CO}}$	$f_a^{\text{P}}$	$f_a^{\text{S}}$	$f_a^{\text{N}}$	$f_a^{\text{H}}$	$f_a^{\text{B}}$	$f_{al}^{\text{N}^*}$	$f_{al}^{\text{H}}$	$f_{al}^{\text{O}}$
Parent	0.60	0.4	0.04	0.06	0.11	0.23	0.4	0.07	0.08	0.28	0.06
1	0.63	0.37	0.06	0.07	0.1	0.28	0.37	0.3	0.07	0.15	0.08
2	0.68	0.32	0.07	0.07	0.11	0.51	0.3	0.4	0.05	0.14	0.05
3	0.69	0.31	0.07	0.07	0.11	0.78	0.2	0.62	0.05	0.14	0.06
4	0.75	0.25	0.05	0.05	0.1	0.99	0	0.81	0.02	0.13	0.06

**Table 4.11:** Summary of structural parameters for Coal B and its packed-bed reactor generated samples derived from  $^{13}\text{C}$  Solid state NMR analysis.

Coal	$f_a$	$f_{al}$	$f_a^{\text{CO}}$	$f_a^{\text{P}}$	$f_a^{\text{S}}$	$f_a^{\text{N}}$	$f_a^{\text{H}}$	$f_a^{\text{B}}$	$f_{al}^{\text{N}^*}$	$f_{al}^{\text{H}}$	$f_{al}^{\text{O}}$
Parent	0.64	0.36	0.04	0.06	0.11	0.23	0.41	0.07	0.08	0.28	0.06
1	0.69	0.31	0.09	0.09	0.12	0.45	0.24	0.24	0.11	0.20	0.06
2	0.73	0.27	0.08	0.08	0.10	0.00	1.61	0.00	0.00	0.77	0.05
3	0.75	0.25	0.09	0.09	0.12	0.87	0.00	0.65	0.05	0.19	0.05
5	0.66	0.34	0.09	0.09	0.11	0.82	0.00	0.63	0.12	0.22	0.08

$f_a$  = total fraction of aromatic carbons,  $f_{al}$  = total fraction of aliphatic carbons,  $f_a^{\text{CO}}$  = fraction of carbons bonded to carbonyls,  $f_a^{\text{P}}$  = fraction of carbons bonded to phenolic esters,  $f_a^{\text{S}}$  = fraction of carbons bonded to alkylated carbons,  $f_a^{\text{N}}$  = fraction of non-protonated carbons and CH<sub>3</sub> in aromatic region,  $f_a^{\text{H}}$  = fraction of protonated carbons,  $f_a^{\text{B}}$  = fraction of bridgehead carbons,  $f_{al}^{\text{N}^*}$  = fraction of non-protonated carbons and CH<sub>3</sub> in aliphatic region,  $f_{al}^{\text{H}}$  = fraction of protonated carbons and CH<sub>3</sub> in aliphatic region,  $f_{al}^{\text{O}}$  = aliphatic carbons bonded to oxygen

Quantitative analysis confirmed that both parent coal samples (Coal A and B) were rich in aromaticity; the fraction of aromatic carbons ( $f_a$ ) on these coals was 0.60 (60%) and 0.64 (64%) respectively. This analysis also revealed that as the temperature increased,

## CHAPTER 4: RESULTS AND DISCUSSION

---

the aromaticity increases with a corresponding decrease in aliphaticity. Fraction of aromatic carbons and fraction of aliphatic carbons are the only structural parameters that show a variation for Coal A and B packed-bed reactor generated samples. The fraction of aromatic carbons bonded to carbonyls ( $f_a^{CO}$ ), phenolic esters ( $f_a^P$ ) and alkylated carbons ( $f_a^S$ ) remained unchanged. Fractions of aromatic carbons bonded to non-protonated carbons and  $CH_3$  ( $f_a^N$ ) increased with a decrease in aromatic carbons bonded to protonated carbons in both Coal A and B packed-bed reactor samples. This was due to the fact that protonated carbons have weak bonds and tend to break faster when compared to non-protonated carbons.

The fraction of bridge-head aromatic carbons ( $f_a^B$ ) was found to increase as the temperature increased. Bridgehead carbons are aromatic carbons that are connected to other aromatic carbons. The structure of coal is connected by bridge head structures, so when heat is applied to the coal, the aliphatic carbons on the bridge head aromatic carbons tend to break and released as volatiles are released. The aromatic bridge heads will remain and reconnect with other aromatic ring structures forming well ordered crystallites and be consumed at significantly higher temperatures. Hence a good correlation between volatile matter and fraction of aromatic carbon is observed from parent coal sample to the middle of pyrolysis zone (sample 4), as illustrated in Figure 4.13.



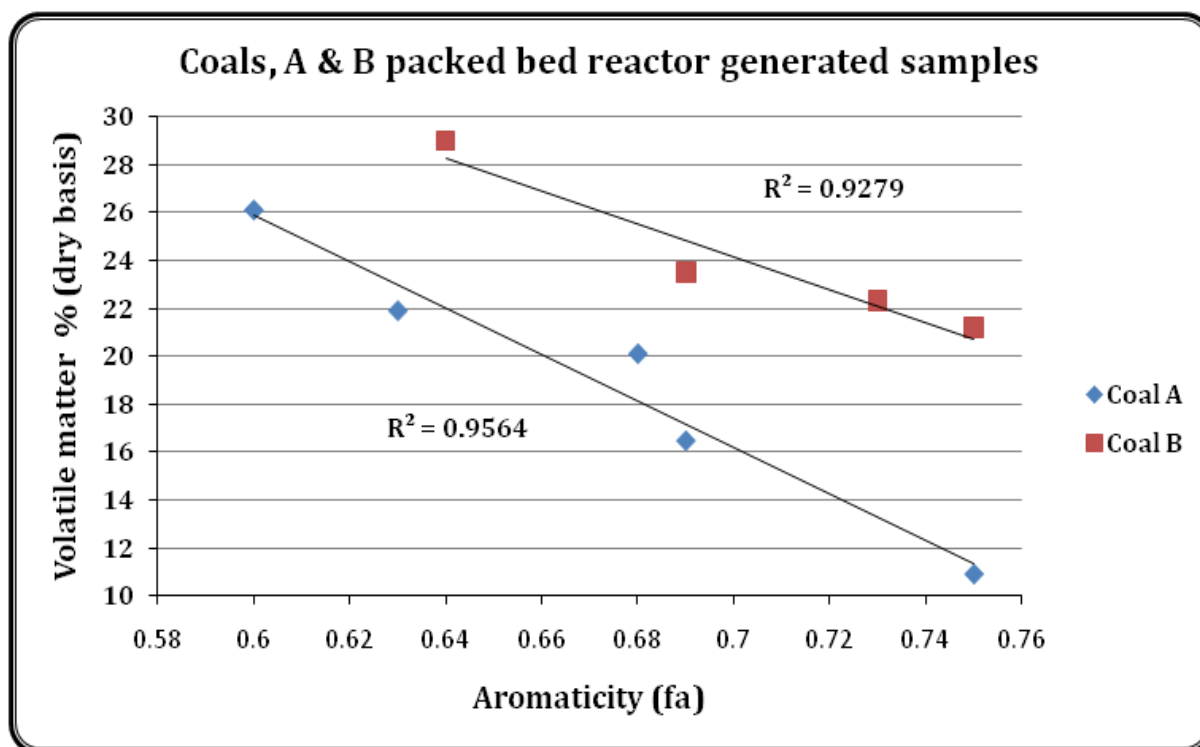


**Figure 4.13:** Correlation of volatile matter content of Coal A and B as a function of aromaticity value.

A good correlation between volatile matter content and the aromaticity values for the Coals, A and B parent coal samples and the packed-bed reactor generated samples was obtained. This is due to the fact that proximate analysis reflects the nature of the coal atomic bonding and good correlations are expected to exist between the volatile matter or fixed carbon and many other coal properties. As the aromaticity increases the volatile matter content decreases. This was in agreement with the statement made when discussing the FTIR analysis results in Section 4.2.2, i.e. during pyrolysis the weakest bonds break producing molecular fragments and the fragments abstract hydrogen from hydroaromatics or aliphatics, thus increasing the aromatic hydrogen concentration of coal (Solomon et al. 1988).

## CHAPTER 4: RESULTS AND DISCUSSION

---

No discussion will be given on the fraction of aliphatic carbons bonded to the non-protonated, protonated carbons, and fraction of aliphatic carbons bonded to the oxygen groups since they did not show variation with an increase in temperature.

Samples in the reduction and combustion zone were not quantified due to the high conductivity and the presence of paramagnetic species in these samples. This leads to high signal to noise ratio of the spectra. High conductivity of the coal chars results in the under-estimation of the internal carbons in the aromatic ring structures, or these tend not to be observed during analysis due to saturation. This was also observed by Miyoshi et al. (1997).

Thus the above results revealed that the Coal A parent coal sample appeared to have fewer aromatic rings when compared to the Coal B parent coal sample.  $^{13}\text{C}$  Solid state NMR data gave a clear insight into the changes occurring in the parent coal samples from the drying zone to the end of pyrolysis zone with regard to heat treatment. This was not the case in the reduction and combustion zones due to the highly ordered crystallite structure of the chars. The samples in the reduction and combustion zones were shown to be highly conductive, and the conductivity results are attached in the Appendix G. To obtain good results for quantitative analysis for coal samples, a good demineralization method is required. Both packed-bed reactor generated samples (Coal A and B) appear to follow the same trend with regard to heat treatment. Whilst  $^{13}\text{C}$  SSNMR proved to be a good analysis when it came to structural characterization of coal and char samples, there is still a room for improvement so that this analysis can possibly be considered for use on a daily basis to improve coal conversion processes. This is further discussed in Chapter 5 under recommendations.

### 4.2.6 Summary of Phase 2

The combined use of FTIR, XRD, BET adsorption and  $^{13}\text{C}$  SSNMR gave a significant insight into the structural changes occurring as a result of heat treatment from the four reaction zones identified in the packed-bed reactor. The combination of the above mentioned techniques revealed that structural disordering occurs as early as the drying zone, and that the major structural changes are observed to occur in the pyrolysis zone. Qualitative FTIR analysis was able to show only the changes occurring within the four reaction zones of the packed-bed reactor combustor unit and unable to reveal which coal was converted more efficiently. FTIR also revealed that Coal A and B are rich in aromatic carbons, and this was evidenced from the presence of the prominent  $-\text{C}=\text{C}-$  band at  $1600\text{ cm}^{-1}$  and the presence of the less prominent  $-\text{CH}_2$  and  $-\text{CH}_3$  at  $2918$  and  $2859\text{ cm}^{-1}$ . BET surface area analysis using  $\text{CO}_2$  as adsorbent gas showed that the Coal A parent coal sample and the corresponding packed-bed reactor generated samples have a higher surface area when compared to the Coal B samples. It is well documented in literature that high surface area leads to fast internal heat treatment (Sadhukhan et al., 2009). XRD revealed that structural ordering for the Coal A packed-bed reactor generated samples starts at  $290\text{ }^\circ\text{C}$  whereas for the Coal B packed-bed reactor generated samples it starts above  $400\text{ }^\circ\text{C}$ . This means that the Coal B is more ordered and has a high quantity of aromatic crystallites, which is proven by difference in  $L_c$  values, where the Coal B had high values of  $L_c$  when compared to the Coal A.  $^{13}\text{C}$  SSNMR studies showed that the Coal B parent coal sample is rich in aromatic rings compared to the Coal A parent coal sample. This might explain the observation revealed by XRD analysis, whereby structural ordering of the Coal A packed-bed reactor generated samples were

## CHAPTER 4: RESULTS AND DISCUSSION

---

observed to start at different temperatures when compared to the Coal B packed-bed reactor generated samples.

The above coal structural findings obtained from the four analytical techniques are in agreement with each other. Coal samples with high surface areas are generally more reactive due to faster internal heat transfer; this might lead to earlier structural ordering of the coal char samples.  $^{13}\text{C}$  SSNMR studies also confirmed that the Coal A has fewer aromatic rings when compared to Coal B. It is also known that fewer aromatic rings lead to high probability of the coal's ability to react faster to heat treatment.

No conclusive structural changes were obtained in the reduction and combustion zone due to the high conductivity of chars and since these two processes occur at higher temperatures. This implies that it is difficult to obtain char structural information using some of the above mentioned techniques, and the use of organic petrographic analysis can possibly also become very useful in the classification of chars in these zones. This is discussed further in phase 3.

A combination of molecular structural analysis together with organic petrographic analysis can thus possibly be useful in the understanding, advancement and manipulation of the lump coal conversion process outcome. Significant findings determined from FTIR, BET, XRD and  $^{13}\text{C}$  SSNMR are summarized in Table 4.12 below.

## CHAPTER 4: RESULTS AND DISCUSSION

**Table 4.12:** Summary of significant findings obtained from FTIR, BET adsorption studies, XRD and  $^{13}\text{C}$  SSNMR.

Analytical technique	Coal A	Coal B
<b>FTIR</b>	<ul style="list-style-type: none"> <li>➤ -C=C- band at <math>1600\text{ cm}^{-1}</math> was more prominent and -CH<sub>2</sub> and -CH<sub>3</sub> bands at <math>2918</math> and <math>2859\text{ cm}^{-1}</math> were less prominent, the coal is rich in aromatic carbons.</li> </ul>	<ul style="list-style-type: none"> <li>➤ -C=C- band at <math>1600\text{ cm}^{-1}</math> was more prominent and -CH<sub>2</sub> and -CH<sub>3</sub> bands at <math>2918</math> and <math>2859\text{ cm}^{-1}</math> were less prominent, the coal is rich in aromatic carbons.</li> </ul>
<b>BET adsorption</b>	<ul style="list-style-type: none"> <li>➤ Parent coal sample has high surface area.</li> <li>➤ Re-opening of micro-pores occurs at lower temperatures of <math>289\text{ }^{\circ}\text{C}</math> to <math>419\text{ }^{\circ}\text{C}</math>.</li> <li>➤ Micro-pore transformation to meso-pore occurs at <math>671\text{ }^{\circ}\text{C}</math>.</li> </ul>	<ul style="list-style-type: none"> <li>➤ Parent coal sample has low surface area.</li> <li>➤ Re-opening of micro-pores occurs at lower temperatures of <math>342\text{ }^{\circ}\text{C}</math> to <math>693\text{ }^{\circ}\text{C}</math>.</li> <li>➤ Micro-pore transformation to meso-pore occurs at <math>980\text{ }^{\circ}\text{C}</math>.</li> </ul>
<b>XRD</b>	<ul style="list-style-type: none"> <li>➤ Parent coal sample has low <math>L_c</math> value, structurally less ordered.</li> <li>➤ Coal structure becomes more ordered at temperatures above <math>289\text{ }^{\circ}\text{C}</math>.</li> </ul>	<ul style="list-style-type: none"> <li>➤ Parent coal sample has high <math>L_c</math> value, structurally more ordered.</li> <li>➤ Coal structure becomes more ordered at temperatures above <math>693\text{ }^{\circ}\text{C}</math>.</li> </ul>
<b><math>^{13}\text{C}</math> SSNMR</b>	<ul style="list-style-type: none"> <li>➤ Parent coal sample has <math>f_a</math> value of <math>0.60</math> (60%), less aromatic carbons.</li> <li>➤ Parent coal has <math>f_{al}</math> value of <math>0.40</math> (40%).</li> <li>➤ Volatile matter decreases as aromaticity (<math>f_a</math>) increases from parent coal sample to pyrolysis zone.</li> </ul>	<ul style="list-style-type: none"> <li>➤ Parent coal sample has <math>f_a</math> value of <math>0.64</math> (64%), more aromatic carbons.</li> <li>➤ Parent coal has <math>f_{al}</math> value of <math>0.36</math> (36%).</li> <li>➤ Volatile matter decreases as aromaticity (<math>f_a</math>) increases from parent coal sample to pyrolysis zone.</li> </ul>

### 4.3 PHASE 3: Petrographic results

The third phase of this study involves petrographic analysis of two different feed lump coal samples (Coal A and B) and their packed-bed reactor generated samples. This study was undertaken to investigate the morphological nature and behaviour of the organic and inorganic matter within the four reaction zones of the packed-bed reactor.

Petrographic analysis deals with the identification and characterization of organic and inorganic constituents of coal and the degree of metamorphosis to which they have been subjected at their time of burial. Petrography is of great importance as it is known that the different petrographic constituents of coal will behave differently under various processing conditions (Hessley et al., 1985). There are three coal components that can be determined by petrographic analysis, namely: maceral, microlithotype and mineral matter, and these are discussed in detail in Chapter 2, Section 3.3.3. In addition, petrography can be used to characterize the carbon conversion by analyzing devolatilized coal and char morphology as discussed in Chapter 2, Section 3.3.3.2.

The generated packed-bed reactor samples resembled the morphological structure of cokes. This led to the utilization of the petrographic carbon particle type analysis classification method proposed by Wagner (2005); and this method is discussed further in Chapter 3, Section 3.3.3.2. Total reflectance analysis was also performed in attempt to correlate temperature changes of the packed-bed reactor generated samples within the four reaction zones identified.

## CHAPTER 4: RESULTS AND DISCUSSION

### 4.3.1 Maceral group analysis

Maceral group analysis was performed on the parent coal samples (Coal A and B). Since South African coals are known to be inertinite-rich, it was a necessity to further subdivide this maceral (inertinite) into three different subgroups (as illustrated in Table 4.13). The inertinite subgroups were further divided into reactive and inert maceral components.

**Table 4.13:** Maceral group analysis and rank value for the parent coal.

Macerals, vol %	Coal A	Coal B
Vitr	22.2	23.8
Lipt	4.8	3.4
Inrt SMF	34.0	31.6
Rct SMF	2.6	4.0
Inrt INTD	19.8	5.2
Rct INTD	5.0	22.4
Fus	2.4	3.2
Mic	1.6	5.4
Min	7.6	4.8
Rank (mr RoV %)	0.62	0.64

Vitr = Vitrinite, Lipt = Liptinite, Inrt SMF = Inert Semifusinite, Rct SMF = Reactive Semifusinite, Inrt INTD = Inert Inertodetrinite, Rct INTD = Reactive Inertodetrinite, FUS = Fusinite, Micr = Micrinite, MIN = Minerals, mr RoV % = mean random vitrinite reflectance

The two parent coal samples illustrated in Table 4.13 do not differ significantly in terms of the main maceral groups and coal rank. The rank values indicate that the coals are of

## CHAPTER 4: RESULTS AND DISCUSSION

---

bituminous rank C coals. The vitrinite content indicates a low vitrinite coal, which is typical of RoM coals from Highveld. The vitrinite, liptinite, inert semifusinite, reactive semifusinite, fusinite and micrinite of both parent coal samples did not differ significantly in their content. Inert inertodetrinite and reactive inertodetrinite appeared to be very different in their maceral contents; Coal A having high content of inert inertodetrinite (19.8 vol %) and Coal B having high reactive inertodetrinite content (22.4 vol %). South African coal typically have less than 5 vol % of liptinite content, with sporite and cutinite being the most dominant liptinite submacerals. No attempt was made in identifying the types of mineral matter present in these coals by petrographic analysis as this was beyond the scope of the current investigation. Typically the mineral matter consists of silicates (clays and quartz) with minor amounts of pyrite and carbonate.

Steyn and Smith (1977) determined that the maceral regarded as inert (inertinite) are in fact reactive and they proved that the typical Gondwana coals produce a better coke than the vitrinite-rich coals from Northern Hemisphere. Reactive inertinite is not a separate maceral but a sub-category of inertinite (Semifusinite and Inertodetrinite) that undergoes radical changes during carbonization. Reactive inertinite is believed to be of reflectance intermediate between that of vitrinite and inertinite (Kruszewska, 1989). Allocation of the inertinite group maceral into reactive and inert sub-categories has a significant impact in the coal conversion processes (as illustrated in Table 4.14). The term “reactive” in this context refers those macerals that ignite and combust rapidly in the presence of oxygen. Inert macerals are those macerals that are slow to change and they require more heat and oxygen in order to ignite and take longer time to burn out (Falcon and Ham, 1988).



## CHAPTER 4: RESULTS AND DISCUSSION

---

**Table 4.14: A summarized reactive and inert macerals for the parent coal samples.**

<b>Macerals</b>	<b>Coal A, vol %</b>	<b>Coal B, vol %</b>
Total Reactive macerals	34.6	53.6
Total Inert macerals	57.8	45.4
Total Inertinites	65.4	71.8

Total Reactive macerals = Lipt + Vitr + Rct SMF + Rct INTD; Total Inert Macerals = Int SMF + Int INTD + Fusinite + Micrinite; Total Inertinites = Rct SMF + Inrt SMF + Rct INTD + Inrt INTD + Mic + Fus

From Table 4.14, Coal A comprises of 34.6 vol % reactive macerals of which, 78 % is from liptinite and vitrinite. Coal B has 53.6 vol % of reactive macerals of which 49 % is from liptinite and vitrinite, the other 51 % is from reactive semifusinite and reactive inertodetrinite contents. Both parent coals have high inertinite contents with Coal B having a slightly higher inertinite content value relative to Coal A. The 49/51 split between reactive maceral for Coal B may explain the lower reactivity compared to Coal A. Inertinites are aromatic in nature, whereas liptinite and vitrinite are aliphatic in nature meaning that their reactivity will not be the same during gasification or combustion. This is also supported by Borrego et al. (1997) whereby it was suggested that inertinite-rich parent coals will have low reactivity as the inertinite content increases. Hence, this was attributed to highly cross-linked structure of the inertinites. The aromatic rings tend to restrict the aliphatic structure from igniting and combusting leading to a slower coal conversion reaction process, and thus the lower reactivity for Coal B. This also causes Coal B to run cooler in the drying zone (sample 1-2) and achieve higher temperatures in the hotter regions of the reactor (as illustrated in Table 4.1). The 78 % reactive macerals from liptinite and vitrinite macerals makes Coal A to be more reactive due to

## CHAPTER 4: RESULTS AND DISCUSSION

---

the aliphatic nature of liptinite and vitrinite macerals; and thus, the reactive inertinite do not restrict the aliphatic structures from igniting since they are lower in content. This leads to higher temperatures in the drying zone (sample 1-2), and lower temperatures in the hotter regions of the reactor; sample 5-7 (as illustrated in Table 4.1) and thus, a higher reactivity for Coal A. Nomura et al. (1998) and Kidena et al. (1998) studied the nature of plastic phenomena of vitrinite-rich and inertinite-rich fractions of two bituminous coals utilizing a number of techniques. They reported that the inertinite-rich fractions exhibited little fluidity in the plastic temperature.  $^{13}\text{C}$  NMR suggested that they had a larger size of aromatic clusters, a less amount of substituent (alkyl- and oxygen functional groups) on aromatic rings and a higher density of cross-linking than the vitrinite-rich fractions (Nomura et al., 1998 and Kidena et al., 1998). In all, this indicates that the reactivity behaviour of the parent coal samples is highly influenced by the petrographic composition of coal samples.

Thus whilst the total inertinite content is comparable, the breakdown between the reactive and inert macerals has provided some indication to a possible reason for the difference in performance between the two coals. The difference is beyond possible margins of error and is likely to be big enough for a difference in coal behaviour during heating. A difference of greater than 10 % can be considered to be of significance petrographically (as per personal communication with N.J. Wagner, 2011).

### **4.3.2 Carbon particle type analysis**

Carbon particle type analysis was conducted to determine the petrographic constituents of the packed-bed reactor generated samples and their maceral associations (micro-

## CHAPTER 4: RESULTS AND DISCUSSION

---

lithotype), together with the morphological structural changes. This analysis was undertaken as petrography is a useful analytical tool when considering carbon conversion as the formation and consumption of chars can be tracked. This information can be used to support and confirm results presented in Phases 1 and 2. It is hoped that this section will bring more insight in to what is occurring within the reduction and combustion zones of the packed-bed reactor; the structural analysis discussed in Phase 2 provided limited information regarding the conversion behaviour at higher temperatures.

Petrographic photographs of coal, devolatilizing coal and char particles observed for the packed-bed reactor generated samples are illustrated in Figures 4.14 - 4.16. The first Figure presents the type of coal macerals before heat treatment observed in the two coal samples. As the temperature is increased, the first phase of the coal softening process is the formation of pores in the reactive macerals (as shown in Figure 4.15). Thereafter chars are produced as illustrated in Figure 4.16. Stach et al. (1982) revealed that in the plastified mass only the inertinites can be recognized and distinguished from the softening coal by a discernible relief. When the resolidification temperature has been reached, there is no longer any difference in relief between the reactive and inertinite macerals. The raw data of the carbon particle type analysis results for both Coal A and B packed-bed reactor generated samples is attached in the Appendix H. Figures 4.17 and 4.18 represent results of the carbon particle type analysis.

**Coal macerals**

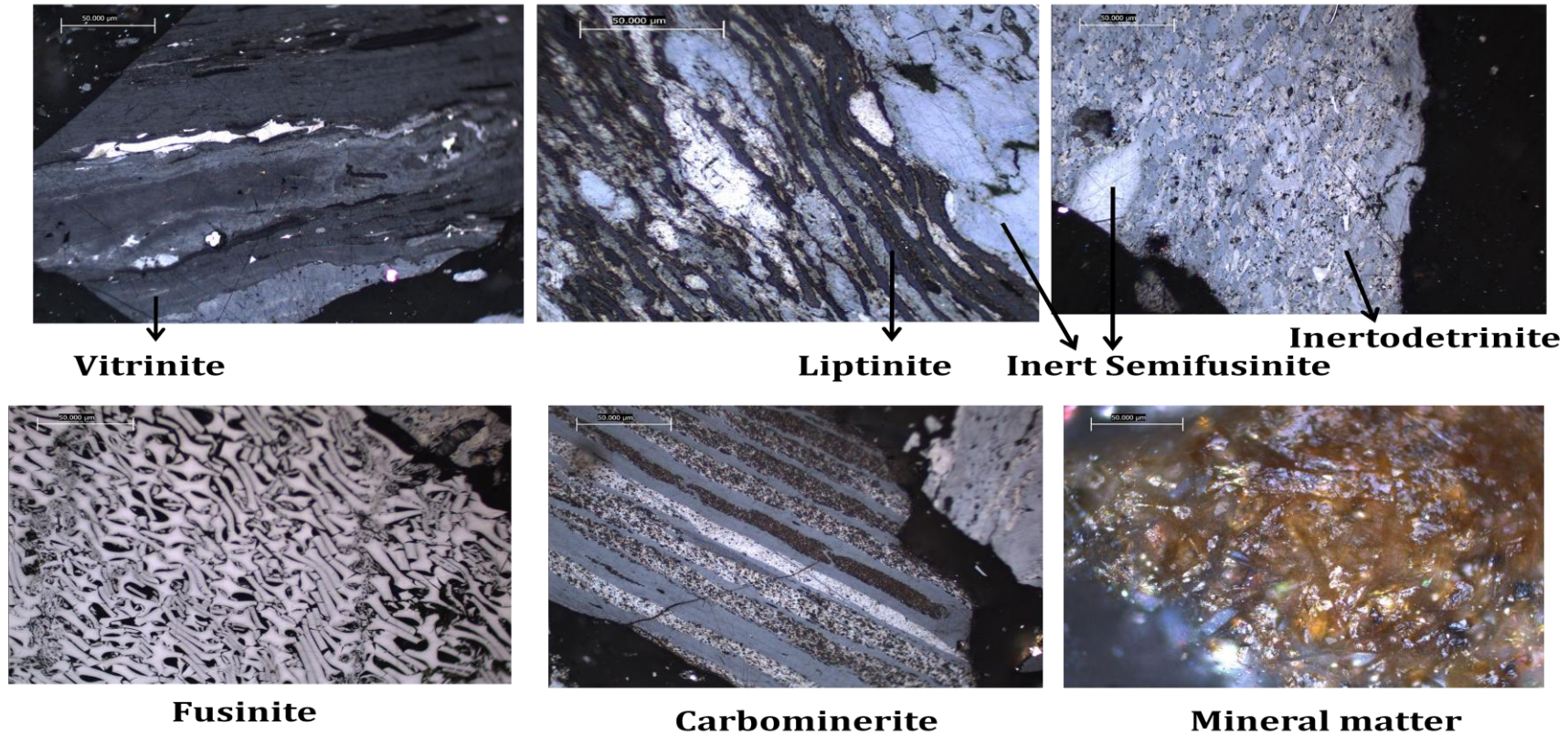
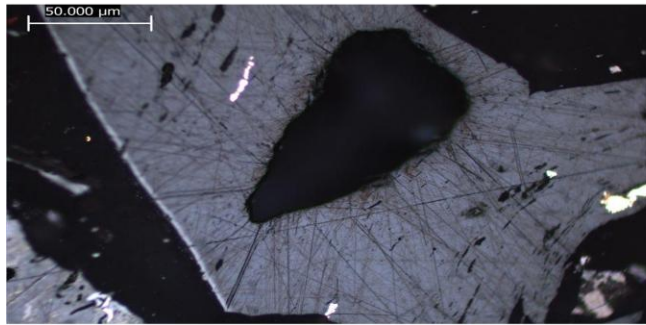


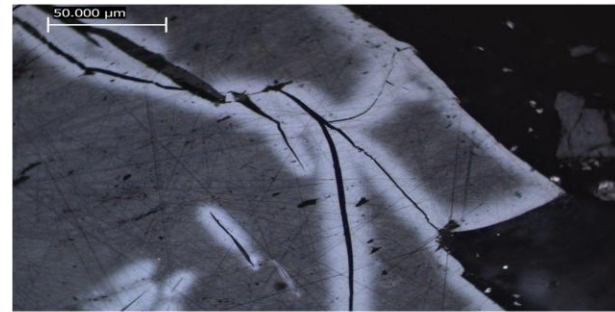
**Figure 4.14:** Micrographs showing coal groups observed from the packed-bed reactor samples (magnification x500, oil immersion, reflected light).



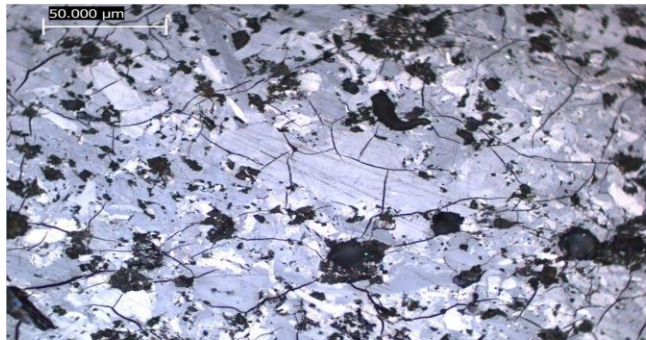
**Devolatilized Coals**



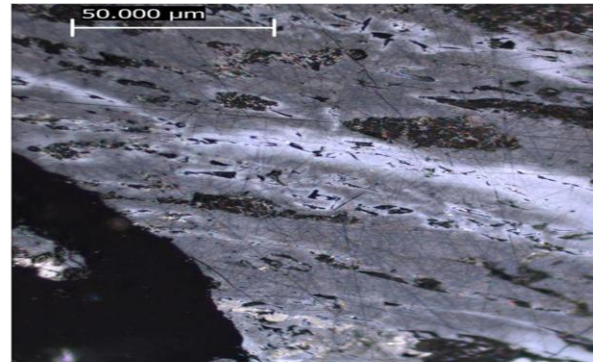
**Porous devolatilizing coal**



**Cracked with colour change devolatilized coal**



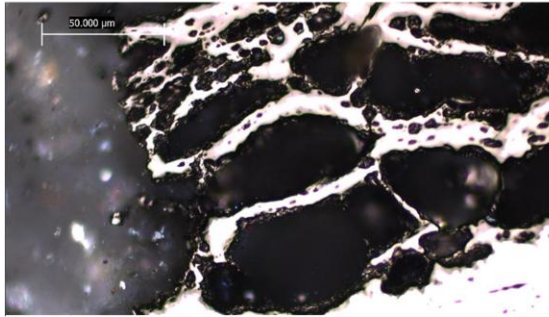
**Cracked devolatilizing coal**



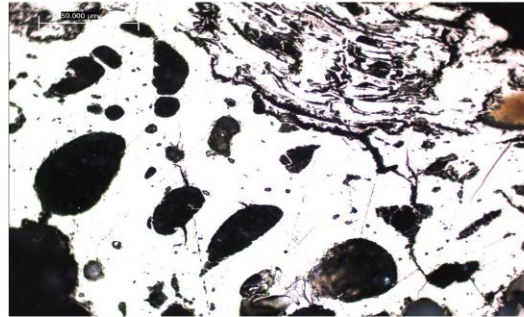
**Colour changed devolatilized coal**

**Figure 4.15:** Micrographs showing devolatilizing coals observed from the packed-bed reactor samples (magnification x500, oil immersion, reflected light).

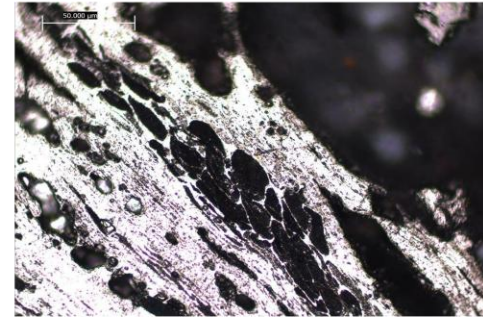
**Char particles**



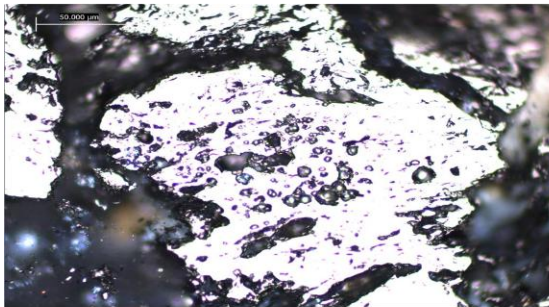
**Porous with thin walls**



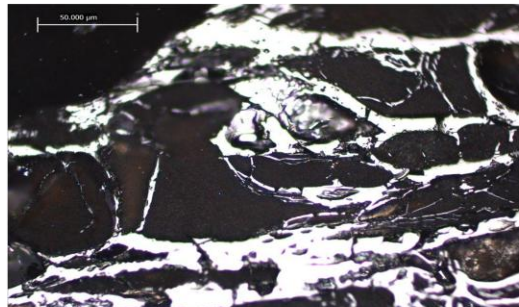
**Porous with thick walls**



**Intermediate char**



**Inert char**



**Carbo char**



**Ash**

**Figure 4.16:** Micrographs showing char particles observed from the packed-bed reactor samples (magnification x500, oil immersion, reflected-light)

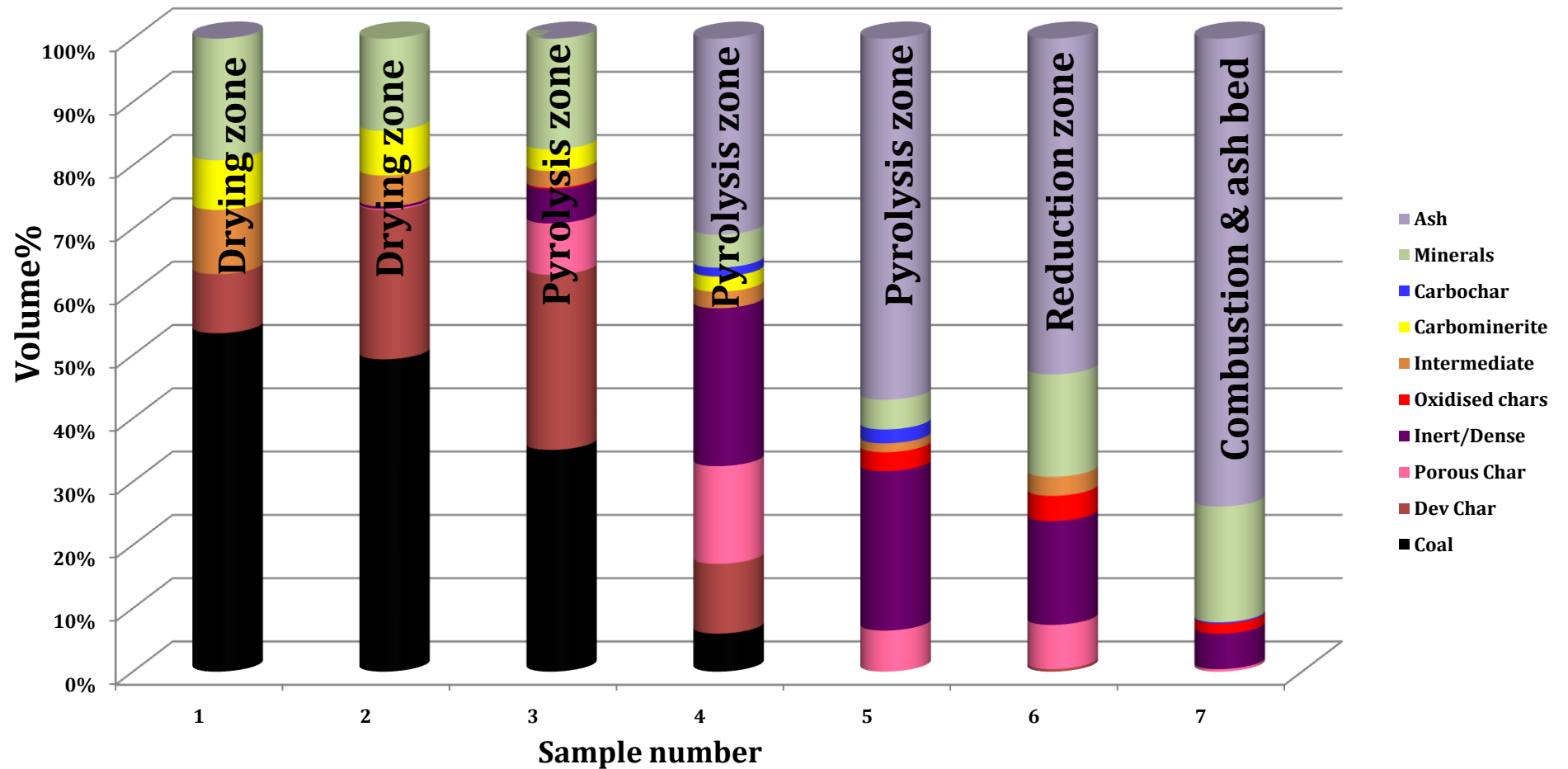


Figure 4.17: Carbon Particle Type Analysis results for Coal A packed-bed reactor generated samples.

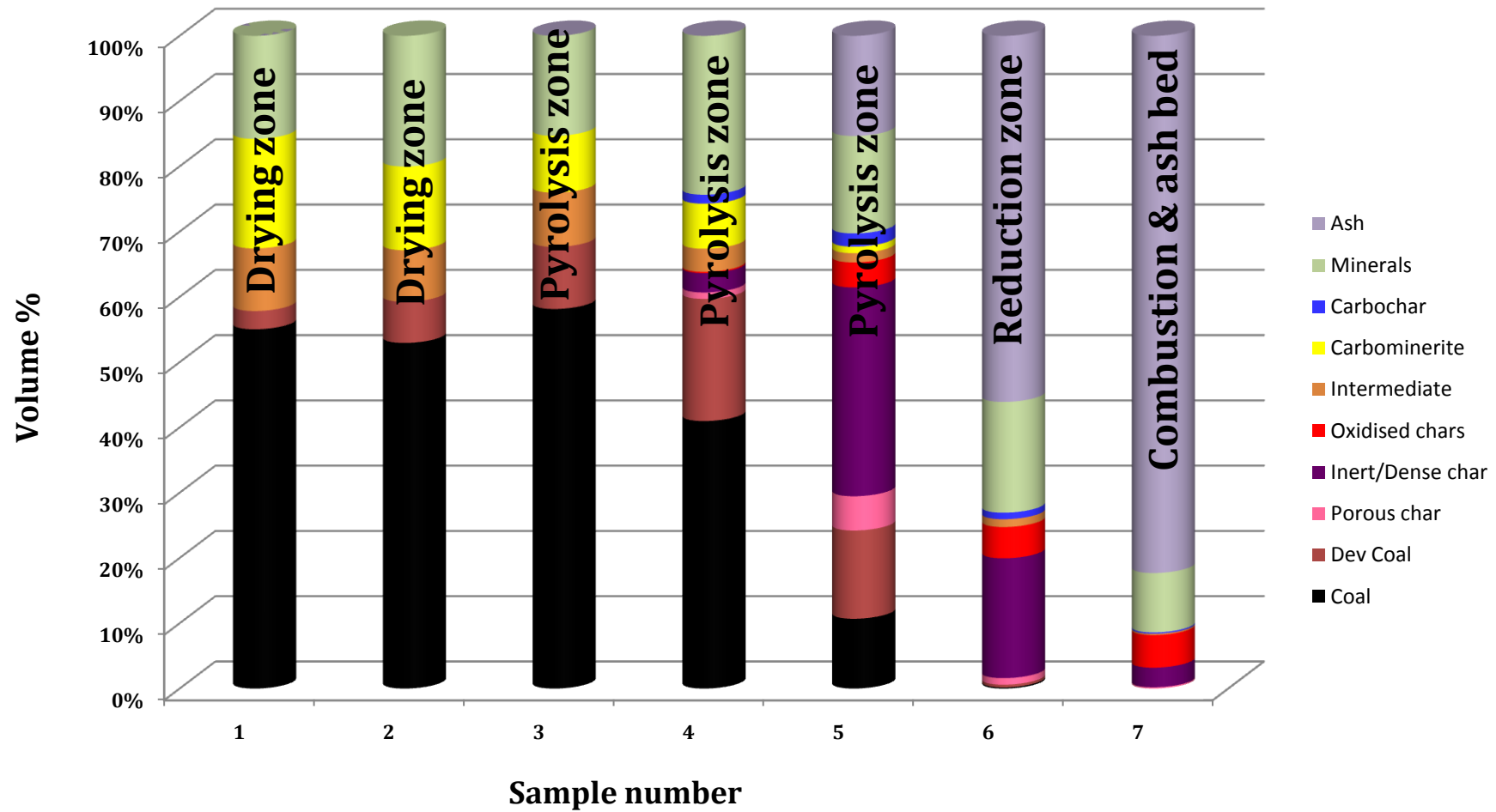


Figure 4.18: Carbon Particle Type Analysis results for the Coal B packed-bed reactor samples.



## CHAPTER 4: RESULTS AND DISCUSSION

---

Figure 4.17 shows the carbon particle type analysis results for Coal A packed-bed reactor generated samples with regard to reaction zones. Carbon conversion is clearly observed between all the reaction zones. This can be seen by the decreasing proportion of coal with an increase and subsequent decrease in char particles throughout the reactor. The effect of heat appeared to be visible as early as the drying zone with the formation of devolatilized coal particles. The devolatilized coal particles were observed as heated sections on the prepared coal blocks. In the pyrolysis zone, the formation of inert char particles was noticeable, and they seemed to dominate to the end of pyrolysis zone. The formation of inert char particles in this zone can be explained by the presence of the high content of inertodetrinite in the feed lump coal samples. Inertodetrinite is a highly matured subgroup of inertinite, and it tends to have high thermal stability and lower volatile matter yield leading to formation of inert chars during heat treatment processes (Cook, 2009).

Figure 4.18 shows the carbon particle type analysis results for the Coal B packed-bed reactor generated samples. It was noticed that this coal follows a similar trend compared to Coal A packed-bed reactor generated samples during the heat treatment process. There was still 10 vol % of coal present in sample 5 for Coal B packed-bed reactor generated samples; whereas for Coal A all of the coal had been converted to char particles by this stage. Devolatilized coal particles were observed from the drying zone to the end of pyrolysis zone. The devolatilization process seems to take longer for Coal B, as the devolatilized particles were still observed in sample 5 (the end of pyrolysis zone) in moderate amounts (13.4 vol %). The inert and porous char particles became visible in sample 4; whereas for Coal A packed-bed reactor generated samples the chars appeared in sample 2. This can be

## CHAPTER 4: RESULTS AND DISCUSSION

---

linked to the reactivity results (Section 4.1.2) which showed that Coal A is more reactive compared to Coal B. XRD also revealed that the Coal B packed-bed reactor generated samples became well aligned and ordered at temperatures above 400 °C due to high aromaticity. Unexpectedly porous char particles seemed to be formed in lower quantities in sample (Coal B) due to higher inertinite content in the parent coal (as shown in Table 4.14). Unreacted mineral matter and oxidised char particles were also observed in the ash bed in Coal B, and this confirms the high unburnt fixed carbon content observed in Section 4.1.1.2 from the proximate analysis results, resulting in incomplete carbon conversion.

Inert char particles were also observed in the ash bed zone (as illustrated in Figure 4.19). These include oxidised char and inert char particles. The presence of inert char particles in the ash bed zone supports the observation from the proximate analysis results. Volatile matter and fixed carbon were observed at the ash bed zone due to incomplete carbon conversion. Thus, this can be attributed to these carbon forms.

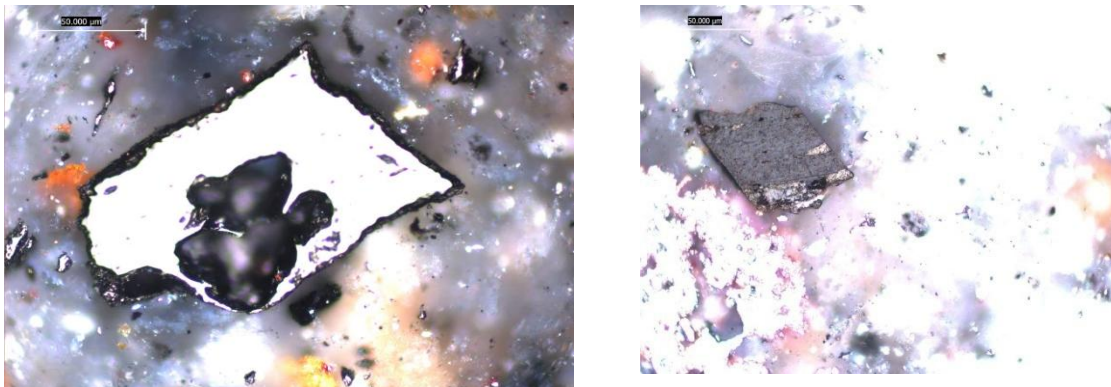


**Figure 4.19:** Micrographs showing a char particle and coal particle within ash bed (magnification x500, oil immersion, reflected light).

Oxidised inert char particles at the end of pyrolysis zone were observed in both Coal A and B packed-bed reactor generated samples. Oxidised inert char particles differ from normal inert char particles by appearing to have brown layering along the edges of the particle, or where there are extensive cracks and pores in the particle. It is suspected that this brown layering is formed where there is the presence of carbon active sites. At this point no concrete conclusion can be drawn as to the origin of these char particles, or the implications in carbon conversion efficiency. Further investigation by Electron microprobe is discussed in Section 4.3.4.

### **3.4.1.2 Devolatilization coal particles profile for Coal A and B packed-bed reactor generated samples.**

As mentioned in Chapter 3, section 3.4.3.2, devolatilized coal particles are those coal particles that are partially heated and exhibit physical changes with the development of colour change, cracks and pores as indicated in Figure 4.15. Relative to char particles, devolatilized coals show a slight change in the shade of grey from the parent coal sample under the reflected light microscopy, progressing to white in colour for char particles.

It is clearly shown in Figure 4.20 that both Coal A and B packed-bed reactor generated samples follow similar trends in the formation of devolatilized coal particles with regard to heat treatment within the four reaction zones. In the drying zone (at temperatures below 200 °C), devolatilized coal particles starts to form as early as sample 1, with Coal A having a higher content when compared to Coal B (10.4 vol % and 2.8 vol % respectively) at this

---

## CHAPTER 4: RESULTS AND DISCUSSION

---

zone. The devolatilized coal particles form at an earlier stage for Coal A from the drying zone to the middle of the pyrolysis zone. The increase in proportion of devolatilized coal particles content for Coal A is observed up to sample 3 (29.4 vol %); whereas for the Coal B, it is observed up to sample 4 (19 vol %). The devolatilization process is governed by the amount of reactive macerals, the sample with higher content of liptinite and vitrinite as reactive macerals will have quicker devolatilization process.

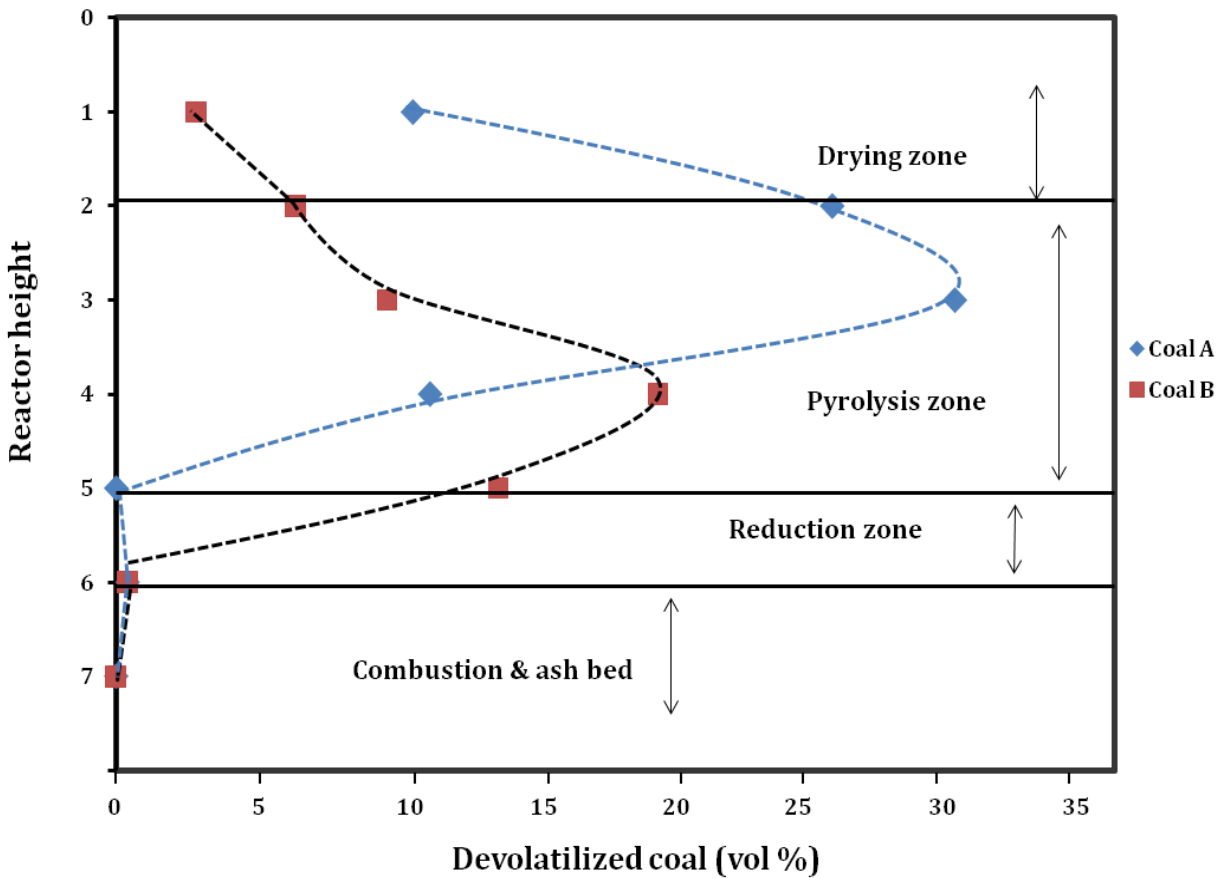


**Figure 4.20:** Devolatilization coal particles profile for the Coal A and B packed-bed reactor generated samples as a function of reactor height.

## CHAPTER 4: RESULTS AND DISCUSSION

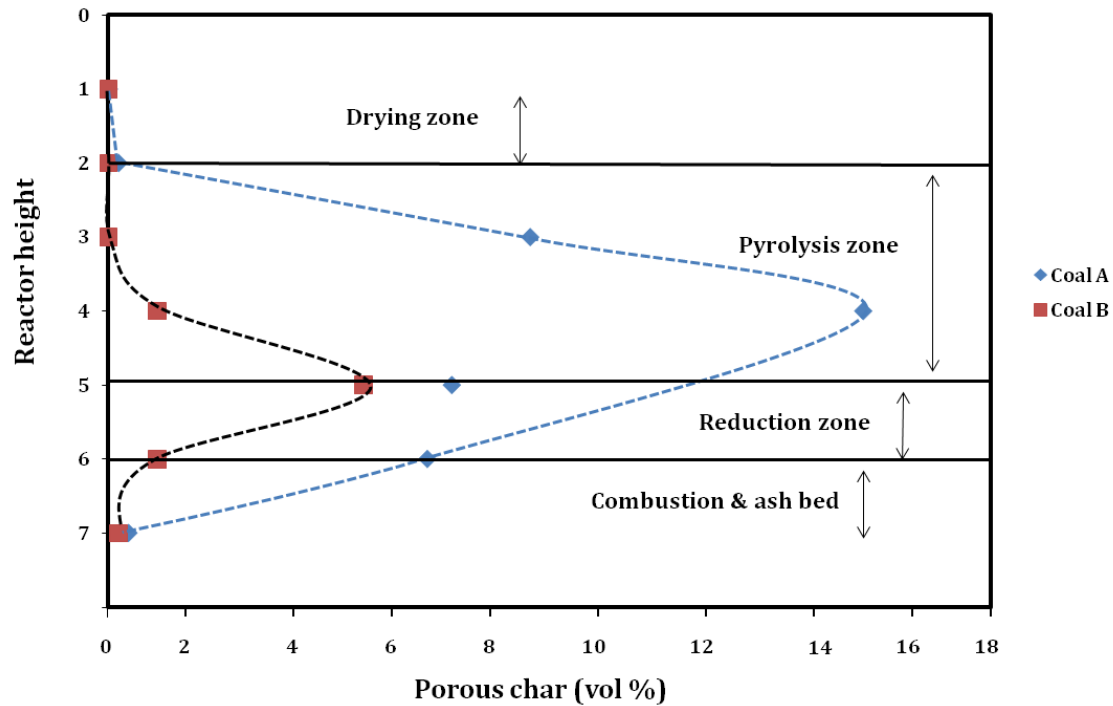
---

It is believed that devolatilized coal particles evolve from vitrinite and reactive inertinite (Bailey et al., 1990) and maceral content plays a vital role in coal burning behaviour. As shown in Table 4.14, Coal A had 78 % of its reactive macerals from liptinite and vitrinite whereas this was not the case with Coal B. Higher devolatilized coal can be attributed to the difference in reactive maceral content of both Coal A and B parent coals.

The burning behaviour these two coals (Coal A and B) can also be linked to the higher surface area of the Coal A parent coal sample when compared to the Coal B parent coal sample and therefore resulting in faster internal heat transfer. From the middle of the pyrolysis zone to the end of pyrolysis zone (samples 3-5), the amount of devolatilized coal particles in both coals decreases due to higher temperatures (temperatures above 700 °C), and the formation of char particles. The decrease in the devolatilized content is further observed from the reduction zone to the ash bed zone.

### **3.4.2.2 Porous char particles profile for the coal A and B packed-bed reactor generated samples.**

Porous char particles comprises of pores moderately or largely distributed in the char particle as indicated in Figure 4.21. Some of these porous char particles have thick walls or thin walls depending on the initial maceral. The porous char particles with thin walls are believed to have formed from vitrinite and reactive inertinites since they are easily heated (Bailey et al., 1990). Porous char particles with thick walls appear to be formed from reactive semifusite or a banded coal with vitrinite in the middle (Bailey et al, 1990).



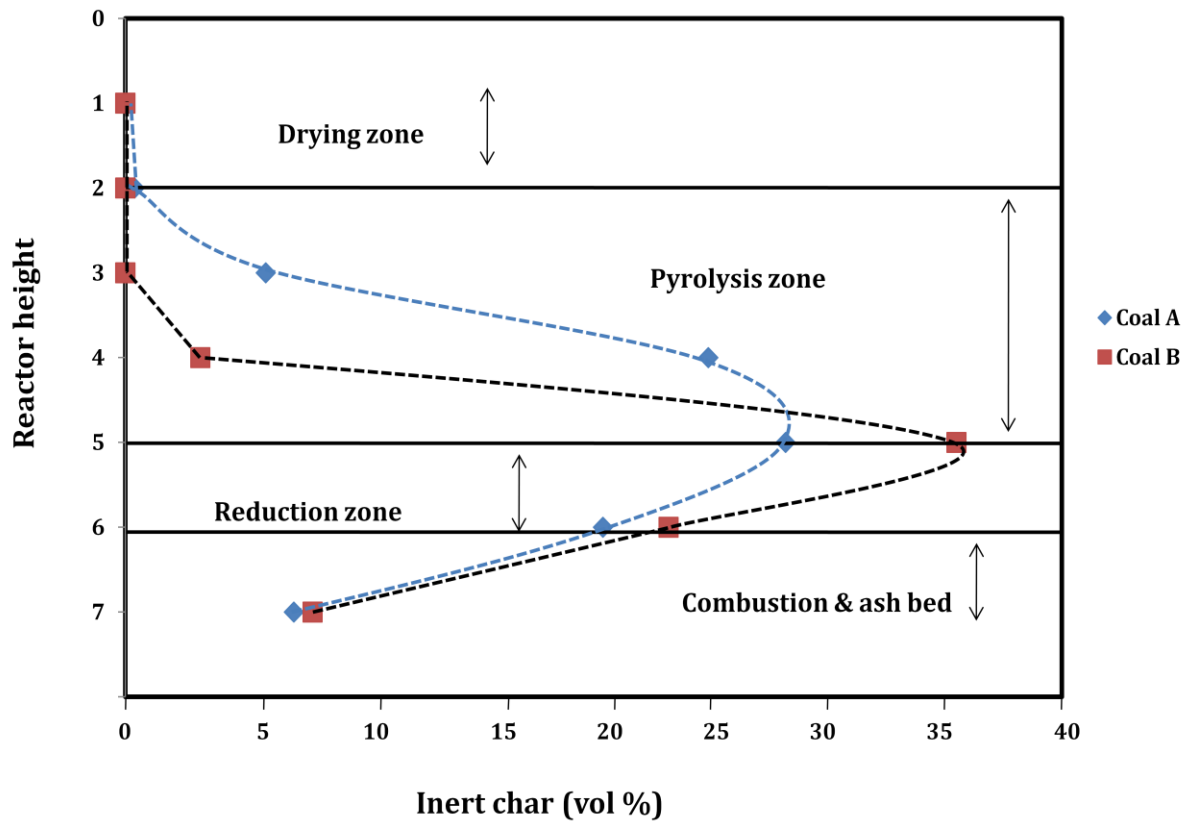
**Figure 4.21:** Porous char particles (vol %) profile for the Coal A and B packed-bed reactor generated samples as a function of reactor height.

Figure 4.21 presents the porous char particles profile for the Coal A and B packed-bed reactor generated samples as a function of packed-bed reactor height within the four reaction zones identified. It is observed that Coal A and B follow similar trends in the development of porous char particles with regard to heat treatment within the four reaction zones. Porous char particles begin to form in the pyrolysis zone (8.6 vol % and 1 vol % for Coal A and B respectively) to the middle of the pyrolysis zone for Coal A, and to the end of the pyrolysis zone for Coal B (15.4 vol % and 5.2 vol % for Coal A and B respectively) due to an increase in temperature (temperatures above 300 °C). Coal A appears to form porous char

particles at an earlier stage and at a higher rate relative to Coal B, from sample 2 (0.2 vol %) and sample 3 (1 vol %) respectively. This shows that Coal A has a higher reactivity than Coal B. From the middle of the pyrolysis zone to the ash bed, a decrease in porous char particles (0.2 vol % and 0.4 vol % for Coal A and B respectively) in both coals occur due to reaction of char particles with the reactant gases, resulting in carbon consumption and collapsing of the porous char particles walls. The low content of porous char particles observed in the ash bed is from porous char particles having thick walls and not thin walled char particles.

### **3.4.3.2 Inert char particles profile for the Coals, A and B packed-bed reactor generated samples.**

The inert char particles that were observed in this study were: fusinoids, inert chars and oxidised chars, and are discussed in detail in Chapter 3, section 3.4.3.2. Figure 4.22 presents an inert char particles profile for the Coal A and B packed-bed reactor generated samples as a function of the reactor height.



**Figure 4.22:** Inert char particles (vol %) profile for the Coal A and B packed-bed reactor generated samples as a function of reactor height.

The formation of inert char particles is clearly visible from the beginning of the pyrolysis zone for Coal A (sample 2, 0.4 vol %), and from the middle of the pyrolysis zone for Coal B (sample 4, 3.2 vol %). This shows the difference in reactivity of these two coals with regard to heat treatment even though they follow similar trends within the four reaction zones of the packed-bed reactor, [Coal A begins to form inert chars at the beginning of the pyrolysis zone (sample 2), at temperatures above 200 °C when compared to Coal B which begins to form inert char particles in sample 3, at temperatures above 342 °C]. This supports the



## CHAPTER 4: RESULTS AND DISCUSSION

---

variation in the reactivity of these two coals leading to the difference in their burning behaviour. An increase in the formation of inert char particles is observed in the pyrolysis zone for both coals, Coal B forming inert char particles at a higher rate (sample 5, 35.5 vol %) when compared to Coal A (sample 5, 28.2 vol %). This can be linked to Coal B having higher inertinite content (as illustrated in Table 4.14) relative to Coal A. The variation in the formation of inert char particles can also be linked to the XRD and  $^{13}\text{C}$  SSNMR findings which show that Coal B is highly ordered and more aromatic when compared to Coal A. Inert char particles are highly ordered crystallite aromatic carbons remaining when the volatile matter has been driven off from coal at higher temperatures. Since the Coal B parent coal sample is highly ordered and more aromatic, during heat treatment, this coal will tend to form more inert char particles relative to the Coal A parent coal sample as can be observed in Figure 4.22. In the beginning of reduction zone to the ash bed, the inert char particle content decreases due to consumption of carbon at higher temperatures within the reactor bed. In both coals, A and B packed-bed reactor generated samples, inert char particles are observed in less than 10 % (by volume) in the ash bed. This type of char particle indicates that it is the less reactive relative to the porous char particles. The presence of unburnt carbon in the ash bed zone is supported by proximate analysis whereby both coals were observed to have unburnt carbon in the ash bed zone. This may be attributed to the fact that both coals are inertinite-rich, as it is known inertinite coals comprises of aromatic ring structures which are not easily broken even at higher temperatures.

### 4.3.3 Total Reflectance analysis results

Total reflectance analysis was performed to determine the reflectance changes for Coal A and B with regard to heat treatment within the four packed-bed reactor reaction zones identified. This analysis was conducted on vitrinite and semifusinite coal particles, and their char derivatives that were observed under the reflected light microscope. This analysis was not conducted on inertodetrinite particles since it consists of fine particles normally smaller than 30 microns and these fine particles are fragments or remains of fusinite, semifusinite, macrinite and sclerotinite (Stach et al., 1982). In addition, due to the small size, it is difficult to find a suitable spot to take a reflectance reading. Two hundred and fifty counts were taken on each sample to allow for a more acceptable standard deviation. It was hoped that the inclusion of the reflectance analysis would support findings that coal conversion commences as early as drying zone (sample 1 at 111 °C and 93 °C for Coal A and B respectively). Table 4.15 summarizes the obtained reflectance analysis and the standard deviations within the four reaction zones. Total reflectance was not conducted on the ash bed samples since these samples have limited carbon particles, but it could be assumed that the ash bed reflectance reading are comparable to the reduction zone.

## CHAPTER 4: RESULTS AND DISCUSSION

**Table 4.15:** Total reflectance analysis results for the Coal A and B reactor generated samples.

Sample	Reaction zone	Coal A		Coal B	
		Rot %	Std dvt	Rot %	Std dvt
Parent coal		0.62	0.09	0.64	0.11
1	Drying	0.89	0.45	0.91	0.39
2	Drying	0.91	0.43	0.96	0.38
3	Pyrolysis	1.02	0.53	0.97	0.38
4	Pyrolysis	1.62	0.68	1.26	0.44
5	Pyrolysis	4.17	1.53	3.34	1.54
6	Reduction	5.63	2.00	5.36	1.40

Rot = total reflectance; Std dvt = standard deviation

The reflectance analysis showed a great change (from 0.62 to 0.89 mr RoV %) from the parent coals to the samples in the drying zone. This shows that the samples in the drying zone are responding to heat exposure. Figure 4.23 shows that the total reflectance increases as temperature is increased. Total reflectance of both coals slightly increases from the beginning of the drying zone (at temperatures of 111 °C) to the beginning of the pyrolysis zone (at temperatures below 350 °C) for both Coal A and B with regard to heat effect. This is in agreement with the results reported by Stach et al. (1982), whereby the reflectance of various coals from different ranks was studied with regard to temperature of carbonization. The findings were that maximum reflectance of all the studied coals slightly increases at temperatures below 400 °C. This is due to the fact that at temperatures below

## CHAPTER 4: RESULTS AND DISCUSSION

---

400 °C, the original petrographic structure of coal is still visible so most of the coal is partially devolatilized coal and has not been fully affected by high heating temperatures. In this study the random rather than maximum reflectance analysis was conducted. Singh et al. (2007) investigated Jharia coalfield which was carbonized due to igneous intrusives and mine fires. The microstructures and microtextures produced due to extraneous heat were related to the nature and the extent of heat location of the heat source and the quality and quantity of the natural coke produced. It was observed that coals at temperatures below 300 °C had unaltered remnants of the original constituents. However at higher temperatures and under overburden pressures, the coals suffered a twist and fracturing along with an increase in temperature (Singh et al., 2007).

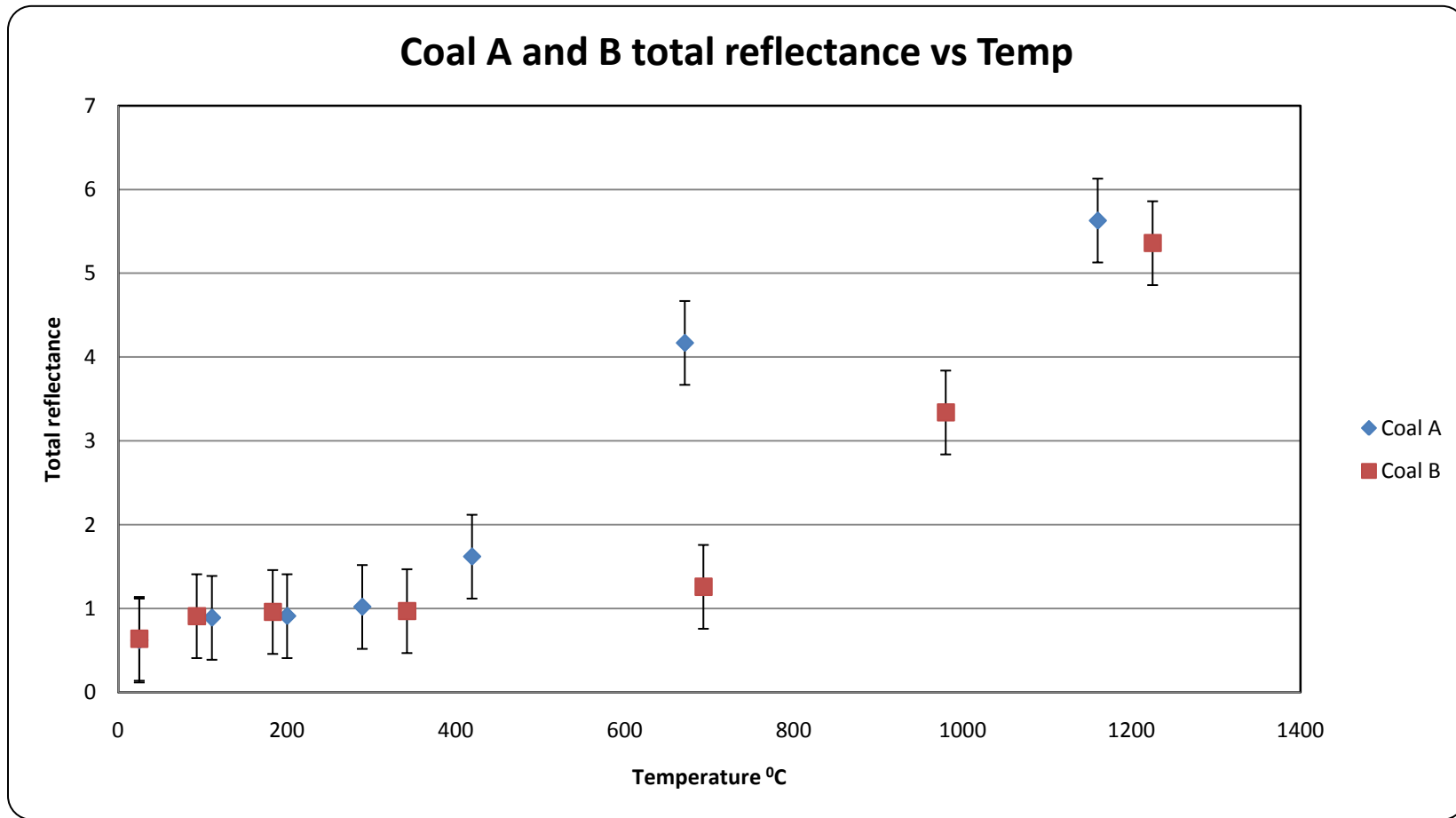


**Figure 4.23:** Total reflectance analysis for Coal A and B parent coal samples and the packed-bed reactor generated samples.

## CHAPTER 4: RESULTS AND DISCUSSION

---

In the middle of the pyrolysis zone (temperatures above 400 °C), the total reflectance shows a greater increase throughout the reactor zones (from 1.62 – 5.63 % Rot for Coal A; and from 1.26 – 5.36 for Coal B); total reflectance for Coal A increases at a lower temperatures when compared to Coal B. This shows that Coal A reacts faster than Coal B under heat exposure. The increase in total reflectance is due to the fact that the original petrographic structure begins to disappear as char particles form, resulting in an increase in the carbon content of the particles, thus leading to higher total reflectance values. Komerek and Morga (2003) determined that the increase in vitrinite reflectance is influenced by temperature increase. At temperatures of 400-500 °C (plastic stage), vitrinite is subjected to substantial alteration. At temperatures of 1200 °C, random reflectance reaches 6.62 % (Komerek and Morga, 2003). In this study, at temperatures of 1160-1225 °C, the total reflectance ranged between 5.36-5.63 %, for both Coal A and B. The difference in the increase of total reflectance of these coals can only be linked to the fact that the Coal A is converted faster than Coal B, based on the carbon particle type analysis results presented in Figures 21 and 22. In addition to this, since Coal B have high inertinite content, this sample tends to retain temperature within its aromatic structure more than Coal A. Bunt et al. (2008) did a similar study on Sasol-Lurgi MK IV FBDB gasifier whereby lump coals (-75mm +5mm) were utilized as parent coals. A linear correlation between reflectance of vitrinite and reaction temperatures was obtained. Bunt et al. (2008) determined that at the bottom of the gasifier, the reflectance of vitrinite decreases as the vitrinite samples are consumed. Ascough et al. (2010) obtained similar results to that of Bunt et al. (2008). Ascough et al. (2010) utilized different charcoal species which were assessed by reflectance analysis. A linear correlation was obtained between random mean reflectance and reaction temperatures.

### 4.3.4 Electron Microprobe study on char particles.

The Electron microprobe is an analytical tool used non-destructively to determine the chemical composition of small volumes of solid materials. When this analysis is performed the sample is bombarded with an electron beam, and signals emanating from the sample are collected. This analysis enables the determination of elements present within the sample in volumes of 10-30 cubic micrometers or less.

During the petrographic analysis, particles showing oxidation rims and brown discolouration were observed. In order to determine the significance of these oxidized particles, further investigation was required. The electron microprobe enabled the determination of the difference in elemental composition between oxidized and non-oxidized sections in inert char particle. A typical oxidised inert char particles with two sections (oxidized and non-oxidized section) as observed under the electron microbe is illustrated in Figure 4.24. As this aspect is only exploratory at this stage, and not core to the aims and objective of this thesis, it was decided that this analysis will be conducted on one coal block sample that showed the presence of oxidised and non-oxidised inert char particles. From the selected oxidised char particle, eight points were selected and analyzed. Four points were selected from the oxidized section, and the other four, points were selected from the non-oxidized section. A detailed method used for this analysis is discussed in Chapter 3, Section 3.3.3.3.

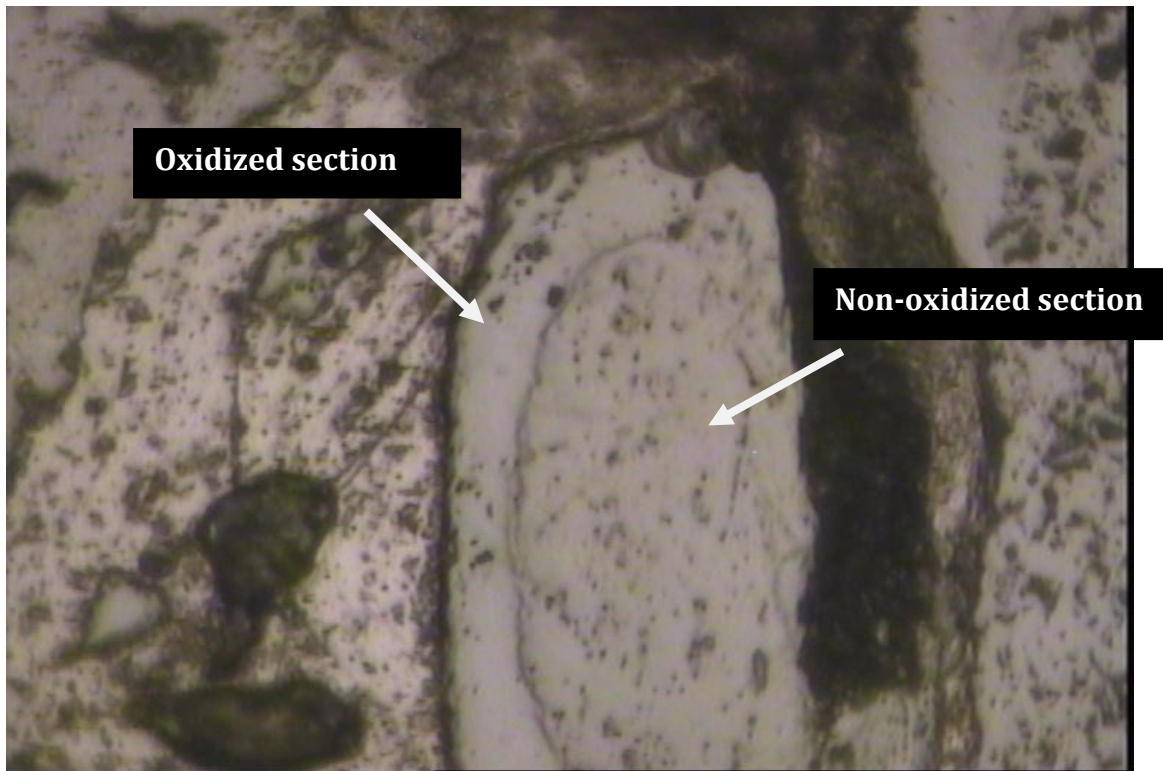


**Figure 4.24:** A photograph of inert char particle with both non-oxidized and oxidized sections.



## CHAPTER 4: RESULTS AND DISCUSSION

**Table 4.16:** Elemental Composition in mass for sample 5 (Coal A packed-bed reactor)

%.

No.	S	Ca	Ti	Si	C	O	N	Fe	Al	Total
1*	0.68	0.22	0.22	0.00	<b>90.44</b>	<b>5.21</b>	1.49	0.00	0.9	99.18
2*	0.73	0.21	0.11	0.03	<b>90.55</b>	<b>4.36</b>	1.93	0.00	0.9	98.82
3*	0.70	0.25	0.15	0.06	<b>90.15</b>	<b>4.47</b>	1.93	0.00	0.9	98.66
4*	0.68	0.17	0.12	0.04	<b>91.22</b>	<b>4.77</b>	2.17	0.00	0.9	100.12
5+	0.40	0.06	0.73	0.08	<b>87.99</b>	<b>8.13</b>	0.91	0.00	0.0	98.31
6+	0.39	0.08	0.74	0.01	<b>88.04</b>	<b>9.18</b>	0.40	0.08	0.0	98.93
7+	0.40	0.07	0.96	0.01	<b>87.96</b>	<b>8.72</b>	1.05	0.00	0.0	99.17
8+	0.44	0.09	0.30	0.05	<b>90.41</b>	<b>6.88</b>	0.34	0.07	0.8	99.39

\* non-oxidized section, + oxidized section

The elemental composition for the selected particles is summarised in Table 4.16. The element that showed the greatest variation between the oxidised section and the non-oxidized section is the oxygen content value. The non-oxidized sections have lower oxygen content and the oxidized section have a high oxygen content value, almost double. As mentioned earlier that it was suspected that these oxidised inert char particles are formed by excess air in the samples. When the air reacts with the char's active sites, due to the low proportion of these sites, the air tends to be in excess on these particles and it becomes absorbed in the surface area of these particles leading to what appears as a brown layer covering the edges of these inert char particles. This provides evidence concerning to the origin of oxidized inert chars discussed in Section 4.3.2.3. It is recommended that more still needs to be investigated about the appearance of these oxidised chars.

### **4.3.5 Comparative results of Coal A and B parent coal samples and packed-bed reactor generated samples.**

Maceral group analysis of the feed lump coal samples showed that both coals A and B did not differ significantly which is typical of Highveld coals. This analysis revealed that Coal B had higher reactive maceral content than Coal A. The difference in the reactive maceral content leads to the difference in reactivity of both parent coal samples. Coal B higher inertinite (71.8 vol %) content than Coal A (65.4 vol %). Petrographic carbon particle type analysis was able to show the morphological structural differences that occurred within the four zones for both Coal A and B parent coal samples. Both coals followed similar trends with regard to heat treatment, and the pyrolysis zone seemed to be the most crucial zone during the coal conversion process. This is due to the fact that most of the coal structural morphology was developed in this zone; i.e. different char particles were formed in this zone. Within the reduction zone, carbon consumption is clearly observed by a decrease in the char particles through the ash bed.

Once more it was confirmed that Coal A has higher reactivity relative to Coal B during the coal conversion process. This was confirmed by the following points:

- Devolatilized coals were formed as early as the drying zone (at temperatures below 111 °C) for both coals A and B packed-bed reactor generated samples. Coal A had a higher vol % of devolatilized coal particles in sample 1 (10.4 vol %) relative to Coal B packed-bed reactor generated sample (2.8 vol %). An increase in the development of devolatilized coal particles for Coal A packed-bed reactor generated samples occurred to sample 3

## CHAPTER 4: RESULTS AND DISCUSSION

---

(29.4 vol %), and to sample 4 (19 vol %) for the Coal B packed-bed reactor generated sample. The devolatilization process for the Coal B packed-bed reactor generated samples appeared to be longer than the Coal A packed-bed reactor generated samples.

- The development of porous char particles were observed at an earlier stage (at temperatures above 183 °C), and at a greater concentration for the Coal A packed-bed reactor generated samples (sample 2, 0.2 vol %), when compared to Coal B (sample 3, 1 vol %, at temperatures above 289 °C). An increase in the development of porous char particles for the Coal A packed-bed reactor samples was observed up to sample 4 (15.4 vol %), and to sample 5 (5.2 vol %) for Coal B packed-bed reactor generated samples.
- Once more the development of inert char particles begins at an earlier stage for the Coal A packed-bed reactor samples (sample 2, 0.4 vol %) when compared to the Coal B packed-bed reactor samples (sample 4, 3.2 vol %).

An increase in the development of inert char particles for the Coal B packed-bed reactor generated samples was observed to be higher at the end of the pyrolysis zone (sample 5, 35.5 vol %) when compared to the Coal A packed-bed reactor generated samples (sample 5, 28.2 vol %). This was attributed to higher inertinite content for Coal B compared to Coal A. A link was also observed between the structural parameters and the formation of inert char particles of the coals studied in this project. The variation in the formation of inert char particles can be only be linked to the XRD and <sup>13</sup>C SSNMR findings that Coal B is highly ordered and more aromatic when compared to Coal A. Inert

## CHAPTER 4: RESULTS AND DISCUSSION

---

char particles are highly ordered crystallite aromatic carbons remaining when the volatile matter has been driven off from the coal samples at higher temperatures. Since Coal B parent coal sample is highly ordered and more aromatic, during heat treatment Coal B will tend to form more inert char particles relative to the Coal A parent coal sample. Thus the formation of char particles cannot only be linked to the parent coal maceral analysis results, but can be linked to the structural parameters or properties of the parent coal samples.

Less than 10 vol % of the inert char particles and less than 1 vol % of porous char particles were observed in the ash bed for both coals. This again is in agreement with the proximate analysis results, where volatile matter and fixed carbon were observed in the ash bed zone.

Total reflectance results showed that both Coal A and B packed-bed reactor generated samples vary in reflectance within the four reaction zones. At temperatures below 400 °C (from sample 1 – 3), the reflectance showed a change with an increase in temperature. This was due to the fact that at these temperatures, the coal appearance under the reflected light microscope has not changed its shade from its greyish original maceral colour, meaning that only devolatilized coal particles are observed at these temperatures. At temperatures above 400 °C, an increase in reflectance was observed for both coals. Coal A packed-bed reactor generated samples had higher values of reflectance when compared to the Coal B packed-bed reactor samples. This is due to the fact that at these temperatures, the char particles are formed, changing the coal shade of appearance under the reflected light microscope. The char particles have a high aromatic car-

## CHAPTER 4: RESULTS AND DISCUSSION

---

bon content which tends to increase reflectivity of these packed-bed reactor generated samples.

Electron microprobe revealed that different char particles have a different chemical footprint as can be observed from the analysis of the oxidized and non-oxidized inert char particles. This analysis revealed that oxidized inert char particles have twice the oxygen proportion relative to non-oxidized inert char particles. More work still needs to be done in the investigation of oxidized inert char particles, and its implications.

### CHAPTER 5

#### 5 Summary and Conclusion

This study was initiated after Koekemoer's (2009) studies revealed that two Highveld lump coals (Coals A and B) behave differently during the heat treatment, even though these coals have similar chemical properties. A detailed chemical and physical structural analysis was required to establish an understanding as to why these two Highveld lump coals behave differently during the coal conversion process. The coal conversion process was studied by generating samples in a packed-bed reactor combustor unit. It was claimed that these coal samples do not convert at the same rate even though they are from the same coalfield. Hence an objective was to determine the difference in the conversion process at a structural and microscopic level.

Following the research questions proposed in Chapter 1, they read as follows:

- Can the structural differences of the parent coal samples affect the reactivity of two coals with similar properties during the coal conversion process? This study revealed this question to be true that the structural differences of coals do affect their reactivity during heat treatment.
- Will the carbon particle type analysis determine the reactivity of lump coals during conversion process? This study showed that carbon particle type analysis can determine the burning behaviour of coals during conversion process.

## CHAPTER 5: SUMMARY AND CONCLUSION

---

The characterization techniques were able to show structural changes occurring within the four reaction zones identified within the packed-bed reactor combustor unit i.e. drying, pyrolysis, reduction, and combustion and ash bed zones. These characterization techniques were able to reveal the differences between Coal A and B, and the key findings are noted in the bullet points below.

- It was interestingly to noted from Table 4.1, that Coal B ran cooler (has lower temperatures) in the drying zone when compared to Coal A, and that higher temperatures are reflected in the hotter regions of the reactor (from end of pyrolysis zone to the ash bed zone) for Coal B when compared to Coal A.
- Proximate analysis results for the parent coal samples revealed that Coal B had a higher volatile matter and fixed carbon content relative to Coal A. Coal A released 10 % more of volatile matter in the pyrolysis zone to the ash bed relative to the Coal B.
- Unburnt carbon was observed for both coal samples within the ash bed, and this was attributed to incomplete carbon conversion.
- Coal A packed-bed reactor generated samples had 74 % and Coal B had 70 % carbon conversion in the ash bed. This shows that Coal A reaches coal conversion faster than Coal B during heat treatment.
- Coal char CO<sub>2</sub> reactivity results revealed that Coal B has a lower reactivity when compared to Coal A.

From above, the chemical structural analysis results were not able to reveal why Coal A behaves differently from Coal B during coal conversion process. This motivated to further use advanced characterization techniques to obtain structural differences of these two lump coals, and the following significant findings were obtained:

## CHAPTER 5: SUMMARY AND CONCLUSION

---

- FTIR analysis results showed that both parent coal samples were rich in aromatic rings. This was observed by a prominent appearance of  $\text{-C=C-}$  band at  $1600\text{ cm}^{-1}$ , and a lesser appearance of the  $\text{-CH}_2$  and  $\text{-CH}_3$  bands for aliphatics at  $2918$  and  $2859\text{ cm}^{-1}$ .
- Coal structural characterization by BET surface area revealed that Coal A has high surface area compared to Coal B. This supports the finding that Coal A had a higher reactivity when compared to Coal B. This analysis also confirmed that at low bed temperatures, temperatures above  $200\text{ }^\circ\text{C}$  and  $650\text{ }^\circ\text{C}$  (pyrolysis zone), for the Coal A and B respectively, the reaction is possibly controlled kinetically, creating micropores which results in an increase in the surface area. At high bed temperatures, temperatures above  $700\text{ }^\circ\text{C}$  (reduction to ash bed position) the reaction proceeded through a diffusion controlled regime because the micropores get transformed to mesopores and then to macropores towards the end of combustion zone (as the converted carbon is consumed), and this leads to a decrease in surface area. The transformation of micro-pores to meso-pores occurs at higher temperatures ( $980\text{ }^\circ\text{C}$ ) for Coal B and at lower temperatures ( $671\text{ }^\circ\text{C}$ ) for the Coal A. Once more this shows that Coal A is highly reactive during coal conversion relative to Coal B.
- XRD analysis revealed that Coal A has less aromatic crystallites when compared to Coal B, and this was observed by the fact that Coal A had lower  $L_c$  values compared to Coal B. When XRD structural parameters were plotted against temperature, it was observed that the coal structural properties of Coal A started to become more ordered and aligned at lower temperatures ( $289\text{ }^\circ\text{C}$ , sample 3) at the



## CHAPTER 5: SUMMARY AND CONCLUSION

---

beginning of pyrolysis zone, whereas Coal B starts at higher temperatures (693 °C, sample 4) in the middle of the pyrolysis zone.

- <sup>13</sup>C SSNMR revealed that the Coal A parent coal sample is less aromatic (0.60 or 60%) than the Coal B parent coal sample (0.64 or 64 %). Both Coals, A and B packed-bed reactor generated samples followed the similar trend with regard to heat treatment whereby the aromaticity increases with a decrease in aliphaticity during the coal conversion process. It was observed that volatile matter content decreases with an increase in aromaticity as the temperature increases within the pyrolysis zone.
- Maceral group analysis of the parent coal samples showed that Coal A comprises of 34.6 vol % of reactive macerals of which 78 % is from liptinite and vitrinite contents. Coal B has 53.6 vol % of reactive macerals of which 49 % is from liptinite and vitrinite another 51 % is from reactive semifusinite and inertodetrinite contents. The 49/51 split between reactive macerals for Coal B may explain the lower reactivity compared to Coal A. The inertinites are aromatic in nature, and liptinite and vitrinite are aliphatic in nature. The aromatic rings tend to limit the aliphatic structure from igniting and combusting leading to slow coal conversion reaction process and low reactivity for Coal B. This also causes Coal B to run cooler in the drying zone (sample 1-2) and that higher temperatures are reflected in the hotter regions of the reactor. The 78 % of reactive macerals from liptinite and vitrinite macerals makes this sample to be more reactive due to high aliphatic nature of liptinite and vitrinite macerals and the reactive inertinites does not limit the aliphatic structures from igniting since they are in low content. This leads to hot temperatures at the drying zone (sample 1-2), and low temperatures in the hotter regions of the reactor. The high aromatic nature of Coal B

## CHAPTER 5: SUMMARY AND CONCLUSION

---

is also supported by the XRD and  $^{13}\text{C}$  Solid State NMR results. Coal B have high content of inertinite compared to Coal A and this leads to high inert chars produced by Coal B. This was attributed to the structural ordering and degree of aromaticity of Coal B, where the Coal B parent coal sample appeared to be more ordered and more aromatic which leads to the formation of more inert char particles when compared to the Coal A parent coal sample.

- Total reflectance analysis results showed that reflectance values of both coals showed an increase from parent coal samples to samples at the drying zone. A slight increase in reflectance values at temperatures below 400 °C was observed, this is due to the fact that at these temperatures the shade of coal appearance is still visible. As temperature increases above 400 °C, char particles are formed leading to a change in the shade of appearance of coal from greying to whitish and the reflectance values increases. This was attributed to high-in-carbon content for the char particles.

From the above findings, it can be clearly demonstrated as to why it is claimed that Coal B converts at a slower rate in a commercial coal conversion process when compared to Coal A. The structural analysis results, specifically BET surface area, XRD and  $^{13}\text{C}$ SSNMR, clearly showed the difference in structure of these two coals and their reactivity towards heat treatment. Coal B has a lower surface area, the aromatic crystallites are more ordered and well aligned, and more aromatic in comparison to Coal A. These structural properties lead to its lower reactivity during the coal conversion process.

Petrography analysis clearly showed that the reactivity of lump coals is greatly influenced by the nature of the coal structure rather than by the kinetics of the process.

## CHAPTER 5: SUMMARY AND CONCLUSION

---

It was observed that the coals having high inertinite-rich content will tend to retain temperature in the highly aromatic ring structure of chars, restricting these coals from fully igniting and combusting, thus reducing the reactivity of coals. This leads to remnant volatile matter and fixed carbon in the ash bed zone. Allocation of reactive and inert macerals appeared to be very valuable in this study since the breakdown between the reactive and inert macerals has provided some indication to a possible reason for the difference in performance between the two coals. It is very crucial to further investigate which macerals dominate in the reactive and inert maceral subdivisions since these are derived from vitrinite, liptinite and inertinite groups. The structural nature of the latter maceral groups differs.

In most cases coal processing industries utilized conventional characterization techniques to enhance understanding of coal burning behaviour during coal conversion process. This study showed that these characterization techniques do not always provide appropriate information that could enable detection of abnormal behaviour of coals during the coal conversion process. It is recommended that, in order to effectively understand the burning behaviour of coals, coal processing industries should extensively look at the utilization of alternative techniques or advanced characterization techniques. This can minimize unpredictable behaviour of coals during coal conversion process, thereby minimizing cost to the industries.

### Recommendations

- Mineralogical studies are recommended since it is believed that minerals have a significant effect coal conversion process and this study might assist in finding solution as to why these coals have different temperature profile within the four reaction zones of the packed-bed reactor.
- A more effective demineralization method will be recommended for the extraction of minerals and ash from coal samples if one needs to determine structural analysis of a certain coal. The demineralization method utilized in this study failed to extract all of the ash from sample 6 and 7 within the reduction and ash bed zones. This lead to incomplete structural characterization of the packed-bed reactor generated samples.
- A quantitative analysis of the FTIR needs to be conducted to determine the actual functional group values obtained within the four reaction zones of the packed-bed reactor combustor unit. The quantitative FTIR analysis results can be correlated with the volatile matter as well as fixed carbon content observed within the four reaction zones. These results can also be correlated with the  $^{13}\text{C}$  SSNMR structural parameters that were not discussed in this study since they did not show variation with regard to heat treatment.
- Much more still needs to be done or learnt when it comes to the  $^{13}\text{C}$  Solid state NMR analysis because in this study no conclusive results were obtained within the reduction and ash bed zone. This was due to the fact that NMR Spectroscopy analysis for coals is still new in South Africa and there is limited experience in coal studies.

## CHAPTER 5: SUMMARY AND CONCLUSION

---

- It would be very interesting to determine isotropy and anisotropy variation for the Coal A and B packed-bed reactor generated samples. The obtained results could be utilized as supporting evidence in the physical structural analysis of these samples.
- The thermoplasticity nature of the two coals before and during transformation in packed-bed reactor was not well addressed in this thesis; therefore as need for this will be beneficial for this thesis.

## REFERENCES

---

### References

Alexander, L.E., Sommer, E.C., 1956. Systematic analysis of carbon black structures. *Journal of Physical Chemistry*, 60, pp.1646.

Alonso, M.J., Borrego, A.G., Alvarez, D., Menendez, R., 1999. Pyrolysis behaviour of pulverized coal at different temperatures. *Fuel*, 78, pp.1501.

Ascough, L.A., Bird, M.I., Scott, A.C., Collinson, M.E., Cohem-Ofri, I., Snape, C.E., Le Manquais, K., 2010. *Journal of Archaeological Science*, 37, pp.1590.

Atkins, P., De Paula, J., 2006. *Materials 2: the solid state*. Atkin's Physical Chemistry textbook. Second edition. Oxford, pp.697.

Bailey, J.G., Tate, A., Diesel, C.F.K., Wall, T.F., 1990. A char morphology system with application to coal combustion. *Fuel*, 69, pp.225.

Banwell, C.N., 1972. *Fundamentals of Molecular Spectroscopy*. Second edition, Chapter 3, Infrared Spectroscopy, pp.103.

Bend, L.S., Edwards, I.A., Marsh, H., 1991. Coal provincialism, coal characterization and char formation. *Fuel*, 70, pp.1147.

Bend, L.S., Edwards, I.A., Marsh, H., 1992. The influence of rank upon char morphology and combustion. *Fuel*, 71, pp.493.

Bengtsson M., 1987. Combustion behaviour of Coal containing a high proportion of pseudovitrinite. *Fuel Process Technology*, 15, pp. 1176.

## REFERENCES

---

Berkowitz, N., 1985. Coal Science and Technology 7. *The Chemistry of Coal*. Chapter 3, The Methods of Coal Chemistry, pp.52.

Blauvelt, E., 2008. Coal sector of South Africa, *ABS Energy Research*, World Energy Discussion, Internet: <http://worldenergydiscussion.blogspot.com/2008/02/coal-sector-of-south-africa.html>. Cited 28 May 2009.

Boruah, R.K., Saikia, B.K., Baruah, B.P., Dey, N.C., 2008. X-ray scattering study of the average polycyclic aromatic unit in Ledo coal. *Journal of Applied Crystallography*, 41, pp.27.

Bunt, J.R., 2006. *A new dissection methodology and investigation into coal property transformational behaviour impacting on a commercial-scale Sasol-Lurgi MK IV Fixed-Bed gasifier*. Potchefstroom: North West University, (Thesis-PhD).

Bunt, J.R., Waanders, F.B., 2009. Pipe-reactor gasification studies of a South African bituminous coal blend. Part 1 – Carbon and Volatile matter behaviour as function of feed coal particle size reduction. *Fuel*, 88, pp.585.

Bunt, J.R., Wagner, N.J., Waanders, F.B., 2009. Carbon particle type characterization of the carbon behaviour impacting on commercial scale Sasol-Lurgi FBDB gasifier. *Fuel*, 88, pp.771.

Bunt, J.R., Joubert, J.P., Waanders, F.B., 2008. Coal char temperature profile estimation using optical reflectance for commercial-scale Sasol-Lurgi FBDB gasifier. *Fuel*, 87, pp.2849.

Cannon, C.G., Sutherland, G.B.B.M., 1945. The infra-red absorption spectra of Coals and coal extracts. *Transactions Faraday Society*, 41, pp.279.

Carpenter, A., 1988. *Coal Classification*. London: IEA Coal Research.

## REFERENCES

---

Cartz, L., Hirsch, P.B., 1959. A contribution to the structure of coals from X-ray Diffraction studies. *Royal Society Proceedings of London, Series A*, 252, pp.557.

Choudhury, N., Boral, P., Mitra, T., Adak, A.K., Choudhury, A., Sarkar, P., 2007. Assessment of nature and distribution of inertinite in Indian coals for burning characteristics. *International Journal of Coal Geology*, 72(2), pp.141.

Chunhua, L., Tomokazu, W., Makoto, N., Shigeyuji, U., Toskinori, K., 2001. Gasification kinetics of coal chars carbonized under rapid and slow heating conditions at elevated temperatures. *Journal of Energy Resource Technology*, 123, pp.21.

Coal Fossil Fuel, 2009. Coal. Available at: <http://www.solarnavigator.net/coal.htm>. Cited 28 May 2009.

Cook, A., 2009. Organic Petrological Methods. *ICCP Course in Organic Petrology, Part 2, Chapter 10*, pp.74.

Cooke, N.E., Fuller, O.M., Gaikwad, R.P., 1986. FTIR spectroscopic analysis of coals and coal extracts. *Fuel*, 65, pp.1254.

Crelling, J.C., Hippo, E.J., Woerner, B.A., West, Jr D.P., 1992. Combustion characteristics of selected whole Coals and Macerals. *Fuel*, 71(2), pp.151.

Debelak, K.A., Schrod, J.T., 1979a. Comparison of pore structure in Kentucky coals by mercury penetration and CO<sub>2</sub> adsorption. *Fuel*, 58, pp.732.

Debelak, K.A., Schrod, J.T., 1979b. Diffusion and adsorption in microporous solids: Measurement and effective diffusivities in coal. *Journal of colloid and interface science*, 70, pp.67.



## REFERENCES

---

De Jager, F.S.J., 1976. *Coal*. Republic of South African Department of Mines. Geological Survey, Mineral Resources of the Republic of South Africa. 5<sup>th</sup> edition, pp. 289.

Dempers, J., 2009. *Coal resource assessment – South Africa and neighboring countries*. Clean Coal Fossil Fuel Foundation of Africa. 14<sup>th</sup> Southern African Coal Science and Technology Conference, 11 – 12 March 2009.

Derrepe, J.M., Boudou, J.P., Moreaux, C., Durand, B., 1985. Structural evolution of a sedimentologically homogeneous coal series as a function of carbon content by solid state n.m.r.. *Fuel*, 62, pp.575.

Diamond, R., 1958. A least-Squares Analysis of the Diffuse X-ray Scattering from Carbons. *Acta Crystallographica*, 10, pp.129.

Dubinin, M.M., 1960. The Potential Theory of Adsorption of Gases and Vapours for Adsorbent with Energetically Nonuniform Surfaces. *Chemical Reviews*, 60(2), pp.235.

Dyrkacz, G.R., Bloomquist, C.A.A., Ruscic, L., 1984a. Chemical variations in coal macerals separated by density gradient centrifugation. *Fuel*, 63, pp.1166.

Dyrkacz, R., Bloomquist, C.A., Solomon, P.R., 1984b. Fourier Transform Infrared study of high purity maceral types. *Fuel*, 63, pp.536.

Emmerich, F.G., 1995. Evolution with heat treatment of crystallinity in carbons, *Carbon*, 33, pp.1709.

Ergun, S., Tiensuu, V.H., 1959. Interpretation of the intensities of X-rays scattered by coals. *Fuel*, 38, pp.64.

## REFERENCES

---

Eskom, Coal Power. Available at:[http://www.eskom.co.za/live/content.php?Item\\_ID=279](http://www.eskom.co.za/live/content.php?Item_ID=279).

Cited 23 May 2009.

Everson, R.C., Neomagus, H.W.J.P., Kasaini, H., Njapha, D., 2006. Reaction Kinetics of Pulverized Coal Chars Derived from Inertinite-rich Coals Discards: Gasification with Carbon Dioxide and Steam. *Fuel*, 85, pp.1076.

Falcon, L.M., Falcon R.M.S., 1987. The Petrographic Composition of Southern African Coal in relation to friability, hardness and abrasive indices. *Journal of South African Institute of Mining and Metallurgy*, 87(10), pp.323.

Falcon, R.M.S., Snyman, C.P., 1986. *An introduction in Coal Petrography: Atlas of Petrographic Constituents in the Bituminous Coal of South Africa*. First edition. South Africa.

Falcon, R.M.S., 1986a. A Brief review of the origin, formation and distribution of coal in the Southern Africa. *Mineral Deposits of Southern Africa*, pp.1879.

Falcon R.M.S., 1986b. Classification of coals in Southern Africa, *Mineral Deposits of Southern Africa*, vol I & II, pp.1899.

Feng, B., Bhatia, S.K., 2003. Variation of the pore structure of coal chars during gasification". *Carbon*, 41(3), pp.507.

Franklin, R.E., 1950. The interpretation of diffuse X-ray diagrams of carbon. *Acta Crystallographica*, 3, pp.107.

Fletcher, T.H., Bai, S., Pugmire, R.J., Solum, M.S., Wood, S., Grant, D.M., 1993. Chemical structural features of pyridine extracts and residues of the Argonne Premium coals using solid state C-13 NMR spectroscopy. *Energy and Fuels*, 7, pp.734.

## REFERENCES

---

Fujii, S., Dsawa, Y., Sugimura, H., 1970. Infra-red spectra of Japanese coal: The absorption band at 3030, 2920 and 1600  $\text{cm}^{-1}$ . *Fuel*, 43, pp.48.

Gan, H., Nandi, S.P., Walker Jr, P.L., 1972. Nature of the porosity in American coals. *Fuel*, 51, pp.272.

Genetti, D, Fletcher, T.H., Pugmire, R.J., 1999. Development and Application of a correlation of  $^{13}\text{C}$  NMR Chemical Structural Analyses of Coal based on Elemental composition and Volatile matter content. *Energy and Fuels*, 13, pp.60.

Given, P.H., Marzec, A., Barton, W.A., Lynch, L.J., Gerstein, B.C., 1986. The concept of a mobile or molecular phase within the macromolecular network of coals: A debate. *Fuel*, 65, pp.155.

Goodarzi, F., 1985. Organic Petrology of Hat Creek coal deposit No.1, British Columbia. *International Journal of Coal Geology*, 5, pp.337.

Gregg, S.J., Sing, K.S.W., 1967. *Adsorption, surface area and porosity*. Academic express, London, Chapter 1, pp.1.

Gumz, W., Kirsch, H., Mckowsky, M. T., 1958. Coal Ash Slagging. International Committee Coal Petrology. Berlin: Springer.

Gupta, R.P., 2005. Coal research in Newcastle – past, present and future. *Fuel*, 84, pp.1176.

Hagelskamp, H.H.B., Snyman, C.P., 1988. On the origin of low-reflecting inertinites in coals from the Highveld Coalfield, South Africa. *Fuel*, 67, pp.307.

## REFERENCES

---

Hambly, E.R., 1998. *A Chemical Structure of Coal Tar and Char During Devolatilization*. Thesis presented to the Department of Chemical Engineering, Brigham Young University.

Hanson, S., Patrick, J.W., Walker, A., 2002. The effect of coal particle size on pyrolysis and steam gasification. *Fuel*, 81(5), pp.531.

Hessley, R.K., Reasoner, J.K., Riley, J.T., 1985. *Coal Science: An Introduction to Chemistry, Technology and Utilization*. pp40.

Hirsch, P.B., 1954. X-ray Scattering from Coals. *Royal Society Proceedings of London, Series A*, 226, pp.143.

Hurt, R.H., Sarofim, A.F., Longwell, J.P., 1991. The role of microporous surface area in the gasification of chars from sub-bituminous coals. *Fuel*, 70, pp.1079.

International Committee for Coal and Organic Petrology (ICCP), 1998. The new vitrinite classification (ICCP System 1994). *Fuel*, 77(5), pp.349.

International Committee for Coal and Organic Petrology (ICCP), 2001. The new inertinite classification (ICCP System 1994). *Fuel*, 80, pp.459.

International Committee for Coal Petrology (ICCP), 1971. *International Hand Book of Coal Petrography*. 2<sup>nd</sup> edition (and 3<sup>rd</sup> Suppl. 1973), CNRS, Paris.

ISO 1171 (International Standards Organization), 1997. *Solid mineral fuels – Determination of ash content*. Standards South Africa.

## REFERENCES

---

ISO 7404 – 2 (International Standards Organization), 1985. *Methods for the petrographic analysis of bituminous coal and anthracite, Part 2: Method of preparing coal samples.* Standards South Africa.

ISO 7404 – 3 (International Standards Organization), 1985. *Methods for the petrographic analysis of bituminous coal and anthracite, Part 3: Method of determining maceral group composition.* Standards South Africa.

ISO 7404 – 4 (International Standards Organization), 1985. *Methods for the petrographic analysis of bituminous coal and anthracite. Part 4: Method of determining microlithotype, carbominerite and minerite composition.* Standards South Africa.

ISO 7404 – 5 (International Standards Organization), 1985. *Methods for the petrographic analysis of bituminous coal and anthracite. Part 5: Method of determining microscopically the reflectance of vitrinite.* Standards South Africa.

Jeffrey, L.S., 2005. Characterization of the coal resources of South Africa. *The Journal of the South African Institute of Mining and Metallurgy*, pp.95.

Jenkins, R., 2000. X-ray Techniques: Overview. *Encyclopedia of Analytical Chemistry*, pp.13269.

John, A.R., 2008. Coal Sampling GDE course. University of Witwatersrand. February 2008. Unpublished.

Jones, R. B., McCourt, C. B., Morley, C., King, K., 1985. Macerals and rank influence on the morphology of coal char. *Fuel*, 64, pp.1460.

## REFERENCES

---

Kalkreuth, W., Steller, M., Wieschenkamper, I., Ganz, S., 1991. Petrographic and chemical characterization of Canadian and German Coals in relation to utilization potential. *Fuel*, 70, pp.683.

Keaton Energy Holdings, 2008. About South African Coalfields. Available at: [http://www.keatonenergy.com/cm/sa\\_coal.asp](http://www.keatonenergy.com/cm/sa_coal.asp). Cited 28 May 2009.

Kidena, K., Mutara, S., Nomura, M., 1998. Investigations on Coal Plasticity: Correlation of the Plasticity and a TGA-Derived. *Energy and Fuels*, 12, pp.782.

Kidena, K., Mutara, S., Nomura, M., 2008. A newly proposed view on coal molecular structure integrating two concepts: Two phase and uniphase models. *Fuel Processing Technology*, 89, pp.424.

Klika, Z., Ambruzova, L., Sykorova, I., Seidlerova, J., Kolomaznik, I., 2009. Critical evaluation of sequential extraction and sink-float methods used for the determination of Ga and Ge affinity in lignite. *Fuel*, 88(10), pp.1834.

Koekemoer, A.F., 2009. *The influence of mineral content and petrographic composition on the gasification of inertinite rich high ash coal*. M.Sc dissertation, Potchefstroom: North West University.

Komerek, J., Morga, R., 2003. Vitrinite reflectance property change during heating under inert conditions. *International Journal of Coal Geology*, 54, pp.125.

Krichko, A.A., Gagarin, S.G., 1990. New ideas of coal organic matter chemical structure and mechanism of hydrogenation processes. *Fuel*, 69, pp. 885.

## REFERENCES

---

Kruger, R.A., Krueger, J.E., 2005. *Historical development of Coal Ash Utilization in South Africa*. International Ash Utilization Symposia and the World of Coal Ash Conference, Policy 3.

Kruszewska, K.J., 1989. The use of reflectance to determine maceral composition and reactive-inert ratio of coal components, *Fuel*, 68, pp.753.

Kruszewska, K.J., 1991. Synthesis: Coal characterisation ENER-C, 91045, *National Energy Council, Pretoria*, pp. 54.

Kuehn, D.W., Snyder, R.W., Davis, A., Painter, P.C., 1982. Characterization of vitrinites concentrates. 1. Fourier Transform Infrared studies. *Fuel*, 61, pp.682.

Lester, E., Watts D., Cloke, M., Clift, D., 2003. Automated Microlithotype analysis on particulate Coal. *Energy and Fuels*, 17, pp.1198.

Lowry, H.H., 1963. Chemistry of Coal Utilization, Coal Analysis and Mineral matter. *Supplementary Volume*, pp.222.

Lu, L., Sahajwalla, K.C., Harris, D., 2001. Quantitative X-ray diffraction analysis and its application to various coals. *Carbon*, 39, pp.1821.

Lu, L., Kong C., Sahajwalla, V., Harris, D., 2002. Chars structural ordering during pyrolysis and combustion and its influence on char reactivity. *Fuel*, 81, pp.1215.

Maciel, G.E., Bartuska, V.J., Miknis, F.P., 1979. Characterization of organic matter in coal by protonated <sup>13</sup>C nuclear magnetic resonance with magic angle spinning. *Fuel*, 58, pp.391.

Mahajan, P., 1991. CO<sub>2</sub> surface area of coals: The paradox. *Carbon*, 29(6), pp.735.

## REFERENCES

---

Maity, S., Mukherjee, P., 2006. X-ray structural parameters of some Indian coals. *Research Communications*, 91(3), pp.337.

Marsh, H., Rand, B., 1970. The characterization of microporous carbons by means of the Dubinin-Radushkevich equation, *Journal of Colloid and Interface Science*, 33(1), pp.101.

Marzec, A., Schulten, H-R., 1989. Chemical nature of species associated with mobile protons in coals; A study by field ionization mass spectrometry. Preprints of papers- *American Chemical Society, Division of Fuel Chemistry*, 34, pp.668.

Melendez, R.B., 2001. *The Characterisation and Combustion of South American coals*. PhD Thesis, University of Nottingham.

Menendez, R., Borrego, A.G., 2007. *Organic Petrology applied to materials and coal by-products characterization*. 24<sup>th</sup> Annual International Pittsburg Coal Conference, Johannesburg: South Africa.

Miyoshi, T, Takegoshi, K, Terao, T., 1997. <sup>13</sup>C High pressure CPMAS NMR Characterization of the molecular motion of polystyrene plasticized by CO<sub>2</sub> gas. *Macromolecules*, 30, pp.6582.

Nandi, S.P., Walker, P.L., 1964. The diffusion of nitrogen and carbon dioxide from coals of various rank, *Fuel*, 43, pp.385.

Nelson J.B., 1954. X-ray Studies of the Ultra-fine Structure of Coal II – Atomic Distribution Functions of Vitrinite from Bituminous Coals. *Fuel*, 32, pp.381.

Oberlin, A., Villey, M., 1980. Influence of Elemental Composition on Carbonization, *Carbon*, 18, pp.347.



## REFERENCES

---

Oka, N., Murayama, T., Matsuoka, H., Yananda, S., Yananda, T., Shinozaki, S., Shibaoka, M., Thomas, C.G., 1987. The influence of rank and maceral composition on ignition and char burnout of pulverized coal. *Fuel Processing Technology*, 15, pp.213.

Painter, P.C., Starsinic, M., Squires, E., Davies, A.A., 1983. Concerning the 1600  $\text{cm}^{-1}$  region in the IR spectrum of coal. *Fuel*, 62, pp.742.

Perry, S.T., Hambly, E.M., Fletcher, T.H., Solum, M.S., Pugmire, R.J., 2000. Solid-state  $^{13}\text{C}$  NMR characterization of matched tars and chars from rapid coal devolatilization. *Symposium (International) on Combustion*, 28(2), pp.2313.

Petersen, T., Yarovsky, I., Snook, I., McCulloch, D.G., Opletal G., 2004. Microstructure of an industrial char by diffraction techniques and Reverse Monte Carlo modeling. *Carbon*, 42, pp.2457.

Prevost, X.M., 2009. *Coal resources for small scale mines – 2009 perspective*. Clean Coal Fossil Fuel Foundation of Africa, 14<sup>th</sup> Southern African Coal Science and Technology Conference. 11 – 12 March 2009.

Prevost, X.M., 2004. *South African reserves and Minerals Act*. Coaltrans South Africa. 1 – 2 March 2004. Cape Town: South Africa. pp.6.

Retcofsky, H.L., Fiedel, R.A., 1973. Carbon-13 magnetic resonance in diamonds, coals and graphite. *Journal of Physical Chemistry*, 77, pp.68.

SABS SM 924 (South African Bureau of Standards), 1978. *Moisture content of coal samples intended for general analysis: Vacuum oven method*. Council of the South African Bureau of Standards.

## REFERENCES

---

SAinfo reporter, 2008. South Africa's energy supply, *South Africa .info*. Available at: <http://www.southafrica.info/business/economy/infrastructure/energy.htm> Cited 27 May 2009.

Sadhukhan, A.K., Gupta P., Saha R.K., 2009. Characterization of porous structure of coal char from a single devolatilized coal particle: Coal Combustion in a fluidized bed, *Fuel Processing Technology*, 90, pp.692.

Schmidt S., 2007. Coal deposits of South Africa – the future of coal mining in South Africa, *Oberseminar*. Available at: [http://www.geo.tu-freiberg.de/oberseminar/os07\\_08/Stephan\\_Schmidt.pdf](http://www.geo.tu-freiberg.de/oberseminar/os07_08/Stephan_Schmidt.pdf). Cited 28 May 2009.

Schoening, F.R.L., 1983. X-ray structure of some South African coals before and after heat treatment at 500 and 1000<sup>o</sup> C. *Fuel*, 62, pp.1315.

Senneca, O., Salatino, P., Masi, S., 1998. Microstructural changes and loss of gasification reactivity of chars upon heat treatment. *Fuel*, 77(13), pp.1483.

Serio, M.A., Hamblers, D.G., Markham, J.R., Solomon, P.R., 1987. Kinetics of volatile product evolution in Coal Pyrolysis: Experiment and Theory. *Energy and Fuels*, 1, pp.138.

Shinn, J.H., 1984. From coal to single-stage and two-stage products: a reactive model of coal structure. *Fuel*, 63, pp.1187.

Sigh, A.K., Singh, M.P., Sharma, M., Srivastava, S.K., 2007. Microstructures and microtextures of natural cokes: A case study of heat affected coking coals from the Jharia coal-field, India. *International Journal of Coal Geology*, 71, pp.153.

## REFERENCES

---

Solomon, P.R., Beer, J.M., 1987. Fundamentals of coal conversion and relation to coal properties. Chapter 12, Longwell J. P., *Energy*, 12 (8-9), pp.837.

Solomon, P.R., Hamblen D.G., Carangelo R.M., Serio M.A., Deshpande G.V., 1988. General Model of Coal Devolatilization. *Energy and Fuels*, 2, pp.405.

Solum, M.S., Pugmire R.J., Grant D.M., 1989. <sup>13</sup>C Solid State NMR of Argonne Premium Coals. *Energy and Fuels*, 3, pp.187.

Spiro, C.L., Kosky, P.G., 1982. Space-filling models of coals. 2. Extension to coals of various ranks. *Fuel*, 61, pp.1080.

Stach, E., 1992. *Coal Petrology*. Third Edition (Eds Stach, E., Mackowsky, M.-Th., Teichmuller, M., Taylor, G.H., Chandra, D., Teichmuller, T.), Gebruder Borntraeger, Berlin, pp.87.

Steyn, J.G.D., Smith, W.H., 1977. Coal petrography in the evaluation of South African Coals. *Coal, Gold and Base Metals*, September.

Straka, P., Brus, J., Endrysova, J., 2002. Solid State NMR Spectroscopy of Ostrava-Karvina Coals, *Chemical papers*, 56(3), pp.182.

Stopes, M.C., 1935. On the petrology of banded bituminous coal, *Fuel*, vol 14, pp 4.

Suggate, R.P., Dickson, W.W., 2004. Carbon NMR of Coals: the effect of coal type and rank, *International Journal of Coal Geology*, 57, pp.1.

Van Krevelen, D.W., 1993. *Coal: Typology-Chemistry-Physics-Constitution*. Third edition. Amsterdam: Elsevier Science, Chapter 12 (Coal as a colloidal), pp.127; Chapter 25, Mechanism of Carbonization pp.471.

## REFERENCES

---

- Van Krevelen, D.W., Schuyer J., 1957. *Coal Science*. Amsterdam, Elsevier.
- Van Niekerk, D., Pugmire, R.J., Solum M.S., Painter, P.C., Mathews, J.P., 2008. Structural characterization of vitrinite rich and inertinite rich Permian aged South African bituminous coals. *International Journal of Coal Geology*, 76, pp.290.
- Van Vutch, H.A., Rietveld, B.J., Van Krevelen, D.W., 1955. Chemical Structure and Properties of Coal VIII – Infra-red Absorption Spectra. *Fuel*, 34, pp.50.
- VanderHart, D., Retcofsky, H.L., 1976. Estimation of coal aromaticities by proton-decoupled carbon-13 magnetic resonance spectra of whole coals. *Fuel*, 55, pp.202.
- Vasallo, A.M., Wilson, M.A., Edwards, H.J., 1987. <sup>13</sup>C n.m.r. aromaticity balance on the products from flash pyrolysis of five Australian coals. *Fuel*, 66, pp.622.
- Wagner, N.J., 2005. Enhanced understanding of carbon conversion process during gasification as determined petrographically. *Fossil Fuel Foundation Indaba November 2005*.
- Wagner, N.J., Matjie, R.H., Slaghuis, H., van Heerden, J.P., 2008. Characterization of unburned carbon present in coarse gasification ash. *Fuel*, 87, pp.683.
- Walker, P.L. Jr, 1971. Chemistry and Physics of carbon. Volume 7. Marcel Dekker, Inc. New York. The Chemistry of the pyrolytic conversion of organic compounds to carbon: Parameters of crystalline order. pp269.
- Walker, P.L. Jr, Cariaso, O., Patel, R.L., 1968. Surface Areas of Coals, *Fuel, London*, 47, pp322.
- Ward, J.H.W., 2009. Summary of Economic Geology Provinces: Mpumalanga Province, *Council of Geosciences*. Available at

## REFERENCES

---

[http://www.geoscience.org.za/index.php?option=com\\_content&task=view&id=163&Itemid=45](http://www.geoscience.org.za/index.php?option=com_content&task=view&id=163&Itemid=45)

Q. Cited 28 May 2009.

Warren, B.E., 1941. X-ray diffraction in random layer lattices, *Physical Review*, 59, pp.693.

Weisz, P.B, Goodwin, R.D., 1963. Combustion of carbonaceous deposits within porous catalyst particles. 1. Diffusion-controlled kinetics, *Journal of Catalysis*, 2, pp397.

Wemmer, D.E., Pines, A., Whitehurst, D.D., 1981. <sup>13</sup>C NMR studies of coal and coal extracts, *Philosophical Transactions of Royal Society of London, Series A, Mathematical and Physical Sciences*, 300(1453), pp.15.

Wertz, D.L., Bissell M., 1994. Relating the nonideal diffraction from the grapheme layer stacking peak to the aliphatic carbon abundance in bituminous coals. *Energy and Fuel*, 8, pp.613.

Wertz, D.L., Quin, J.L., 1998. X-ray analysis of liquid treated coals. 1. Effects of pyridine on the short range structuring in Beulah Zap lignite. *Energy and Fuels*, 12, pp.697.

Wertz, D.L., 1998. X-ray scattering analysis of the average polycyclic aromatic unit in Argonne premium coal 401. *Fuel*, 77(1-2), pp.43.

Wilson, M.G.C., 2009. Mineral profile of Limpompo region, *Council of Geosciences*. Available

at:[http://www.geoscience.org.za/index.php?option=com\\_content&task=view&id=428&Itemid=](http://www.geoscience.org.za/index.php?option=com_content&task=view&id=428&Itemid=448-47K)

[448-47K](http://www.geoscience.org.za/index.php?option=com_content&task=view&id=428&Itemid=448-47K). Cited 28 May 2009.

## REFERENCES

---

Wilson, M.A., Pugmire, R.J., Karas, J., 1984. Carbon Distribution in Coals and Coal Macerals by Cross Polarization Magic Angle Spinning Carbon-13 Nuclear Magnetic Resonance Spectrometry. *Analytical Chemistry*, 56, pp.933.

World Coal Institute, 2009. Coal Facts 2008 edition with 2007 data. Available at: [http://www.worldcoal.org/assets\\_cm/files/PDF/coalfacts08.pdf](http://www.worldcoal.org/assets_cm/files/PDF/coalfacts08.pdf). Cited 23 May 2009.

World Coal Institute, 2000. Coal, power for progress, 4th Edition. London: WCI.

World Coal Institute, 2009. The Coal Resource, a comprehensive overview of coal. Available at: [www.worldcoal.org/coal\\_info.asp](http://www.worldcoal.org/coal_info.asp). Cited 5 March 2009.

Wu, Y., Wu, S., Gu, J., Gao, J., 2009. Differences in physical properties and CO<sub>2</sub> gasification reactivity between coal char and petroleum coke. *Process Safety and Environmental protection*, 87, pp.323.

Xuguang, S., 2005. The investigation of chemical structure of coal macerals via transmitted-light FT-IR microspectroscopy. *Spectrochimica Acta Part A*, 62, pp.557.

Yen, T.F., Erdman, J.G., Pollack, S.S., 1961. Investigation of the structure of petroleum asphaltene by X-ray diffraction. *Analytical Chemistry*, 33, pp.1587.

Yu, J., Lucas, J.A, Wall, T.F., 2007. Formation of the structure of chars during devolatilization of pulverized coal and its thermoproperties: A review. *Progress in Energy and Combustion Science*, 33, pp.135.

Zhu, X., Sheng, C., 2010. Evolution of the Char structure of Lignite under Heat Treatment and its Influences on Combustion Reactivity. *Energy and Fuels*, 24, pp. 152.

## REFERENCES

---

Zilm, K.W., Pugmire, R.J., Larter S.R., Allan, J., Grant, D.M., 1981. Carbon-13 CP/MAS spectroscopy of coal macerals. *Fuel*, 60, pp.717.

## APPENDICES

---

### Appendix A

#### Proximate analysis

**Table A-1:** Table presenting proximate analysis data for the Coal A packed-bed reactor samples.

<b>-75mm, +5mm</b>	<b>Proximate analysis (dry basis)</b>		
	<b>Volatiles</b>	<b>Fixed C</b>	<b>Ash</b>
<b>Sample</b>	<b>%</b>	<b>%</b>	<b>%</b>
<b>1</b>	21.9	46.6	31.4
<b>2</b>	20.1	48.0	31.8
<b>3</b>	16.4	50.8	32.7
<b>4</b>	10.9	53.2	35.8
<b>5</b>	4.44	55.0	40.4
<b>6</b>	1.38	40.3	58.3
<b>7</b>	1.02	12.7	86.2

**Table A-2:** Table presenting proximate analysis data for the Coal B packed-bed reactor samples.

<b>-75mm, 5mm</b>	<b>Proximate analysis (dry base)</b>		
	<b>Volatiles</b>	<b>Fixed C</b>	<b>Ash</b>
<b>Sample</b>	<b>%</b>	<b>%</b>	<b>%</b>
<b>1</b>	23.5	47.6	28.8
<b>2</b>	22.3	46.7	31.0
<b>3</b>	21.2	44.6	34.2
<b>4</b>	17.9	45.3	36.8
<b>5</b>	9.2	30.8	60.0
<b>6</b>	4.5	32.1	63.3
<b>7</b>	3.3	14.9	81.8



## APPENDICES

---

### Appendix B

#### Coal char CO<sub>2</sub> reactivity results

**Table B-1:** Summarized coal char CO<sub>2</sub> reactivity of Coal A and B packed-bed reactor samples.

Sample	Reactivity @ 50%burnoff	
	Coal A	Coal B
Feed coal	3.5	3.2
1	3.7	3.0
2	3.2	2.5
3	3.5	2.8
4	2.9	2.7
5	2.5	1.9
6	0.8	0.8

**Appendix C**

**Proximate analysis results after demineralization**

## APPENDICES

---

### Appendix D

#### BET adsorption results (raw data)

BET adsorption analysis was conducted using both CO<sub>2</sub> and N<sub>2</sub> as adsorbent gases. The CO<sub>2</sub> surface area results are discussed in Chapter 4, section 4.2.3. Due to the reasons mentioned in Section 4.2.3, the N<sub>2</sub> results were not utilized and are presented in Table D2 and D3 for both Coal A and B packed-bed reactor generated samples. Table D1 summarizes BET CO<sub>2</sub> isotherm pore volume results for both Coals, A and B packed-bed reactor generated samples.

**Table D-1:** Summarized BET CO<sub>2</sub> isotherm pore volume results for both Coals, A and B packed-bed reactor generated samples.

Sample	Coal A, Temp °C	Coal A, Pore Volume (Å)	Coal B, Temp° C	Coal B, Pore Volume (Å)
1	111	297.5	93	262.9
2	200	476.2.	183	532.4
3	289	181.1	342	338.4
4	419	181.8.	693	147.8
5	671	84.3	980	100.4
6	1160	56.2	1225	43.31
7	1250	42.5	1260	79.1

---

## APPENDICES

---

Table D-2: **Summarized BET N<sub>2</sub> isotherm raw data for the Coal A packed-bed reactor generated samples**

Surface Area	Sample 1	Sample 2	Sample 3	Sample 4	Sample 5	Sample 6	Sample 7
--------------	----------	----------	----------	----------	----------	----------	----------

## APPENDICES

Single point surface area at P/Po = 0.324207454:	0.8556 m <sup>2</sup> /g	0.6081 m <sup>2</sup> /g	2.2198 m <sup>2</sup> /g	1.9514 m <sup>2</sup> /g	7.9035 m <sup>2</sup> /g	13.8039 m <sup>2</sup> /g	9.4175 m <sup>2</sup> /g
<b>BET Surface Area:</b>	<b>0.9807 m<sup>2</sup>/g</b>	<b>0.6936 m<sup>2</sup>/g</b>	<b>2.3456 m<sup>2</sup>/g</b>	<b>2.0905 m<sup>2</sup>/g</b>	<b>8.4979 m<sup>2</sup>/g</b>	<b>14.3241 m<sup>2</sup>/g</b>	<b>9.8212 m<sup>2</sup>/g</b>
t-Plot Micropore Area:	3.5994 m <sup>2</sup> /g	2.7049 m <sup>2</sup> /g	0.6965 m <sup>2</sup> /g	2.8063 m <sup>2</sup> /g	12.8337 m <sup>2</sup> /g	5.6017 m <sup>2</sup> /g	4.0829 m <sup>2</sup> /g
t-Plot External Surface Area:	-2.6187 m <sup>2</sup> /g	-2.0113 m <sup>2</sup> /g	1.6491 m <sup>2</sup> /g	-0.7158 m <sup>2</sup> /g	-4.3359 m <sup>2</sup> /g	8.7225 m <sup>2</sup> /g	5.7383 m <sup>2</sup> /g
<b>BJH Adsorption cumulative surface area of pores</b>							
between 17.000 Å and 3000.000 Å diameter:	0.475 m <sup>2</sup> /g	0.650 m <sup>2</sup> /g	0.957 m <sup>2</sup> /g	0.727 m <sup>2</sup> /g	1.088 m <sup>2</sup> /g	6.756 m <sup>2</sup> /g	4.233 m <sup>2</sup> /g
<b>BJH Desorption cumulative surface area of pores</b>							
between 17.000 Å and 3000.000 Å diameter:	1.9532 m <sup>2</sup> /g	2.3106 m <sup>2</sup> /g	2.7543 m <sup>2</sup> /g	2.4409 m <sup>2</sup> /g	3.8402 m <sup>2</sup> /g	7.8759 m <sup>2</sup> /g	2.1375 m <sup>2</sup> /g
<b>Pore Volume</b>							
Single point adsorption total pore volume of pores							
less than 1606.339 Å diameter at P/Po = 0.987809378:	0.007293 cm <sup>3</sup> /g	0.008258 cm <sup>3</sup> /g	0.010617 cm <sup>3</sup> /g	0.009503 cm <sup>3</sup> /g	0.017907 cm <sup>3</sup> /g	0.020112 cm <sup>3</sup> /g	0.010442 cm <sup>3</sup> /g
t-Plot micropore volume:	0.001852 cm <sup>3</sup> /g	0.001374 cm <sup>3</sup> /g	0.000349 cm <sup>3</sup> /g	0.001463 cm <sup>3</sup> /g	0.006506 cm <sup>3</sup> /g	0.002775 cm <sup>3</sup> /g	0.002043 cm <sup>3</sup> /g
BJH Adsorption cumulative volume of pores							
between 17.000 Å and 3000.000 Å diameter:	0.006667 cm <sup>3</sup> /g	0.007904 cm <sup>3</sup> /g	0.009805 cm <sup>3</sup> /g	0.008612 cm <sup>3</sup> /g	0.013613 cm <sup>3</sup> /g	0.016347 cm <sup>3</sup> /g	0.007763 cm <sup>3</sup> /g
BJH Desorption cumulative volume of pores							
between 17.000 Å and 3000.000 Å diameter:	0.007294 cm <sup>3</sup> /g	0.008268 cm <sup>3</sup> /g	0.010643 cm <sup>3</sup> /g	0.009537 cm <sup>3</sup> /g	0.016689 cm <sup>3</sup> /g	0.017162 cm <sup>3</sup> /g	0.006506 cm <sup>3</sup> /g
<b>Pore Size</b>							
<b>Adsorption average pore width (4V/A by BET):</b>	<b>297.4819 Å</b>	<b>476.2097 Å</b>	<b>181.0599 Å</b>	<b>181.8362 Å</b>	<b>84.2881 Å</b>	<b>56.1617 Å</b>	<b>42.5280 Å</b>
BJH Adsorption average pore diameter (4V/A):	561.974 Å	486.426 Å	409.656 Å	474.084 Å	500.540 Å	96.781 Å	73.361 Å
BJH Desorption average pore diameter (4V/A):	149.370 Å	143.132 Å	154.566 Å	156.285 Å	173.839 Å	87.163 Å	121.749 Å

### Appendix E

## APPENDICES

**Table E-1:** Summarized BET N<sub>2</sub> isotherm raw data for the Coal B packed-bed reactor generated samples.

Surface Area	Sample 1	Sample 2	Sample 3	Sample 4	Sample 5	Sample 6	Sample 7
Single point surface area at P/Po = 0.322546992:	1.1190 m <sup>2</sup> /g	1.0008 m <sup>2</sup> /g	0.9205 m <sup>2</sup> /g	3.2549 m <sup>2</sup> /g	7.0583 m <sup>2</sup> /g	14.8948 m <sup>2</sup> /g	5.3029 m <sup>2</sup> /g
<b>BET Surface Area:</b>	1.2358 m <sup>2</sup> /g	1.1034 m <sup>2</sup> /g	1.0210 m <sup>2</sup> /g	3.5216 m <sup>2</sup> /g	7.4464 m <sup>2</sup> /g	15.6621 m <sup>2</sup> /g	5.5815 m <sup>2</sup> /g
t-Plot Micropore Area:	1.9208 m <sup>2</sup> /g	1.6954 m <sup>2</sup> /g	1.2748 m <sup>2</sup> /g	1.9250 m <sup>2</sup> /g	7.4661 m <sup>2</sup> /g	12.5936 m <sup>2</sup> /g	4.7237 m <sup>2</sup> /g
t-Plot External Surface Area:	-0.6850 m <sup>2</sup> /g	-0.5920 m <sup>2</sup> /g	-0.2538 m <sup>2</sup> /g	1.5966 m <sup>2</sup> /g	-0.0197 m <sup>2</sup> /g	3.0685 m <sup>2</sup> /g	0.8578 m <sup>2</sup> /g
<b>BJH Adsorption cumulative surface area of pores</b>							
between 17.000 Å and 3000.000 Å diameter:	0.688 m <sup>2</sup> /g	0.960 m <sup>2</sup> /g	0.682 m <sup>2</sup> /g	1.128 m <sup>2</sup> /g	1.455 m <sup>2</sup> /g	1.582 m <sup>2</sup> /g	3.804 m <sup>2</sup> /g
<b>BJH Desorption cumulative surface area of pores</b>							
between 17.000 Å and 3000.000 Å diameter:	2.3076 m <sup>2</sup> /g	3.7394 m <sup>2</sup> /g	2.3021 m <sup>2</sup> /g	3.2865 m <sup>2</sup> /g	4.2345 m <sup>2</sup> /g	4.0897 m <sup>2</sup> /g	2.5468 m <sup>2</sup> /g
<b>Pore Volume</b>							
Single point adsorption total pore volume of pores less than 1862.662 Å diameter at P/Po = 0.989510833:	0.008122 cm <sup>3</sup> /g	0.014686 cm <sup>3</sup> /g	0.008639 cm <sup>3</sup> /g	0.013013 cm <sup>3</sup> /g	0.018694 cm <sup>3</sup> /g	0.016959 cm <sup>3</sup> /g	0.011035 cm <sup>3</sup> /g
t-Plot micropore volume:	0.000991 cm <sup>3</sup> /g	0.000877 cm <sup>3</sup> /g	0.000696 cm <sup>3</sup> /g	0.001056 cm <sup>3</sup> /g	0.003792 cm <sup>3</sup> /g	0.006181 cm <sup>3</sup> /g	0.002335 cm <sup>3</sup> /g
<b>BJH Adsorption cumulative volume of pores</b>							
between 17.000 Å and 3000.000 Å diameter:	0.007679 cm <sup>3</sup> /g	0.014292 cm <sup>3</sup> /g	0.008276 cm <sup>3</sup> /g	0.011867 cm <sup>3</sup> /g	0.015566 cm <sup>3</sup> /g	0.010056 cm <sup>3</sup> /g	0.010256 cm <sup>3</sup> /g
<b>BJH Desorption cumulative volume of pores</b>							
between 17.000 Å and 3000.000 Å diameter:	0.008123 cm <sup>3</sup> /g	0.014689 cm <sup>3</sup> /g	0.008640 cm <sup>3</sup> /g	0.013072 cm <sup>3</sup> /g	0.017365 cm <sup>3</sup> /g	0.011673 cm <sup>3</sup> /g	0.010401 cm <sup>3</sup> /g
<b>Pore Size</b>							
<b>Adsorption average pore width (4V/A by BET):</b>	262.8842 Å	532.4000 Å	338.4369 Å	147.8036 Å	100.4179 Å	43.3114 Å	79.0807 Å
BJH Adsorption average pore diameter (4V/A):	446.170 Å	595.527 Å	485.710 Å	420.852 Å	427.865 Å	254.337 Å	107.834 Å
BJH Desorption average pore diameter (4V/A):	140.800 Å	157.123 Å	150.116 Å	159.094 Å	164.030 Å	114.169 Å	163.360 Å

### Appendix F

#### X-ray diffraction calculations.

The XRD structural parameters utilized in section 4.2.4 were determined using the following method. The mean crystallite size of powder composed of relatively perfect crystalline particle can be determined with the familiar Scherrer equation 3 (neglecting the lattice strain),

$$L_{hkl} = k\lambda/\beta_0\cos\theta \quad (3)$$

where  $L_{hkl}$  is the mean dimension of the crystallite perpendicular to the plane (hkl);  $\beta_0$  is the integral breadth or breadth at half maximum intensity of the pure reflection profile in radians;  $k$  is a constant that is commonly assigned a value of unity. For diffuse two-dimensional reflection, if axis 'c' is perpendicular to and axes 'a' and 'b' lie on the plane of the layer, the crystalline reflection will be of the type '001' and two-dimension reflection will be of the index type 'hk'. No general 'hkl' reflection will be observed. The size of two-dimensional layer in the plane of layer can be calculated from the observed breadth of 'hk' reflection, using the Scherrer equation (Lowry 1963) with an appropriate value of shape factor  $k$ . The breadth of the reflection on the  $2\theta$  scale at half intensity is,

$$\beta_{1/2} = 2\lambda/L_{hkl} \cos\theta \quad (4)$$

Here,  $L_{hkl}$  is the lamellae diameter of the two dimensional layer in a direction perpendicular to the diameter of the two-dimensional diffracting lattice 'hk' and  $k = 2$ . The av-

## APPENDICES

---

verage number of carbon atoms (N) per aromatic lamellae can be calculated from the equation given elsewhere (Lowry 1963),

$$N = 0.32 L^2 \quad (5)$$

The average interlayer distance of the lamellae can be computed from the position of the '002' reflection, where as the average dimension of the packets of the lamellae in the direction perpendicular to their planes may be estimated from its half width.

Table F-1: XRD structural parameters for the Coal A feed coal and the corresponding packed-bed reactor generated samples.

Sample	Temp ( <sup>o</sup> C)	Reaction Zones	d <sub>002</sub>	L <sub>c</sub> (Å)	L <sub>a</sub> (Å)	N
Feed coal			3.44	7.49	9.65	3.08
1	<b>111</b>	Drying	3.38	7.17	8.61	3.21
2	<b>200</b>	Drying	3.45	6.78	5.75	2.88
3	<b>289</b>	Pyrolysis	3.50	6.50	18.30	2.98
4	<b>419</b>	Pyrolysis	3.57	6.94	27.37	2.91
5	<b>671</b>	Pyrolysis	3.64	7.26	38.09	3.51
6	<b>1160</b>	Reduction	3.64	9.19	61.88	3.00

d<sub>002</sub> = Interlayer spacing of crystallites in a unit cell, L<sub>c</sub> = Average crystallite height in a unit cell, L<sub>a</sub> = Average crystallite diameter in a unit cell, N = number of crystallite in a unit cell



## APPENDICES

---

Table F-2: XRD structural parameters for the Coal B parent coal and its packed-bed reactor generated samples.

Sample	Temp (° C)	Reaction Zones	d <sub>002</sub>	L <sub>c</sub> (Å)	L <sub>a</sub> (Å)	N
Parent			3.46	10.10	16.39	3.30
1	<b>93</b>	Drying	3.46	7.99	14.68	3.91
2	<b>183</b>	Drying	3.49	7.13	27.66	3.04
3	<b>342</b>	Pyrolysis	3.49	7.11	40.07	3.04
4	<b>693</b>	Pyrolysis	3.55	7.18	29.33	3.02
5	<b>980</b>	Pyrolysis	3.64	10.09	7.91	3.76
6	<b>1225</b>	Reduction	<i>Na</i>	<i>Na</i>	<i>Na</i>	<i>Na</i>

d<sub>002</sub> = Interlayer spacing of crystallites in a unit cell, L<sub>c</sub> = Average crystallite height in a unit cell, L<sub>a</sub> = Average crystallite diameter in a unit cell, N = number of crystallite in a unit cell

## Appendix G

### <sup>13</sup>C SS NMR analysis results

<sup>13</sup>C SS NMR structural parameters were calculated following Solomon et al. 1989, and Suggate and Dickson 2004 method. The structural parameters were calculated from the obtained CP/MAS and Dipolar dephasing spectrum. The obtained spectrum was divided into 8 integrals values (from A to G) and is shown in Figure E1.

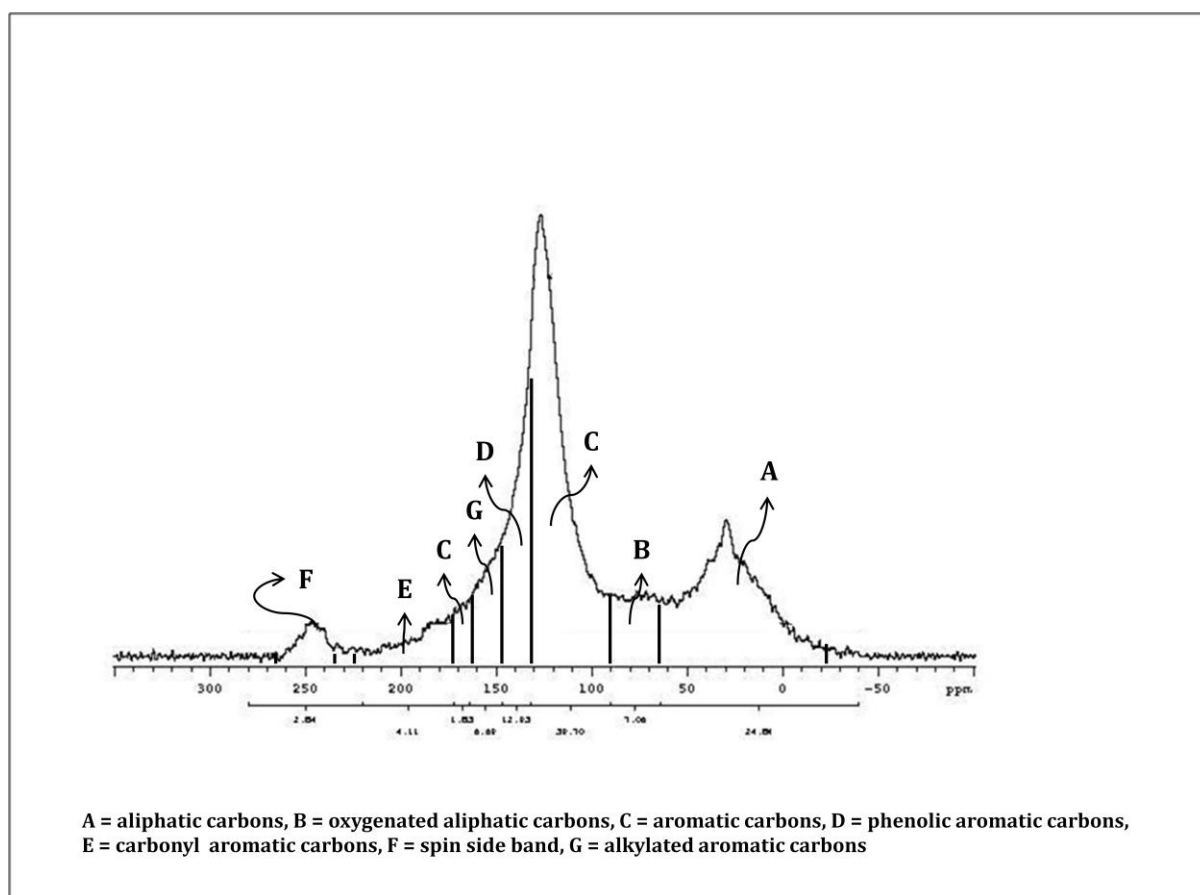


**Figure G-1:** CP/MAS spectrum showing 8 integral values regarding to their structural parameters.

## APPENDICES

---

Table G-1: List of integration regions and values.

Region	Start (ppm)	End (ppm)	Integral
F	280	220	2.83
E	220	172	4.11
C	172	164	1.83
D	164	147	6.69
G	147	132	12.93
C	132	90	39.69
B	90	64	7.06
A	64	-40	24.84

The following calculations were made from the integral values obtained from CP/MAS experiments:

$$f_a = C/(C + A) \quad (6)$$

where  $f_a$  is the fraction of aromatic carbons, C is the integral value of aromatic carbons and A is the integral value of aliphatic carbons.

$$f_{al} = A/(A + C) \quad (7)$$

where  $f_{al}$  is the fraction of aliphatic carbons, C is the integral value of aromatic carbons and A is the integral value of aliphatic carbons.

$$f_a^{CO} = f_a (E/C + E) \quad (8)$$

where  $f_a^{CO}$  is the fraction of carbonyl carbons, C is the integral value of aromatic carbons and E is the integral values of carbonyl carbons.

$$f_a^P = f_a (D/C + D) \quad (9)$$

## APPENDICES

---

where  $f_a^P$  is the fraction of phenolic carbons, C is the integral value of aromatic carbons and D is the integral values of phenolic carbons.

$$f_a^S = f_a (G/C + G) \quad (10)$$

where  $f_a^S$  is the fraction of alkylated aromatic carbons, C is the integral value of aromatic carbons and G is the integral values of alkylated carbons.

The following calculations were made from the dipolar dephasing and CP/MAS experiment results. Dipolar dephasing experiments were performed in order to omit the protonated carbons.

$$f_a^N = f_{a'} / (f_{a'} \times f_a) \quad (11)$$

where  $f_a^N$  is the fraction of non-protonated carbons and CH<sub>3</sub> in aromatic region,  $f_{a'}$  is the integral value of total aromatic carbons from the dipolar dephasing experiments and  $f_a$  is the fraction of aromatic carbons from the CP/MAS NMR experiments.

$$f_a^H = f_a - f_a^N \quad (12)$$

where  $f_a^H$  is the fraction of protonated carbons in the aromatic region,  $f_a^N$  is the fraction of non-protonated carbons and CH<sub>3</sub> in aromatic region and  $f_a$  is the fraction of aromatic carbons from the CP/MAS NMR experiments.

$$f_a^B = f_a^N - f_a^P - f_a^S \quad (13)$$

## APPENDICES

---

where  $f_a^B$  is the fraction of bridgehead carbons,  $f_a^N$  is the fraction of non-protonated carbons and  $\text{CH}_3$  in aromatic region,  $f_a^P$  is the fraction of phenolic carbons and  $f_a^P$  is the fraction of phenolic carbons.

$$f_a^{N*} = f_{al}^* / (f_{al}^* \times f_{al}) \quad (14)$$

where  $f_a^{N*}$  is the fraction of non-protonated carbons and  $\text{CH}_3$  in aliphatic region,  $f_{al}^*$  is the integral value for aliphatic carbons from dipolar dephasing experiments and  $f_{al}$  is the fraction of aliphatic carbons.

$$f_{al}^H = f_{al} - f_a^{N*} \quad (15)$$

where  $f_{al}^H$  is the fraction of protonated carbons and  $\text{CH}_3$  in aliphatic region,  $f_{al}$  is the fraction of aliphatic carbons and  $f_a^{N*}$  is the fraction of non-protonated carbons and  $\text{CH}_3$  in aliphatic region.

$$f_{al}^O = B / (A \times f_{al}) \quad (16)$$

where  $f_{al}^O$  is the fraction of aliphatic carbons bonded to oxygen, B is the integral value of the aliphatic carbons bonded to oxygen and A is the integral value of aliphatic carbons and  $f_{al}$  is the fraction of aliphatic carbons.

**Appendix H**

**Conductivity results**

Electrical conductivity was performed to measure the ability of the Coal A packed-bed reactor generated samples to conduct electricity. This was determined to prove a statement made in section 4.3.5.1, where the spectra of the  $^{13}\text{C}$  CP/MAS NMR for sample 5 appeared to have high signal to noise ratio. High signal to noise ratio lead to speculation that this sample has high electrical conductivity. An electrical conductivity experiments need to be performed in order to prove this. A method used for conductivity analysis is well discussed in Chapter 3, section 3.4.2.1.5. As it can be observed in the figure below, sample 5 and 6 has high electrical conductivity compared to other samples.

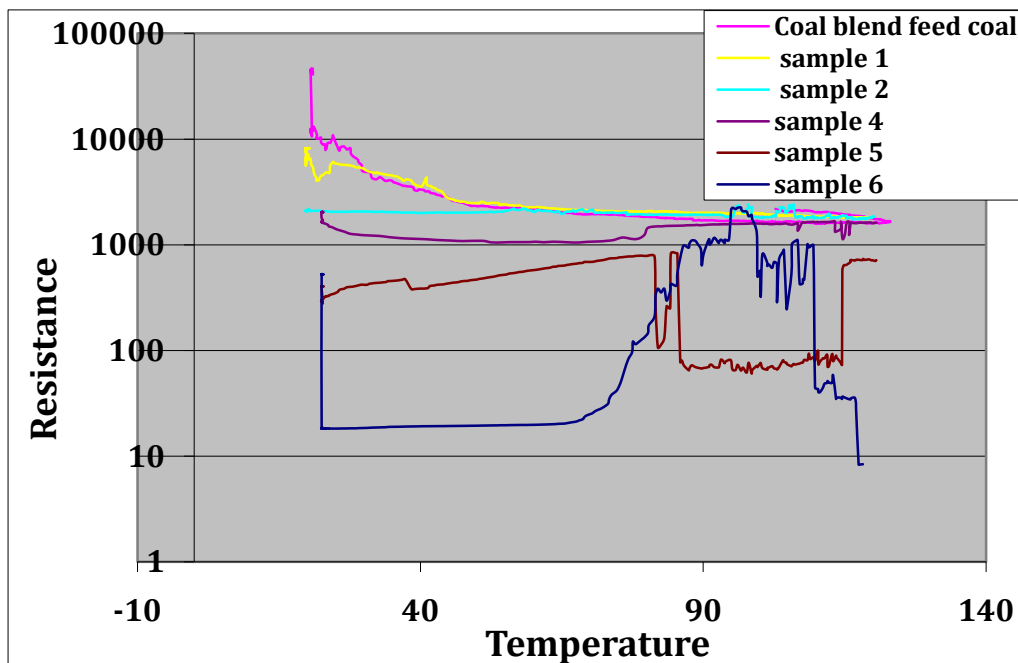


*Figure H-1: Graph showing resistivity of Coal A feed coal sample and the packed-bed reactor generated samples.*

# APPENDICES

---

## Appendix I

### Petrography

Petrography was conducted by maceral and microlithotype group count on feed coal samples, Coal A and B. The maceral results are discussed in Phase 3 and the microlithotype analysis results are summarized in Table H1.

Table I-1: Summarized microlithotype analysis (vol %) for the Coals, A and B feed coal samples.

---

<b>Sample</b>	<b>Microlithotypes (vol %)</b>	<b>Coal A (vol %)</b>	<b>Coal B (vol %)</b>
<b>Coal</b>	<b>Vitrite</b>	16	15.2
	<b>Inertoditrite</b>	41.4	45
	<b>Semifusite/Fusite</b>	19	19
	<b>Intermediate</b>	11.2	12.4
	<b>Carbominerite</b>	8	2.4
	<b>Minerals</b>	5	6.2

---

Table I-2: Tabulated carbon particle type analysis results for the Coal A packed-bed reactor generated samples.

COAL A	MICROLITHOTYPE	SUB GROUP	SAMPLE NUMBER / ID (-75mm, +5mm)						
			1	2	3	4	5	6	7
<b>COAL</b>	<i>VITRITE</i>		13.3	6.5	2.8	1	0	0	0
	<i>LIPTITE</i>		0.2	0.0	0.0	0.0	0.0	0.0	0.0
	<i>INERTITE</i>	<b>SF</b>	13.9	19.4	9.6	1.2	0	0	0
		<b>F</b>	6.5	6.5	4.4	0	0	0	0
		<b>INTD</b>	14.3	19.9	17.2	4	0	0	0
	<b>% TOTAL INERTINITE</b>		<b>34.7</b>	<b>45.8</b>	<b>31.2</b>	<b>5.2</b>	<b>0</b>	<b>0</b>	<b>0</b>
	<i>INTERMEDIATE</i>		11.3	5.2	1.6	0.8	0	0	0
	<i>CARBOMINERITE</i>		8.7	7.5	3.6	2.4	0	0	0
	<i>MINERAL MATTER</i>		21.4	14.3	15.6	5.2	4.7	16.2	18.3
<b>DEV COAL</b>	<i>POROUS COAL</i>		5.8	15.5	18.6	7.6	0	0.4	0
	<i>COLOUR CHANGE</i>		2.2	3.6	5.2	2	0	0	0
	<i>CRACKS</i>		1.4	3.2	0.8	0.8	0	0	0
	<i>MIXED</i>		1	2.8	4.8	0.6	0	0	0
	<b>% TOTAL DEV COAL</b>		<b>10.4</b>	<b>25.1</b>	<b>29.4</b>	<b>11</b>	<b>0</b>	<b>0.4</b>	<b>0</b>
<b>CHARS</b>	<i>POROUS (THIN)</i>		0	0	4.4	5	3	3.8	0.2
	<i>POROUS (THICK)</i>		0	0.2	4.2	10.4	3.5	3.2	0.2
	<b>%TOTAL POROUS CHARS</b>		<b>0</b>	<b>0.2</b>	<b>8.6</b>	<b>15.4</b>	<b>6.5</b>	<b>7</b>	<b>0.4</b>
	<i>INERT CHARS</i>		0	0.4	4	19.5	22.8	14.6	5.6
	<i>FUSINIODES</i>		0	0	1.8	5.4	2.4	1.8	0
	<i>OXIDISED</i>		0	0	0.2	0	3	4	1.6
	<b>% TOTAL INERT CHARS</b>		<b>0</b>	<b>0.4</b>	<b>6</b>	<b>24.9</b>	<b>28.2</b>	<b>20.4</b>	<b>7.2</b>
	<i>INTERMEDIATE</i>		0	0	1.2	1.8	1.4	3	0
	<i>CARBIMINERITE CHARS</i>		0	0	0	1.4	2.2	0	0.2
	<i>ASH</i>		0	0	0	30.9	57.1	53.1	74



Table I-3: Tabulated carbon particle type analysis results for the Coal B packed-bed reactor generated samples.

COAL B	MICROLITHOTYPE	SUB GROUP	SAMPLE NUMBER / ID (-75mm, +5mm)						
			1	2	3	4	5	6	7
<b>COAL</b>	VITRITE		10	6.9	13.6	5.8	2.6	0	0
	LIPTITE		0.0	0.0	0.0	0.0	0.0	0.0	0.0
	INERTITE	SF	16	13.2	13	13.5	5.4	0	0
		F	2.2	2.8	4.1	7.6	0	0	0
		INTD	26.9	30	27.4	14.7	2.6	0.2	0
	<b>% TOTAL INERTINITE</b>		<b>45.1</b>	<b>46</b>	<b>44.5</b>	<b>35.8</b>	<b>8</b>	<b>0.2</b>	<b>0</b>
	INTERMEDIATE		9.6	7.9	8.3	3.2	0	0	0
	CARBOMINERITE		16.8	12.8	8.7	7	1	0	0
	MINERAL MATTER		15.8	20	15.3	24.7	14.8	17	9.1
<b>DEV COAL</b>	POROUS COAL		0.6	1.6	3.3	10.8	7.6	0	0
	COLOUR CHANGE		0	0.4	1.9	3	4.2	0.4	0
	CRACKS		2.2	4.3	4.3	3.4	1.2	0	0
	MIXED		0	0	0	1.8	0.4	0	0
	<b>% TOTAL DEVOLATILIZED COAL</b>		<b>2.8</b>	<b>6.3</b>	<b>9.5</b>	<b>19</b>	<b>13.4</b>	<b>0.4</b>	<b>0</b>
<b>CHARS</b>	POROUS (THIN)		0	0	0	1	2.4	0.2	0
	POROUS (THICK)		0	0	0	0	2.8	0.8	0.2
	<b>%TOTAL POROUS CHARS</b>		<b>0</b>	<b>0</b>	<b>0</b>	<b>1</b>	<b>5.2</b>	<b>1</b>	<b>0.2</b>
	INERT CHARS		0	0	0	3	25.7	15.8	2
	FUSINOIDS		0	0	0	0	6	2.6	1
	OXIDISED		0	0	0	0.2	3.8	4.8	5
	<b>% TOTAL INERT CHARS</b>		<b>0</b>	<b>0</b>	<b>0</b>	<b>3.2</b>	<b>35.5</b>	<b>23.2</b>	<b>8</b>
	INTERMEDIATE		0	0	0	0.2	0	3	0
	CARBO CHARS		0	0	0	1.4	2	1	0.2
	ASH		0	0	2.4	9	33.6	73.4	83.3

6

---

## Appendix J

### Total reflectance analysis results.

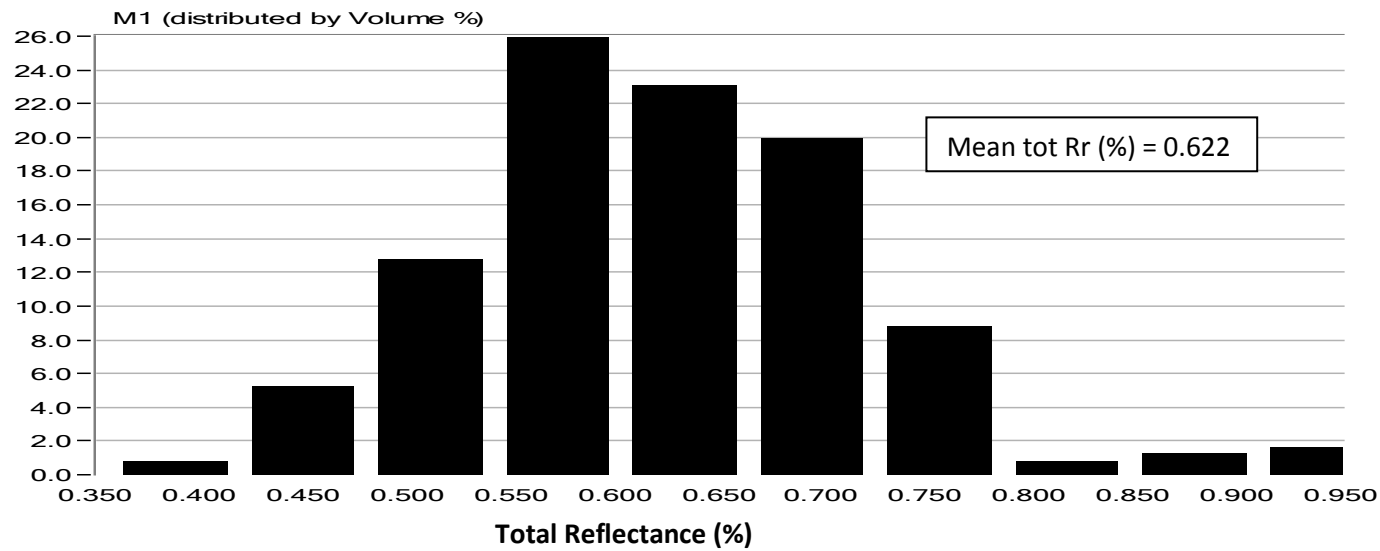


Figure J-1: Total reflectance measurement of coal macerals for the Coal A feed coal sample.

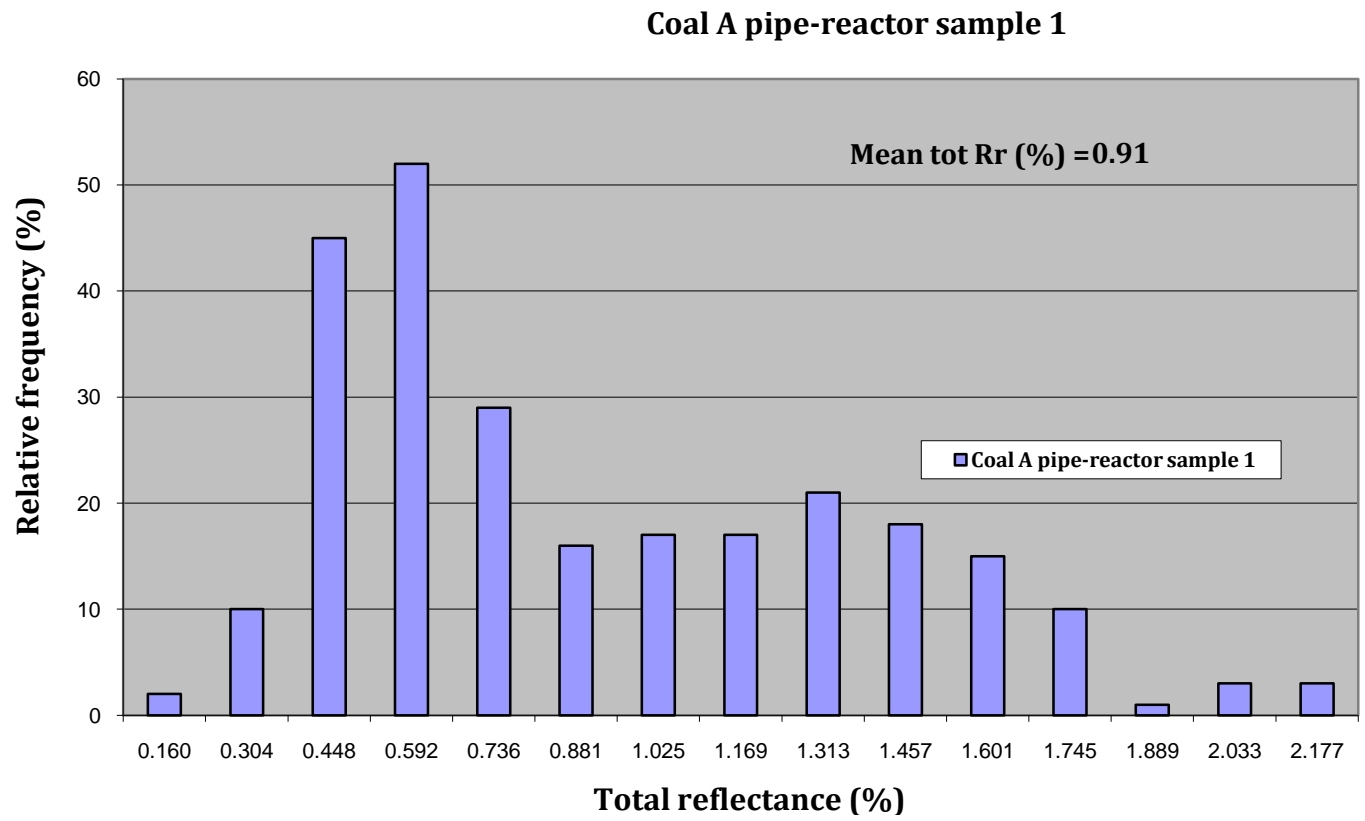


Figure J-2: Total reflectance measurement of coal macerals for the Coal A packed-bed reactor generated sample 1.

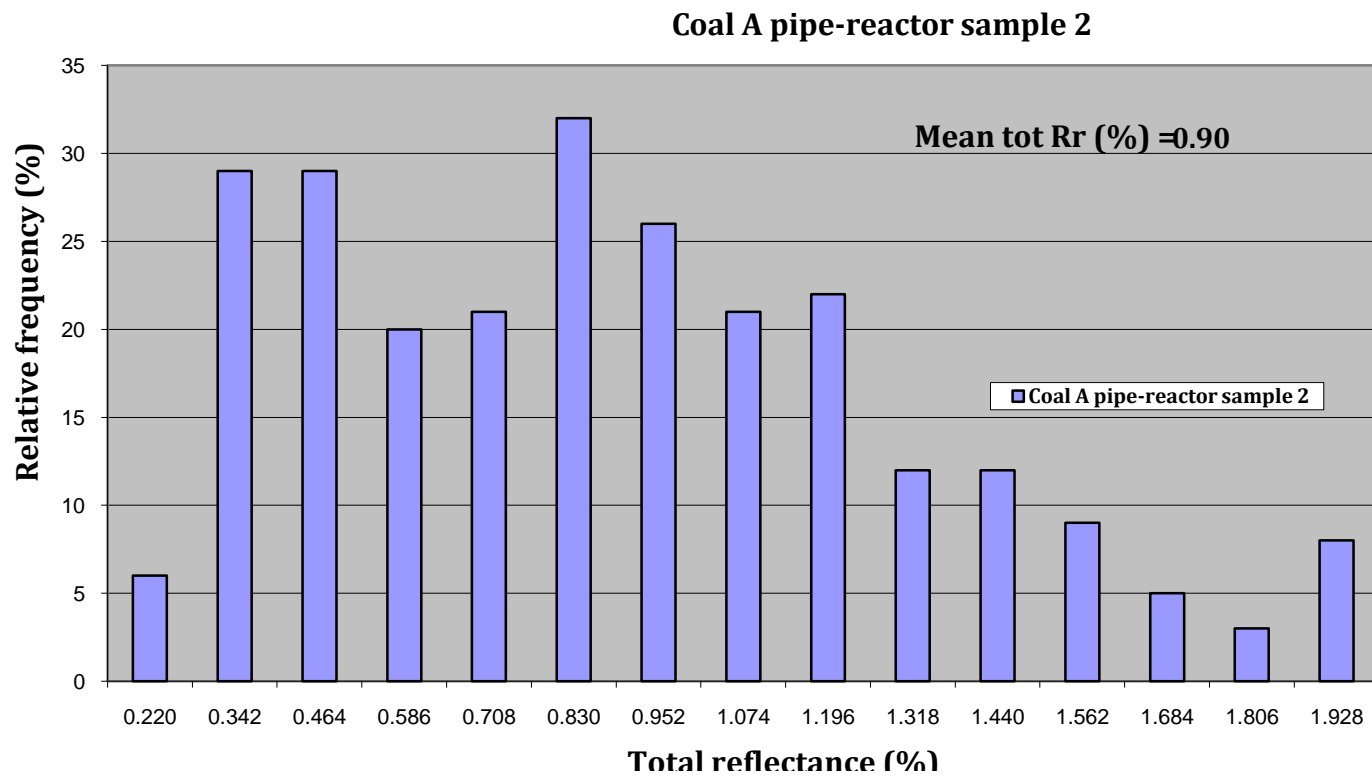


Figure J-3: Total reflectance measurement of coal macerals for the Coal A packed-bed reactor generated sample 2.

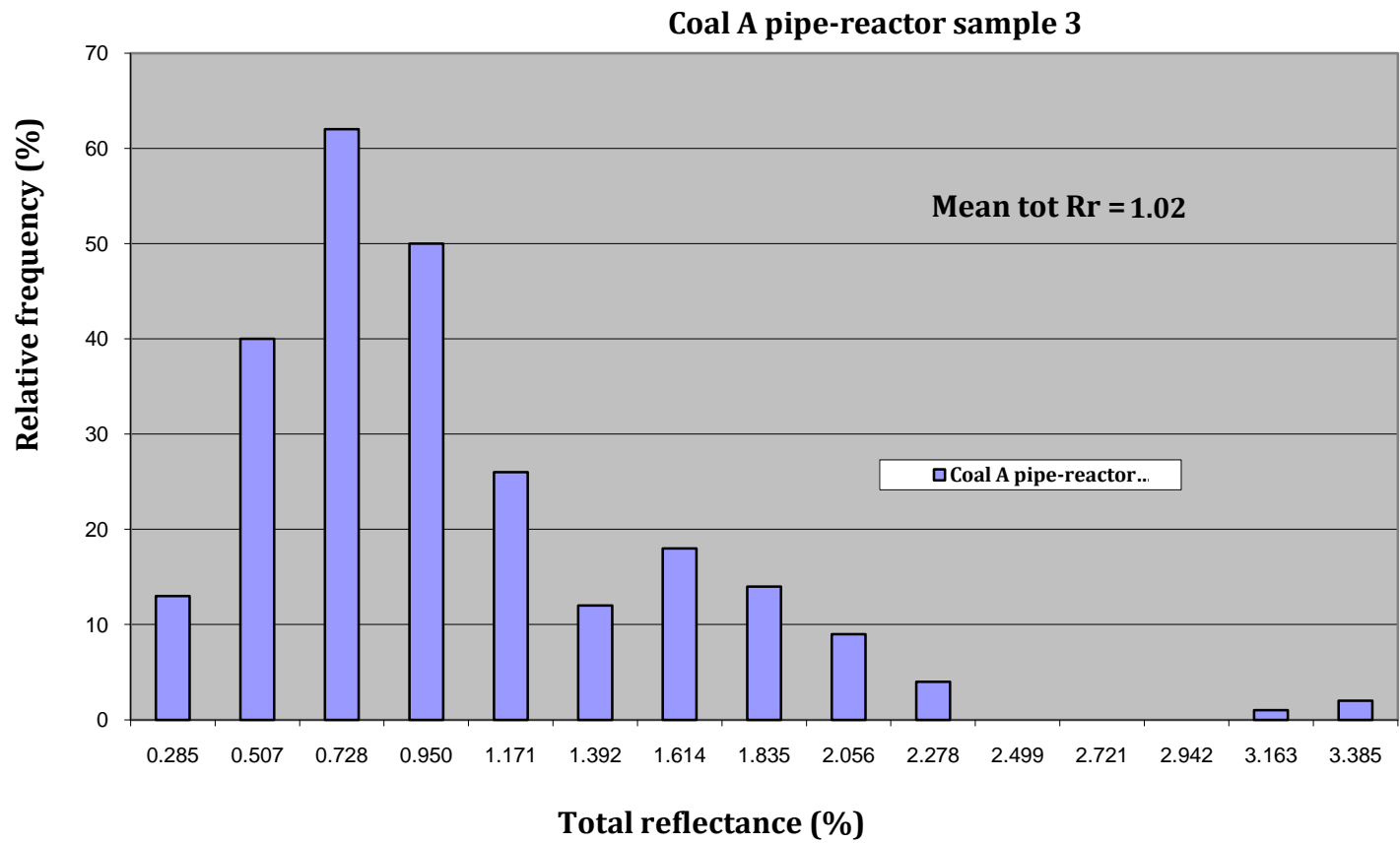


Figure J-4: Total reflectance measurement of coal macerals for the Coal A packed-bed reactor generated sample 3.

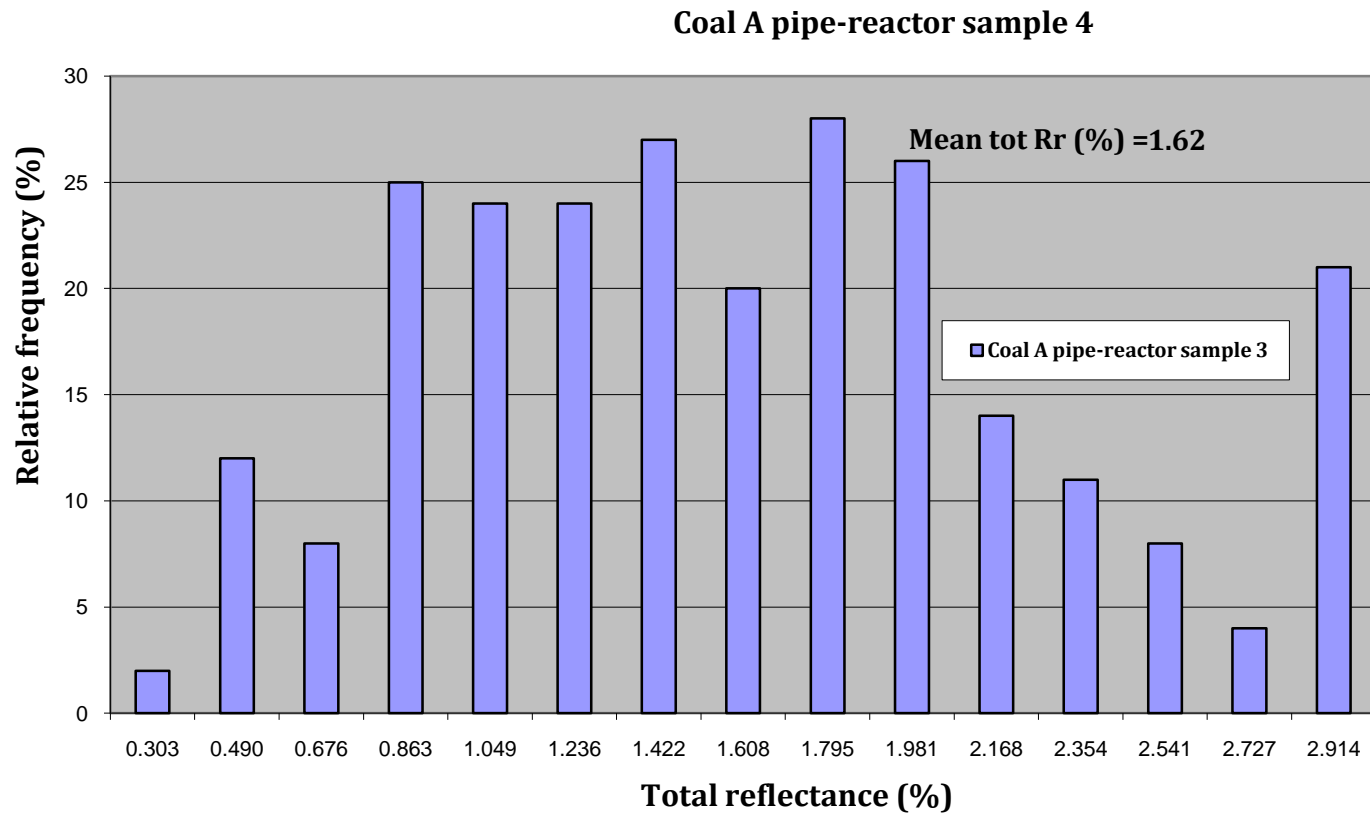


Figure J-5: Total reflectance measurement of coal macerals for the Coal A packed-bed reactor generated sample 4.

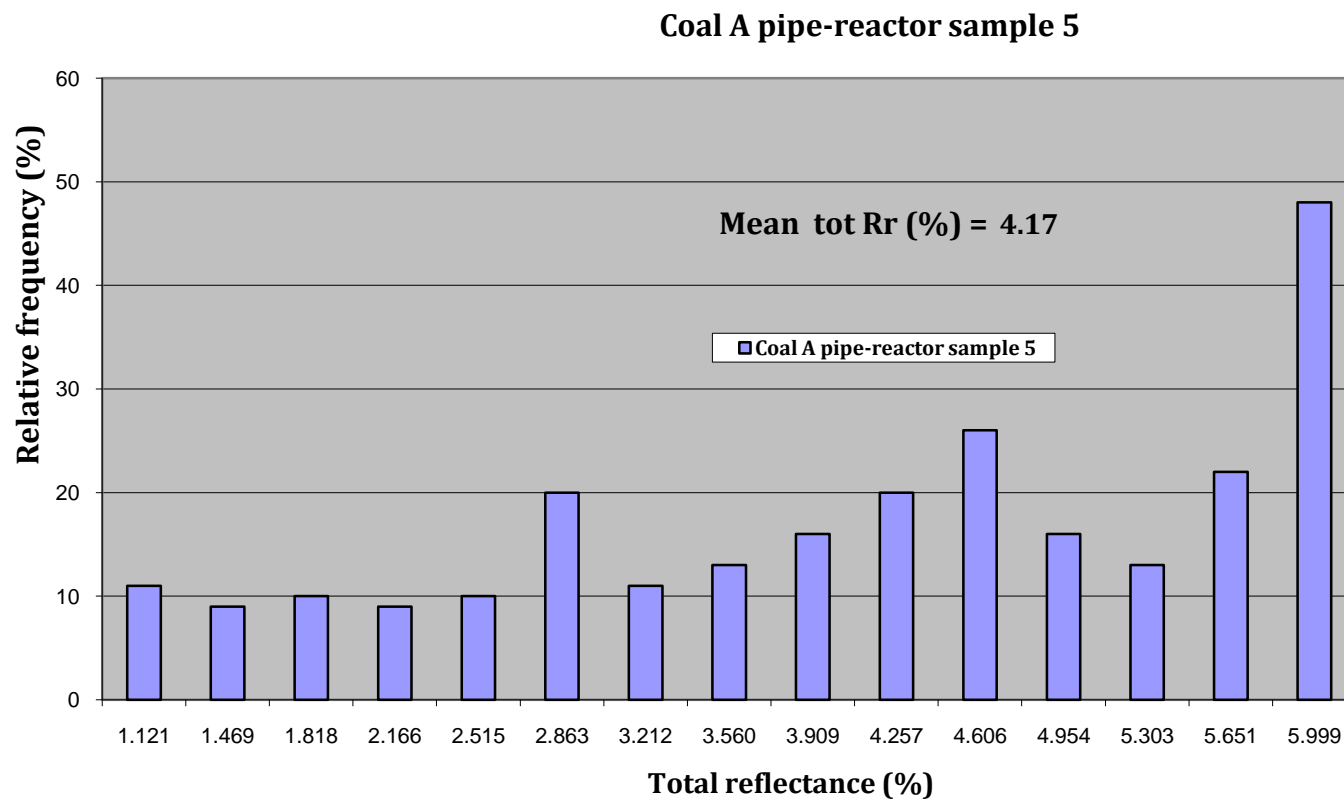


Figure J-6: Total reflectance measurement of coal macerals for the Coal A packed-bed reactor generated sample 5.

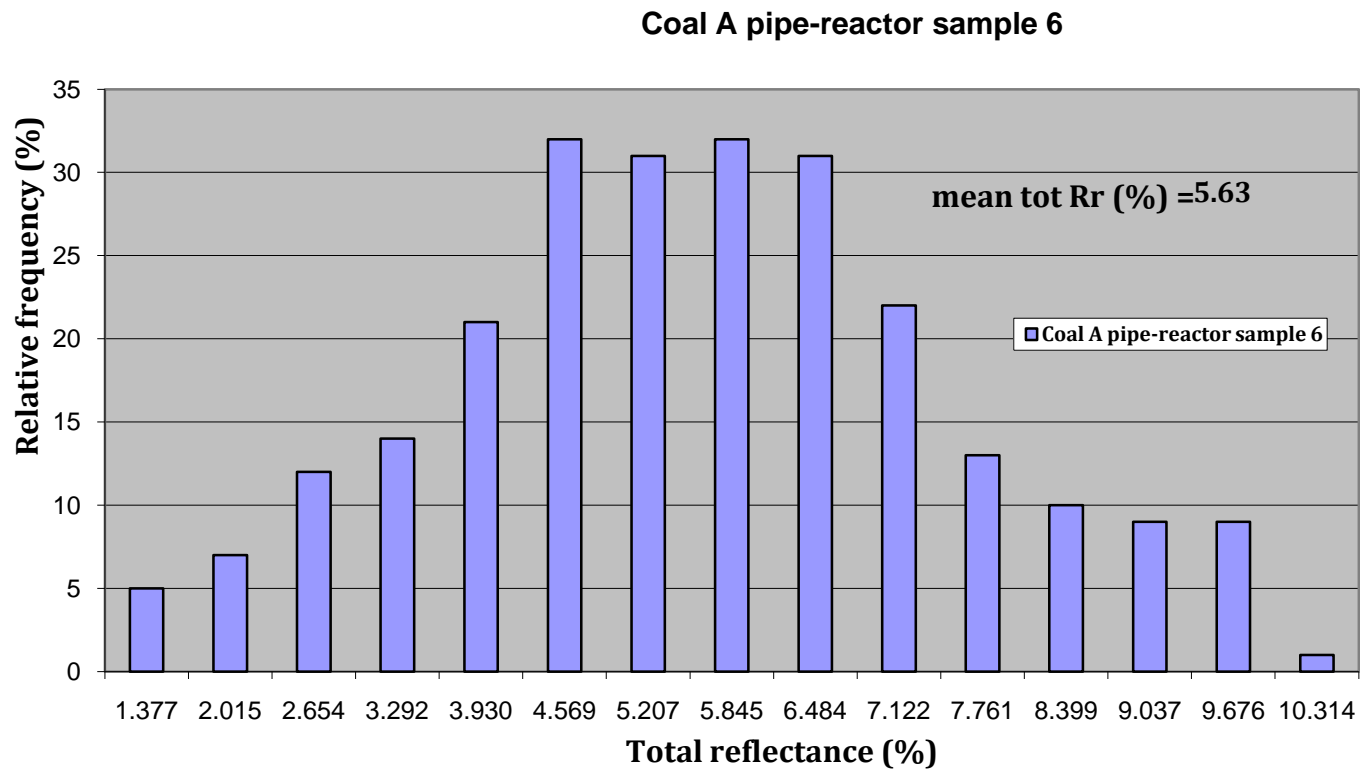


Figure J-7: Total reflectance measurement of coal macerals for the Coal A packed-bed reactor generated sample 6.



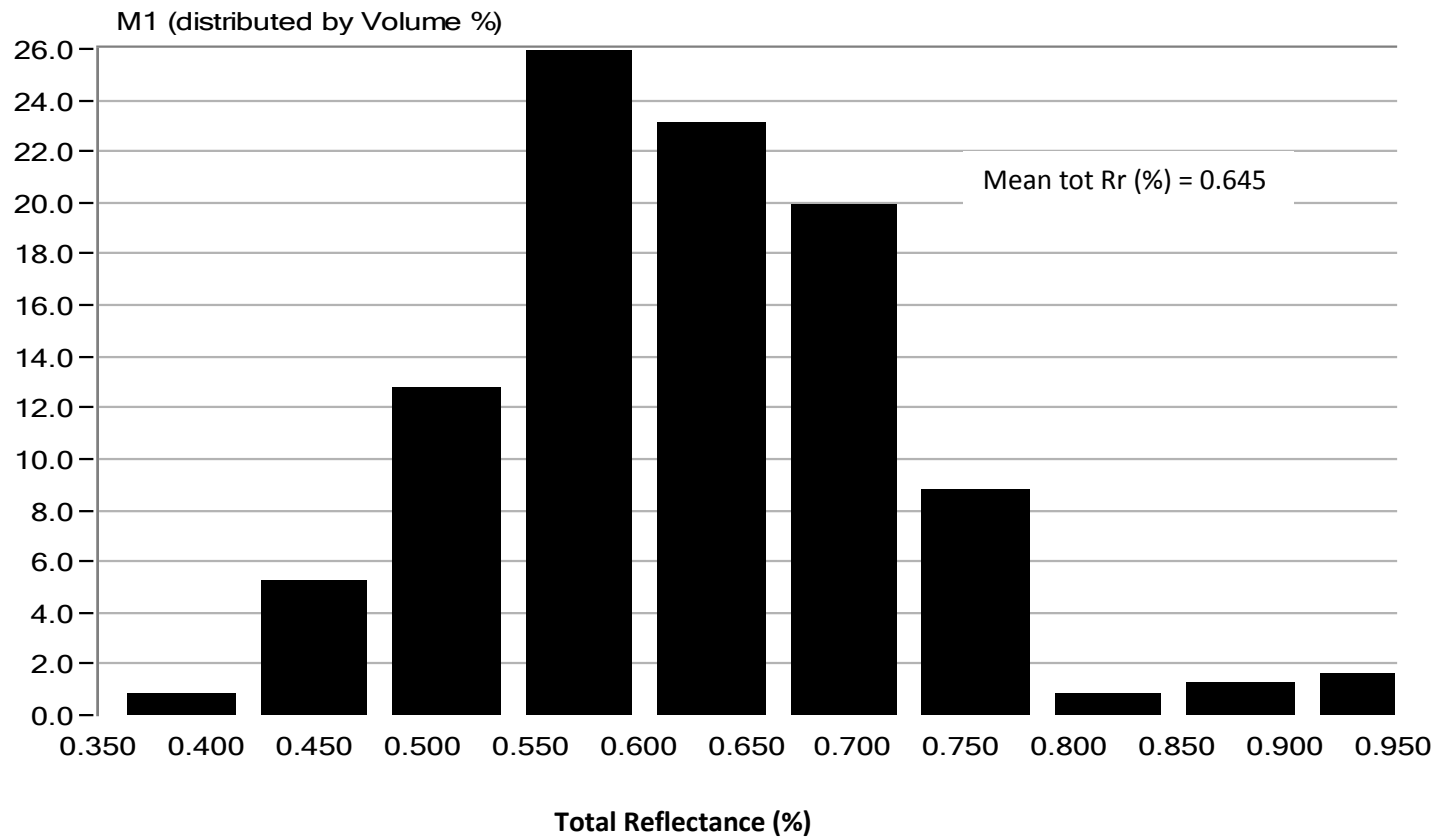


Figure J-8: Total reflectance measurement of coal macerals for the Coal B coal feed sample.

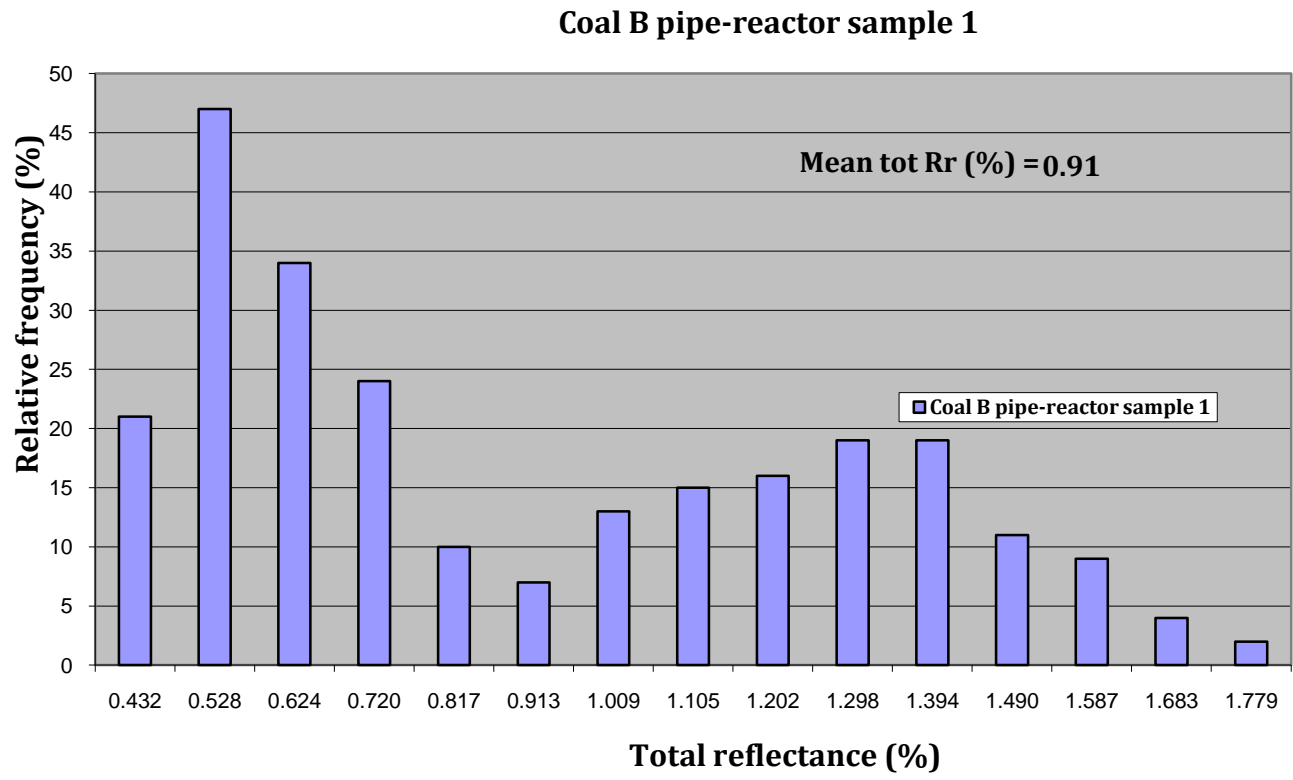


Figure J-9: Total reflectance measurement of coal macerals for the Coal B packed-bed reactor generated sample 1.

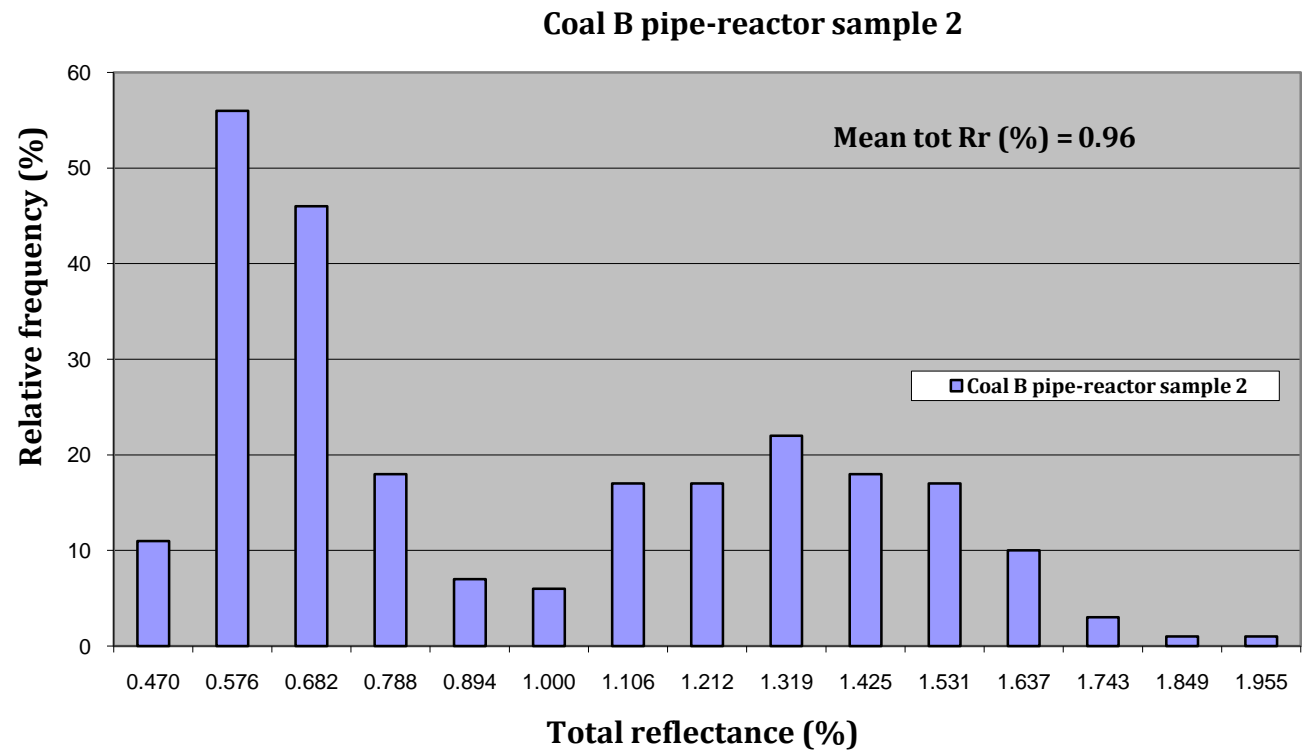


Figure J-10: Total reflectance measurement of coal macerals for the Coal B packed-bed reactor generated sample 2.

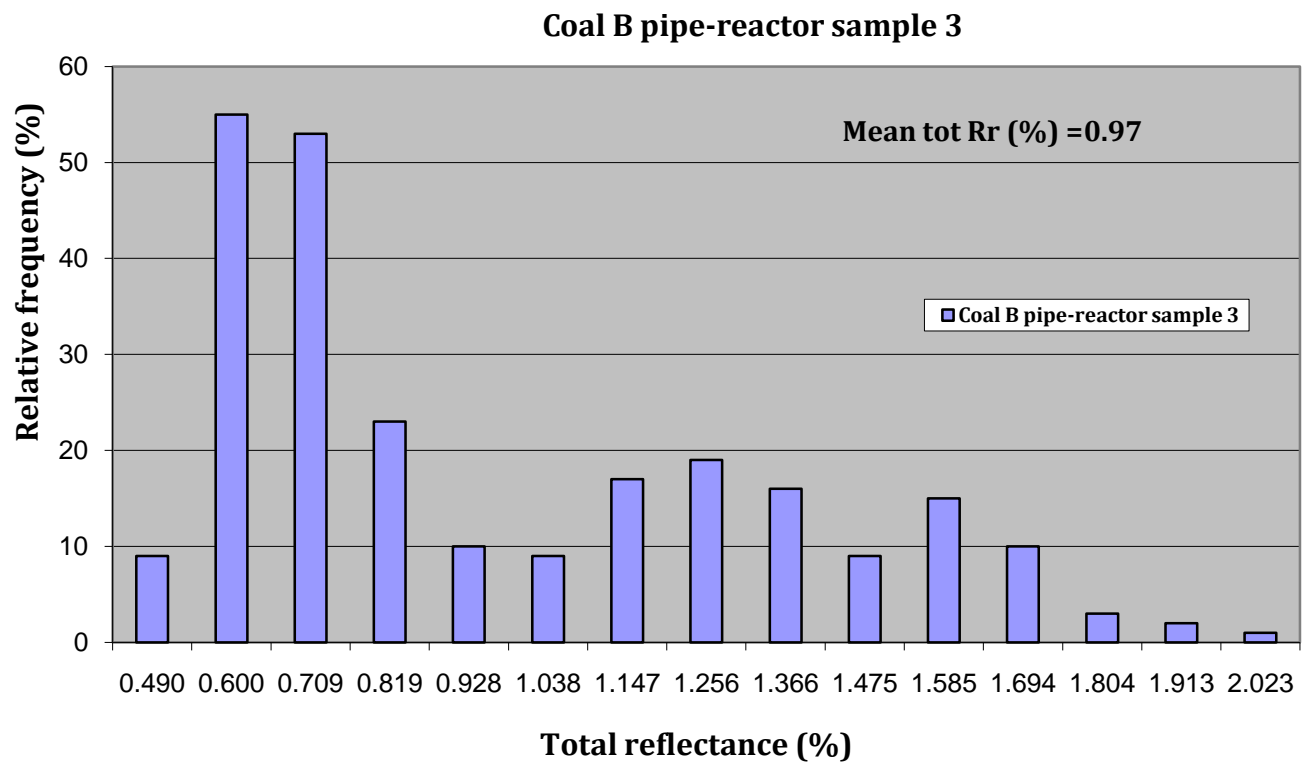


Figure J-11: Total reflectance measurement of coal macerals for the Coal B packed-bed reactor generated sample 3.

**Coal B pipe-reactor sample 4**

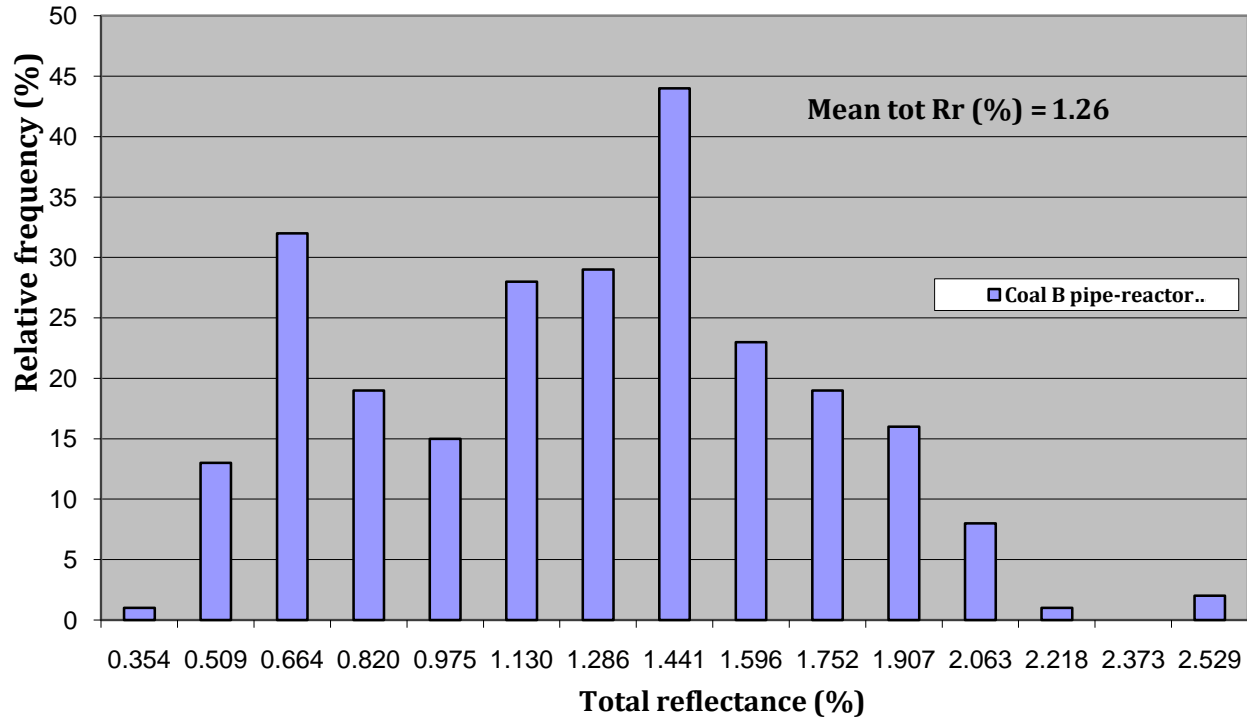


Figure J-12: Total reflectance measurement of coal macerals for the Coal B packed-bed reactor generated sample 4.

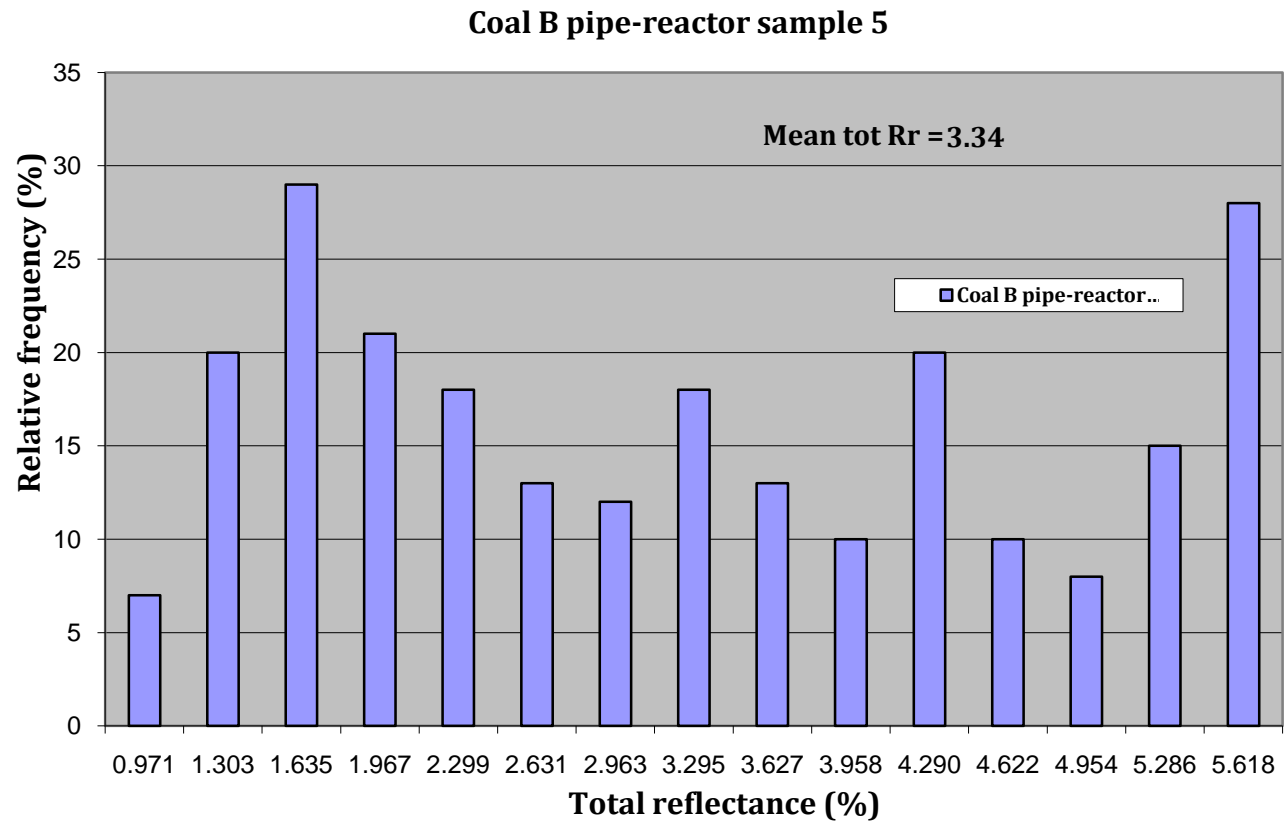


Figure J-13: Total reflectance measurement of coal macerals for the Coal B packed-bed reactor generated sample 5.

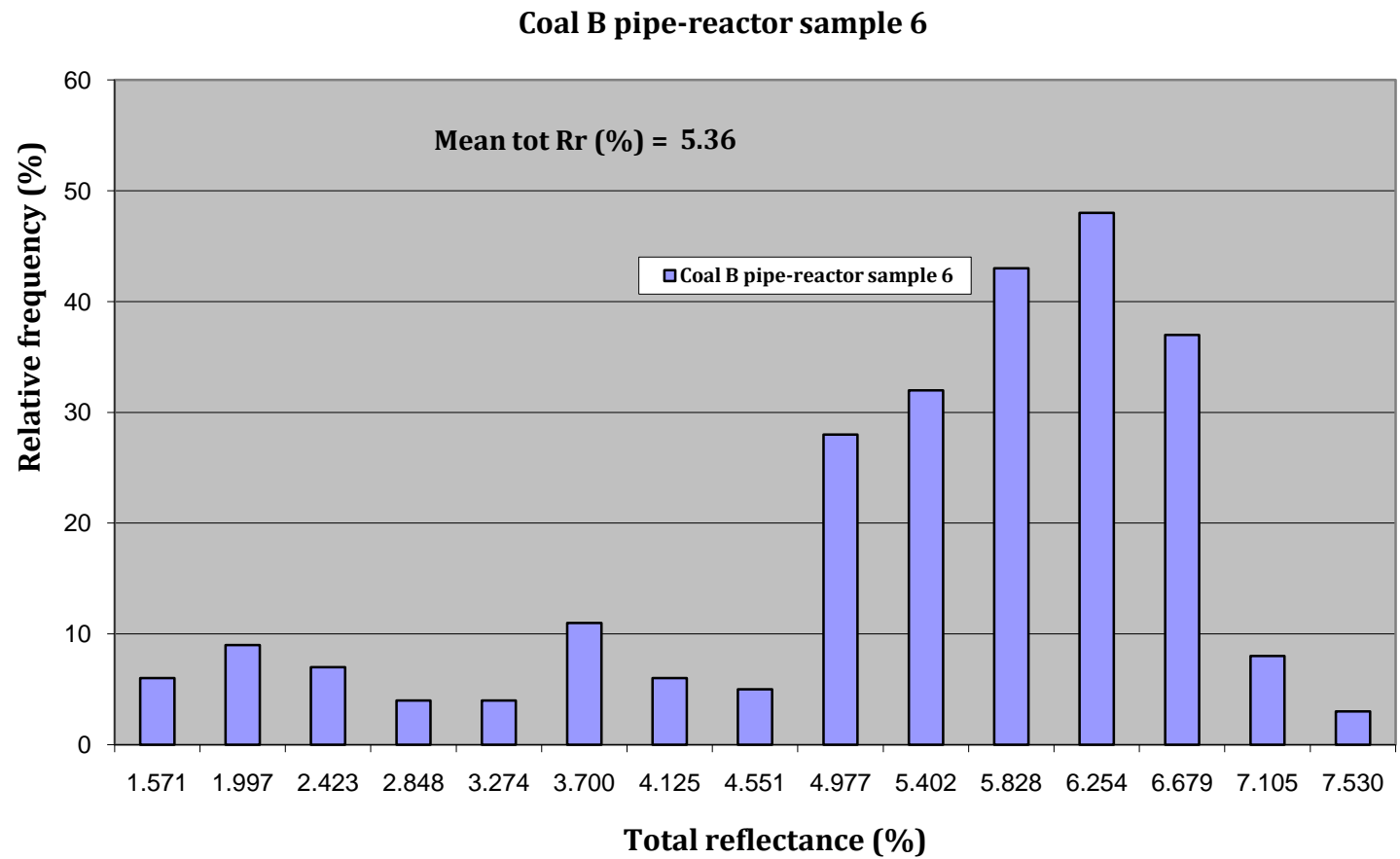


Figure J-14: Total reflectance measurement of coal macerals for the Coal B packed-bed reactor generated sample 6.